Numerical Study on the Seismic Performance of a Demountable Friction-Based Beam-to-Column Connection for Precast Concrete Frames

Xiaoning Sun

Department of Civil Engineering

McGill University, Montreal

March 2025

A thesis submitted to McGill University in partial fulfillment of the requirements of the degree of Master of Engineering.

© Xiaoning Sun 2025

ABSTRACT

To enhance the sustainability and resilience of precast concrete structures, this study adopts a Design for Disassembly (DfD) approach to develop a damage-controlled connection that enables post-earthquake repair and structural component reuse. A Demountable Frictional Energy-Dissipative Beam-to-Column Connection (DFED-BCC) is proposed as a friction-based solution for precast beam-to-column assemblies.

The DFED-BCC incorporates a friction damper at the beam end and employs high-strength bolts and angle steel to provide moment resistance, while corbels and shear bolts are designed to transfer shear forces. The connection features a clear load transfer path and a straightforward assembly process. Under cyclic loading, the response initiates with elastic and minor inelastic deformation in the angle steel, resulting in limited energy dissipation and small residual displacements. As displacement increases, frictional sliding occurs, significantly enhancing energy dissipation while localizing damage within demountable components, thereby protecting the concrete elements and embedded reinforcement. At large displacements, prying action induces plastic deformation in the bolts, leading to irreversible damage. The slot length can be adjusted to control behavioral transitions, providing a means to optimize seismic performance.

Finite element analysis (FEA) was conducted to evaluate the seismic behavior of the proposed connection, focusing on initial stiffness, stiffness degradation, and energy dissipation, while examining the influence of bolt preloads and material properties. The results were compared with those of a monolithic connection. Findings indicated that bolt preloading significantly affects the mechanical response, with the proposed connection exhibiting superior performance, particularly in terms of energy dissipation. At an equivalent design load, the energy dissipation of the monolithic connection was only 39.72% of that of the DFED-BCC.

In conclusion, the DFED-BCC provides a constructible, demountable, and seismically resilient alternative to conventional precast beam-to-column connections. Its ability to simplify

construction, enable post-earthquake repair, and facilitate component reuse highlights its potential for advancing the sustainability and resilience of precast concrete systems.

Résumé

Afin d'améliorer la durabilité et la résilience des structures en béton préfabriqué, cette étude adopte une approche de conception pour le démontage (Design for Disassembly, DfD) visant à développer une connexion contrôlée en termes de dommages, permettant la réparabilité post-sismique et la réutilisation des composants structurels. Une connexion poutre–poteau démontable dissipative d'énergie par frottement (DFED-BCC) est proposée comme solution basée sur le frottement pour les assemblages en béton préfabriqué.

La DFED-BCC intègre un amortisseur à friction à l'extrémité de la poutre et utilise des boulons à haute résistance ainsi que des cornières en acier pour assurer la résistance aux moments fléchissants, tandis que des corbeaux et des boulons de cisaillement sont conçus pour transférer les efforts tranchants. La connexion présente un chemin de transfert de charge bien défini et un processus d'assemblage simple. Sous chargement cyclique, la réponse commence par une déformation élastique et légèrement inélastique des cornières, entraînant une dissipation d'énergie limitée et de faibles déplacements résiduels. Avec l'augmentation du déplacement, un glissement par frottement se produit, augmentant significativement la dissipation d'énergie tout en localisant les dommages dans les composants démontables, protégeant ainsi les éléments en béton et les armatures noyées. À de grands déplacements, l'effet de levier induit une déformation plastique des boulons, entraînant des dommages irréversibles. La longueur des fentes peut être ajustée pour contrôler les transitions de comportement, offrant ainsi un moyen d'optimiser la performance sismique.

Une analyse par éléments finis (FEA) a été menée pour évaluer le comportement sismique de la connexion proposée, en se concentrant sur la raideur initiale, la dégradation de la raideur et la dissipation d'énergie, tout en examinant l'influence de la précontrainte des boulons et des propriétés des matériaux. Les résultats numériques ont été comparés à ceux d'une connexion monolithique. Les résultats ont indiqué que la précontrainte des boulons influence de manière significative la réponse mécanique, la connexion proposée montrant des performances supérieures, notamment en termes de capacité de dissipation d'énergie. À capacité portante

équivalente, la dissipation d'énergie de la connexion monolithique ne représentait que 39,72 % de celle de la DFED-BCC.

En conclusion, la DFED-BCC constitue une alternative constructible, démontable et sismiquement résiliente aux connexions poutre–poteau traditionnelles en béton préfabriqué. Sa capacité à simplifier la construction, à permettre des réparations post-sismiques et à favoriser la réutilisation des composants structurels en fait une solution prometteuse pour renforcer la durabilité et la résilience des systèmes en béton préfabriqué.

ACKNOWLEDGMENT

In the season when hydrangeas first bloomed, I arrived in Montreal; as snowflakes once again adorned the city's streets, my dissertation quietly drew to a close. The changing seasons have witnessed my transformation—the fiery maple leaves of autumn warmed the solitude of life abroad, the tranquility of winter calmed my restless thoughts, and each returning spring brought new hope and strength.

First and foremost, I would like to express my deepest gratitude to my advisor, Professor Shao. Your rigorous academic attitude, sharp insight, and unwavering commitment to academic integrity have not only illuminated my path in research but also taught me how to approach life with clarity and determination. Your guidance has left a profound impact on both my academic development and personal growth.

I am sincerely thankful to all my friends, labmates, and ZeKai. Your companionship, encouragement, and support have accompanied me throughout this journey. When I felt lost, your experience guided me; when I struggled with self-doubt, your words gave me strength; and when I made progress, your genuine joy multiplied my own. The lab discussions, moments of laughter in daily life, and weekend brainstorming sessions are memories I will always treasure.

My deepest thanks go to my mother. Your care across the ocean, the gentle gaze during our video calls, and your unconditional support for every decision I made have always been the firmest anchor in my life. Though far away, my little black cat, Xiao Hei Hei, has accompanied my growth in its own special way. Its curious head tilts during video calls and its "crime scenes" of occupying my desk in photos have brought me unexpected comfort.

I also sincerely thank the Canadian Precast Concrete Institute (CPCI) for their generous financial support of this research.

Lastly, I feel truly fortunate that my story with Montreal does not end here. This city that has witnessed my growth will also be the starting point of a new chapter in my life. As the seasons continue their quiet cycle, I look forward to discovering the beauty that lies ahead.

Table of Contents

Abstract.....I

Résumé.....III

ACKNOWLEDGMENT.....V

Table of Contents.....VI

List of Figures.....VIII

List of Tables.....XI

Chapter 1 Research background.....1

1.1 Research background.....1

1.2 Connections in PC system.....2

1.2.1 Wet connections in PC system.....2

1.2.2 Challenges of wet connections.....2

1.2.3 Dry connections in PC system.....6

1.3 Dry beam-to-column connections.....7

1.3.1 Definition of connection and joint.....8

1.3.2 Multilevel classification system for dry connection design objectives.....8

1.3.3 Connections for moment resisting frame.....10

1.4 Aim and Objective.....24

1.4.1 Aim.....24

1.4.2 Objective.....24

Chapter 2 Design of Demountable Frictional Energy-Dissipative Beam-to-Column connection (DFED-BCC).....26

2.1. Location of the connection.....26

2.2. Constructability.....28

2.3. Proposed design of the connection 29

2.3.1. Introduction of DFED-BCC 30

2.3.2. Rotation point 31

2.4. Load transfer mechanism in DFED-BCC 33

2.5. Replacement and upgrade method 38

Chapter 3 Numerical analysis 40

3.1. Selection of modeling methods 40

3.2. Test arrangements 42

3.2.1. Test specimens 42

3.2.2. Materials 46

3.2.3. Loading protocol 46

3.2.4. Test matrix 47

3.3. FE model validation 47

3.4. FE model for DFED-BCC 51

3.4.1. Basic setup 51

3.4.2. Constitutive models of materials 51

3.4.3. Bolt diameter 58

3.4.4. Bolt preloading forces 58

3.4.5. Interactions 58

3.4.6. Boundary conditions 59

3.5. FE model for monolithic connection 59

3.6. Results and discussion 61

3.6.1. Test phenomenon 61

3.6.2. Hysteresis behaviors 68

3.6.3. Skeleton curves 71

3.6.4. Stiffness degradation curves 72

3.6.5. Energy dissipation capacity 75

Chapter 4 Multi-linear hysteresis model of DFED-BCC 77

4.1. Progressive Working Mechanism of the Proposed Connection 77

4.2. Stage one: Elastic stage 78

4.2.1. Initial Stiffness 79

4.3. Stage two: Localized yielding stage 81

4.4. Stage three: Frictional sliding stage 81

4.4.1. Rotational Stiffness 82

4.4.2. Axial Stiffness of friction damper 84

4.5. Stage Four: Prying-induced plastic stage 85

Chapter 5 Discussion on DFED-BCC 87

5.1. Performance evaluation 87

5.2. Research Limitations 88

Reference list 90

List of Figures

Figure 1-1 Precast Concrete Systems: Factory Fabrication and On-Site Assembly 2

Figure 1-2 The Performance Based Seismic Design (PBSD) method 4

Figure 1-3 Definition of a ‘joint’ and ‘connection 8
Figure 1-4 Classification framework of dry connections 9
Figure 1-5 Endplate-Inspired Connection 13
Figure 1-6 Flange cleats-Inspired Connection 14
Figure 1-7 Normal bolted connections in steel structure 15
Figure 1-8 Hysteretic characteristics for generic PRESSS connection systems [35] 16
Figure 1-9 Specimens for the "Slotted Beam" Concept in the PRESSS Research Program 17
Figure 1-10 Specimen UT-FR and story shear-drift response [35] 18
Figure 1-11 A multi-level damper mechanism induced by preset gaps 21
Figure 1-12 A staged energy dissipation device integrating friction and metallic dampers . 22
Figure 1-13 Four systems in BCC integrating energy dissipation devices 22
Figure 1-14 Beam-to-beam connections 23
Figure 2-1 (1) Beam side sway mechanism (b) Soft storey mechanism 26
Figure 2-2 Construction of precast concrete frame 28
Figure 2-3 Potential connection locations 29
Figure 2-4 Proposed design of the connection 29
Figure 2-5 Components of DFED-BCC 30
Figure 2-6 Location of rotation point 32
Figure 2-7 Displacement with Rotation Centered at Midpoint 32
Figure 2-8 Assumption in Kishi–Chen’s initial stiffness model 34
Figure 2-9 Assumption in Yang–Lee’s initial stiffness model 35
Figure 2-10 Load path: Sagging moment 36
Figure 2-11 Load path: Hogging moment 36
Figure 2-12 Load path in connection with two rows of bolts 37
Figure 2-13 Schematic of height difference 37
Figure 3-1 Dimensions of monolithic connection 42
Figure 3-2 Dimensions of DFED-BCC 43

Figure 3-3 Configurations of the steel components in DFED-BCC 44

Figure 3-4 Materials of DFED-BCC 45

Figure 3-5 Relative Loading History Deformation Amplitudes 46

Figure 3-6 Loading protocol 47

Figure 3-7 Validation of friction-based demountable connection 48

Figure 3-8 Validation of monolithic connection 50

Figure 3-9 Isotropic hardening model and Kinematic hardening model 54

Figure 3-10 Stress-Strain Model proposed for Monotonic Loading of Confined and Unconfined Concrete 56

Figure 3-11 Concrete damage plasticity constitutive model 57

Figure 3-12 Contact relationship of the connection's core area 59

Figure 3-13 USTEEL02 in user-defined subroutine 60

Figure 3-14 0.475% drift ratio hogging moment 63

Figure 3-15 -0.475% drift ratio hogging moment 63

Figure 3-16 1.82% drift ratio hogging moment 64

Figure 3-17 -1.82% drift ratio hogging moment 65

Figure 3-18 5.0% drift ratio hogging moment 66

Figure 3-19 -5.0% drift ratio hogging moment 67

Figure 3-20 Comparison of the hysteresis curves of monolithic connection and P80-1 69

Figure 3-21 Hysteresis curves (1) Pretension load=60kN, A36 (2) Pretension load=80kN, A36 (3) Pretension load=100kN, A36 (4) Pretension load=80kN, A572 70

Figure 3-22 Skeleton curves of P100-1, P80-1 and P60-1 71

Figure 3-23 Skeleton curves of P80-1 and P80-2 72

Figure 3-24 Stiffness degradation curves of P60-1, P80-1 and P100-1 73

Figure 3-25 Stiffness degradation curves of P80-1 and P80-2 74

Figure 3-26 Cumulative energy dissipation 75

Figure 4-1 Proposed four-stage Multi-Linear Hysteresis Model 78

Figure 4-2 Hysteresis behavior of the DFED-BCC in each stage 78

Figure 4-3 Working mechanism in elastic stage 79

Figure 4-4 Working mechanism in localized yielding stage 81

Figure 4-5 Working mechanism in frictional sliding stage 82

Figure 4-6 Parameters of rotational stiffness 83

Figure 4-7 Parameters of stiffness 84

Figure 4-8 Working mechanism in prying-induced plastic stage 85

List of Tables

Table 1-1 Four typical connection types between key parts in dry connections..... 11

Table 1-2 Advantages and disadvantages for typical types of connections between joints and concrete components 12

Table 3-1 Parameters for the steel components in DFED-BCC 45

Table 3-2 Test matrix 47

Table 3-3 Material properties 52

Table 4-1 Comparison of FEA result and Kishi and Chen's model 80

Chapter 1 Research background

1.1 Research background

Reinforced concrete (RC) has been a widely utilized composite material for decades, known for its superior mechanical and fire-resistant performance, adaptability, wide availability, and cost-effectiveness. However, the construction of RC structures through traditional on-site methods is significantly influenced by environmental conditions, workforce variability, and other external factors, which can compromise construction quality and efficiency. Additionally, on-site construction generates considerable pollution and waste, leading to resource inefficiencies and disruptions for surrounding communities. Moreover, the production of cement, a primary component of concrete, is a high-emission process that contributes substantially to greenhouse gas (GHG) emissions and embodied energy in newly constructed RC structures. These challenges have heightened concerns about the environmental sustainability and construction efficiency of traditional RC systems. As a result, the construction industry is transitioning from traditional energy-intensive practices to more efficient, cost-effective, and sustainable approaches.

In this context, the adoption of precast concrete (PC) systems has garnered significant attention as a promising alternative to traditional RC structures. PC systems offer several advantages, including the ability to expedite construction schedules, enhance site management, and minimize both costs and material waste [1–3]. Unlike traditional on-site construction, PC systems involve the production of structural components in a controlled factory environment. These components are then transported to the construction site for assembly, allowing for consistent quality control, reduced material waste, and higher precision. Furthermore, PC systems mitigate many of the risks associated with on-site construction, including errors arising from variable conditions or unskilled labor. This not only improves construction efficiency but also enhances the overall safety and reliability of the structure. Additionally, in PC elements, shrinkage and creep primarily occur before installation, which can significantly reduce in-service stresses and improve long-term performance [4]. These advantages underscore the potential of PC systems as a technically robust and efficient alternative to traditional RC

systems, offering substantial contributions to the advancement of resilient urban infrastructure and the realization of sustainable construction objectives.

Figure 1-1 Precast Concrete Systems: Factory Fabrication and On-Site Assembly

1.2 Connections in PC system

As defined in *ACI 550.2R-13*, PC connections are categorized into two primary types, which are wet and dry connections. For enhanced granularity, a tripartite classification system is often adopted, encompassing wet, hybrid, and dry connections.

1.2.1 Wet connections in PC system

Wet connections, alternatively termed emulative connections, constitute the predominant jointing method in contemporary PC systems. These interfaces integrate precast elements via grout-filled sleeves, welded reinforcement, or lap splices, requiring in-situ concrete placement or grout injection to bridge component gaps. Post-curing, the system attains monolithic behavior, structurally homogenizing discrete elements into a unified load-resisting mechanism. Empirical studies confirm that properly designed wet connections achieve mechanical equivalence to cast-in-place (CIP) monolithic systems [5]. Recent advancements leverage high-performance cementitious materials—including engineered cementitious composites (ECC) and ultra-high-performance concrete (UHPC)—to augment connection durability, strength, and energy dissipation capacity.

1.2.2 Challenges of wet connections

Despite their proven seismic reliability, wet connections present three critical constraints:

- Irreversible structural integrity loss due to post-curing monolithic behavior, leading to limited damage control and reconfigurability.
- Constructability challenges, including construction efficiency, cost, and practical limitations.
- Sustainability concerns, particularly structural demolition triggered by non-structural demands such as functional upgrades.

(1) Irreversible structural integrity

The capacity design philosophy is a methodical approach to controlling post-elastic behavior by enforcing a strong-column, weak-beam hierarchy, effectively preventing undesirable mechanisms such as soft-story failures and confining plastic hinge formation to designated zones. In RC frames, plastic hinges are typically designed at beam ends, while base columns may serve as secondary energy-dissipating regions in specific cases. All other components are provided with sufficient over-strength to remain elastic during seismic events. Plastic hinge zones are meticulously detailed to ensure they possess adequate ductility and energy dissipation capacity after yielding, achieved through optimized reinforcement detailing and confinement.

The capacity design philosophy has been widely validated as a reliable approach for seismic design, effectively preventing structural collapse in numerous recent earthquakes. However, post-earthquake assessments have consistently revealed limitations of this method [6]. The concentration of energy dissipation with plastic hinge zone, resulting extensive and localized structural damage. These dispersive damages lead to substantial economic losses due to prolonged downtime, high repair costs, or deconstruction of affected structures.

To address these challenges, and better control and limit structural damage, the Performance Based Seismic Design (PBSD) method was proposed by the SEAOC Vision 2000 Committee. PBSD establishes higher and more predictable and reliable performance objectives across varying levels of seismic hazards. Unlike force-based design, PBSD explicitly characterizes performance levels through displacement and drift, since it revealed that displacement is more critical than strength in inelastic system. By incorporating nonlinear analysis and considering

the cyclic loading effects and inelastic behavior of RC structure, PBSD provides a more robust and realistic framework for risk assessment and structural design. It allows the realization of specific performance objectives, minimizing post-earthquake repair demands while ensuring resilience and functionality across varying seismic intensities.

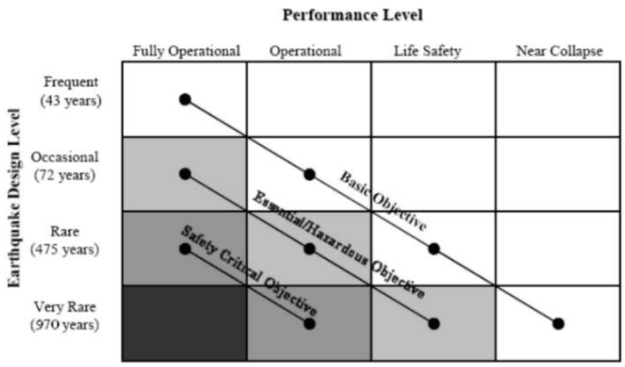

Figure 1-2 The Performance Based Seismic Design (PBSD) method

Wet connections in PC systems can be designed using PBSD method, adapting different seismic conditions by different performance objectives. However, when wet connections are cured, they act as monolithic connections, exhibiting behavior similar to CIP structures. While beam ends are deliberately designed as plastic hinge zones to dissipate energy during seismic loading, this mechanism presents two significant challenges, namely beam elongation and widespread damage dispersion [7].

First, beam elongation occurs due to residual plastic deformation of tensile steel reinforcement and the geometric effects of beam rotation about its neutral axis in finite-depth beams [8]. This phenomenon induces significant axial forces in the beam, activates slab reinforcement, and propagates damage to adjacent slabs, compromising diaphragm action and overall structural integrity [7]. Second, under large displacements, reinforcement yielding and extensive concrete cracking lead to concentrated damage in critical components, including beams, columns, slabs, and their connections. These components, which are integral to the structural system, are typically non-replaceable, and the damage is often interconnected and widespread.

The monolithic continuity of cured wet connections couples beams elongation and damage dispersion, amplifying their combined effects during seismic events. Beam elongation, induced by residual plastic strain in tensile reinforcement, generates axial thrust forces that propagate

cracking to adjacent slabs, while cyclic displacements precipitate widespread yielding in critical components including beams, columns and joints. The severe damage, concentrated in non-replaceable and structurally integral elements, leads to high repair costs. Under high-intensity seismic demands, the interconnected nature of such damage may necessitate partial or full structural decommissioning, and as a result, these failure mechanisms directly contradict the PBSD objectives of controlled damage propagation, cost-effective repairability, and post-earthquake functional resilience.

(2) Constructability

The construction of wet connections necessitates a significant amount of formwork and extensive on-site work, leading to prolonged curing times. Additionally, due to the demand for on-site construction, temporary support or other auxiliary equipment may be required. Furthermore, challenges arise from the concentration of inelastic rotations at the interface and the shear transfer capacity between the newly cast and existing concrete surfaces [9], which are critical to ensuring the structural integrity and long-term performance of the connection.

(3) Sustainability

Engineering practice and research have long recognized structural decommissioning as a critical challenge in RC systems, with conventional demolition processes generating substantial construction and demolition waste (CDW). As previously analyzed, the monolithic nature of cured wet connections fundamentally restricts structural adaptability and reconfigurability. Empirical data reveal a global discrepancy between actual building service lifespans and design lifespans, predominantly driven by functional obsolescence and economic viability rather than structural inadequacies [10,11]. For instance, preliminary surveys in China indicate an average building lifespan of approximately 30 years, with rural residential structures exhibiting even shorter lifespans of 15 years [12]. This trend underscores systemic underutilization of structural capacity, suggesting that modular connection systems could enable component reuse and significantly reduce material waste.

Concurrently, the construction sector faces dual pressures, namely burgeoning demand for new infrastructure in rapidly urbanizing economies, and escalating maintenance/retrofit requirements in aging built environments [13]. This is compounded by impending resource scarcity, as critical concrete constituents, e.g., high-quality sand, limestone, face diminishing availability due to geological and regulatory constraints [14]. When coupled with the carbon-intensive nature of cement production, these factors necessitate urgent adoption of circular construction paradigms.

Within this context, wet connections exhibit inherent incompatibility with sustainable development goals. The irreversible monolithic behavior precludes disassembly-for-reuse strategies, contradicting the precast industry's evolving needs for modularity, material circularity, and life-cycle adaptability. The systemic limitation underscores the imperative to develop dry-jointed or demountable connection systems that align with circular economic principles.

1.2.3 Dry connections in PC system

Demountable concrete structures were first introduced by Reinhardt in 1976 [15], conducting extensive research aimed at developing innovative demountable connection solutions and assessing their performance under various loading conditions. In PC systems, connections typically include beam-to-column connections, column-to-foundation connections, and slab-to-beam connections, among others. To ensure the disassembly and reusability required for a demountable structure, all connections play a critical role. However, among these, beam-to-column connections are widely regarded as the most critical in precast skeletal frames for several reasons. Firstly, beam-to-column connections are fundamental to the overall stability of precast skeletal frames. They are crucial for load transfer and have a direct influence on the deformation characteristics and stability of the frame [16,17]. Secondly, these connections govern the flexural behavior of beams and play a pivotal role in determining the location of plastic hinge zones, which control the yielding mechanism of the frame. The positioning of these plastic hinges significantly affects the load distribution and failure modes of the structural system. Furthermore, as the primary locations for energy dissipation and load transfer, the

performance of beam-to-column connections significantly impacts the global seismic response and overall robustness of the frame.

Despite their critical importance, the design and construction of beam-to-column connections remain particularly challenging. Spatial constraints imposed by surrounding structural elements, such as columns and slabs, and the inherent complexity of the construction process often complicate their implementation. As a result, the industrial application of dry connections has been limited, with notable examples such as the solutions developed by the Piekko Group. Nevertheless, numerous ongoing studies are based on these products, aiming to refine and further improve their performance and applicability.

This limited adoption can be attributed to several factors. Chief among these is the absence of a standardized classification for dry connections and the lack of systematic studies that comprehensively evaluate their structural behavior and load-carrying capacity. Furthermore, much of the existing research focuses on designing connections for highly specific scenarios, often resulting in solutions that are unsuitable for a broad range of beam and column dimensions and shapes. The development and wider implementation of dry connections are further hindered by the absence of specific design codes and guidelines, leaving practitioners without clear directives for their use.

1.3 Dry beam-to-column connections

Although the adoption of PC system has introduced greater flexibility in structural design and construction, the connections between precast elements, particularly beam-to-column, remain a critical challenge in PC system. Destruction of beam-to-column connections is regarded as one of the primary reasons for structural damage [18,19]. This issue is further exacerbated by the fact that, compared to traditional RC structures, PC structures are inherently more sensitive to seismic loads due to their segmented construction and reliance on connections [20].

This section presents a systematic state-of-the-art review of dry connection technologies, with particular emphasis on the structural classification and functional characteristics. Special attention is devoted to externally mounted metallic damper systems integrated with moment-resisting frames, which exhibit superior energy dissipation performance through controlled

yielding mechanisms.

1.3.1 Definition of connection and joint

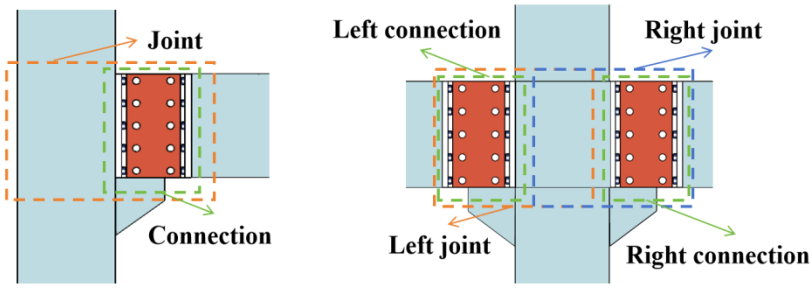

Figure 1-3 Definition of a 'joint' and 'connection'

The performance characteristics discussed above are fundamentally governed by the interaction mechanisms between structural joints and their constituent connections. To establish precise technical terminology for subsequent analysis, Fig. 1-3 provides critical definitions differentiating these key concepts. A 'connection' refers to the set of physical components that mechanically secure elements together; in this context, it includes the embedded bolts within the beam and column, as well as the friction damper. A 'joint', however, encompasses not only the connection itself but also the interaction zone between the connected members, including the configuration of reinforcement and the anchorage of embedded bolts within the concrete.

1.3.2 Multilevel classification system for dry connection design objectives

Current design objectives for dry connections are hierarchically categorized into four levels:

[Level I] Construction simplicity: it prioritizes rapid assembly with minimal onsite operations.

[Level II] Demountability & Performance optimization: it emphasizes reversible configurations and load-path refinement.

[Level III] Damage control & Component replaceability: it focuses on concentrating damage on replaceable components and modular repair capacity.

[Level IV] Reusability: it aims to maximize the reuse of structural components through

standardized design, intelligent tracking systems, and optimized allocation strategies.

This study specifically examines dry connections applicable to moment-resisting frames. First, it can be classified into two principal groups based on self-centering capacity:

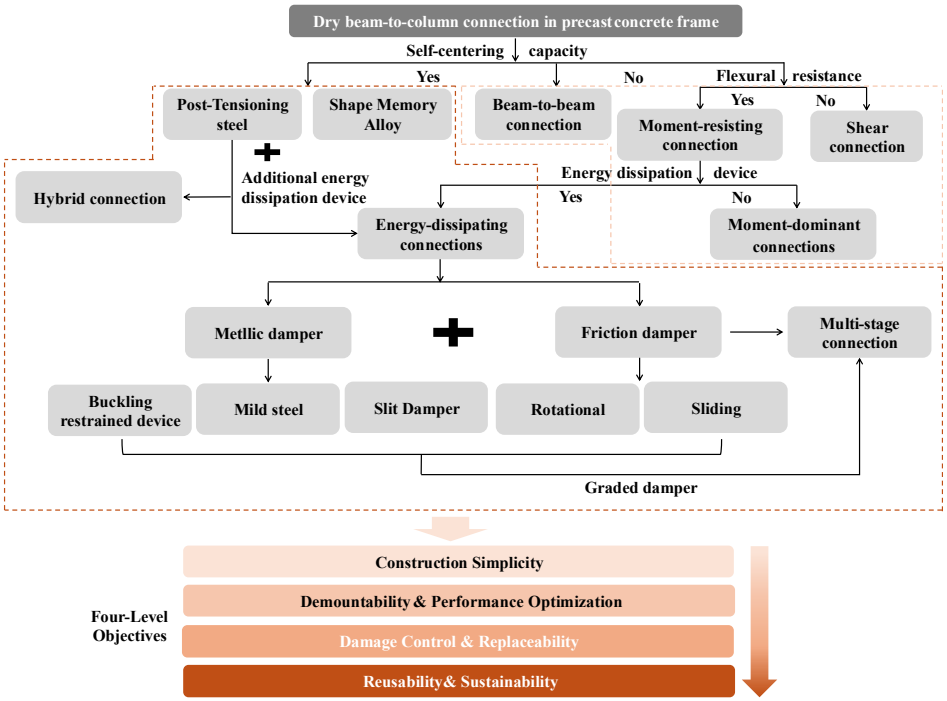

Figure 1-4 Classification framework of dry connections

(1) Self-centering systems:

Utilizing post-tensioned (PT) steel or shape memory alloy (SMA) to achieve elastic recentering. These systems typically require supplemental energy dissipators like friction dampers, mild steel yielding elements to achieve targeted energy dissipation capacity. Although PT strands traverse beam-column interfaces, such connections remain classified as 'dry' due to the replaceable nature of their energy dissipation components which are replaceable.

(2) Non-self-centering systems

It can be subdivided into:

- Basic mechanical connections employing bolted couplers or embedded steel plates targeting level I or II objectives. Their seismic performance parallels conventional monolithic connections, with irreversible damage concentrated in concrete regions and embedded reinforcement.

- Enhanced dissipative connections integrating dedicated damping devices like buckling-restrained devices, friction dampers, mild steel components to achieve level III objectives. Advanced configurations employ staged activation mechanisms where different dampers engage sequentially under increasing drift demands.

Fig. 1-4 systematically maps this classification framework, highlighting functional evolution from basic connectivity to advanced damage-controllable systems. The subsequent sections will systematically examine each connection typology through methodically categorized analyses of their (a) structural composition, (b) functional mechanisms and (c) seismic performance.

1.3.3 Connections for moment resisting frame

As discussed in ***Section 1.3.2***, several dowel connections [21–23] have been developed for PC frames, though they are not primarily designed for moment-resisting frames. Therefore, dowel connections are not the primary focus of this study. Moreover, while this study does not specifically target prestressed frames, research initiatives such as the PRESSS program cannot be overlooked due to their relevance. Consequently, this section provides a comprehensive literature review on dry connections for conventional moment-resisting frames, while also incorporating selected design approaches for prestressed frames that offer valuable insights.

This section consists of two parts:

1. **Typical Connection Types** – A discussion on the common types of dry connections between beams, columns, and joints from a construction perspective.

2. **Review of Dry Connections** – An evaluation of selected dry connection designs and their structural performance.

Table 1-1 Four typical connection types between key parts in dry connections

Type I		Type II		Type III		Type IV	
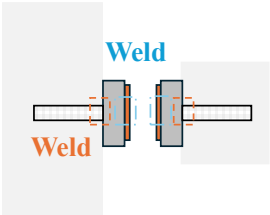 Column zone Beam zone		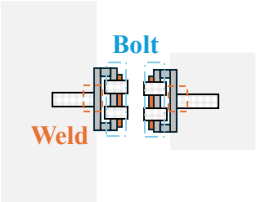 Column zone Beam zone		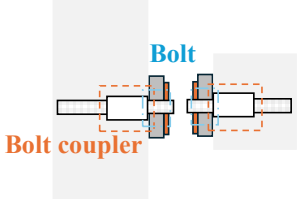 Column zone Beam zone		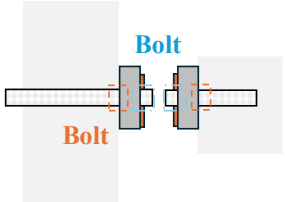 Column zone Beam zone	
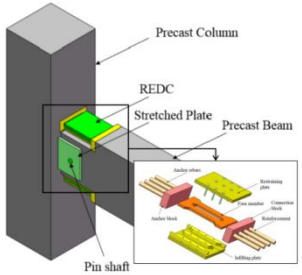	[24]	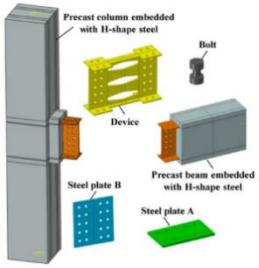	[25]	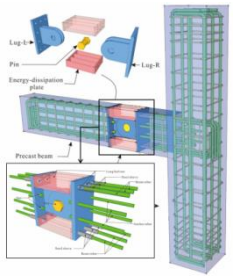	[26]	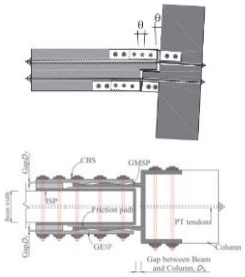	[27]
		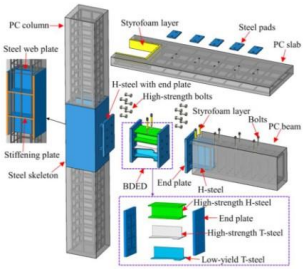	[28]	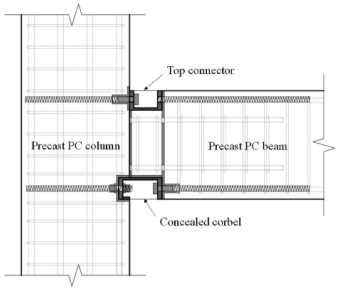	[29]	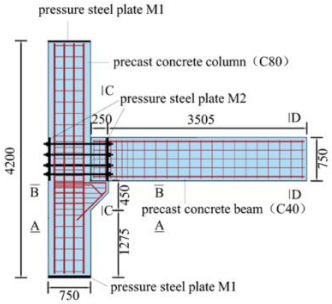	[20]

Table 1-2 Advantages and disadvantages for typical types of connections between joints and concrete components

Types	Advantages	Disadvantages
Type I	**(1) High Structural Integrity**: Ensures continuous load transfer, enhancing overall stability and strength. **(2) Improved Durability**: Resistant to corrosion and loosening overtime, ensuring long-term performance.	**(1) Requires Skilled Labor and On-Site Welding**: Involves high labor costs and is time-consuming, increasing overall construction complexity. **(2) Thermal Effects in Welded Joints**: May introduce residual stresses and material distortions, potentially affecting structural performance.
Type II	**(1) Simplified On-Site Assembly**: Requires only bolt tightening, making construction efficient and timesaving. **(2) Minimal Space Constraints**: Suitable for compact or restricted installation environments.	**(1) High Material Usage**: Requires a large amount of steel components, leading to additional costs. **(2) Transportation Challenges**: Protruding steel components may complicate handling and increase logistical difficulties.
Type III	**(1) Reduces Bolt Shear**: The coupler acts as an extension, minimizing shear forces on individual bolts and enhancing durability. **(2) Enhanced Load Transfer**: The bolt coupler connects two threaded rods, creating a continuous force path like welded connections.	**(1) High Precision Requirements**: Space constraints and the accuracy needed for bolt couplers demand greater precision construction during installation.
Type IV	**(1) High Stiffness & Load Transfer**: Bolt preloading forces eliminate slip, ensuring direct force transfer through friction and reducing the risk of loosening.	**(1) Expensive Equipment**: Requires high-strength bolts and specialized tension tools, increasing initial costs. Additionally, bolt preloading forces loss necessitates regular inspections and maintenance. **(2) Bolt Congestion in Interior Joints**: Through-bolts may lead to crowding issues at internal connection points, complicating assembly and alignment.

Typical Connection Types

As both precast beams and columns lose their removability after curing, their connections to the dry joint are generally designed in a similar way. Table 1-1 illustrates four typical connection types between key parts in dry connections, where the orange sections indicate the interfaces between the concrete components (beam and column) and the dry joint, while the blue sections represent the internal connections within the joint. Table 1-2 provides a detailed description of the advantages and disadvantages of each type.

Review of Dry Connections

1. Steel-Structure-Inspired Moment Connections

Steel-structure-inspired moment connections typically adopt configurations like those widely used in steel structures, such as welded joints and bolted connections, including end plates, flange plates, and cleats. This design approach emphasizes reliable load transfer mechanisms, ensuring consistent and predictable structural performance under various loading conditions. Furthermore, their seismic performance shares similarities with connections in steel structures, making it possible to refer to relevant codes and guidelines for design.

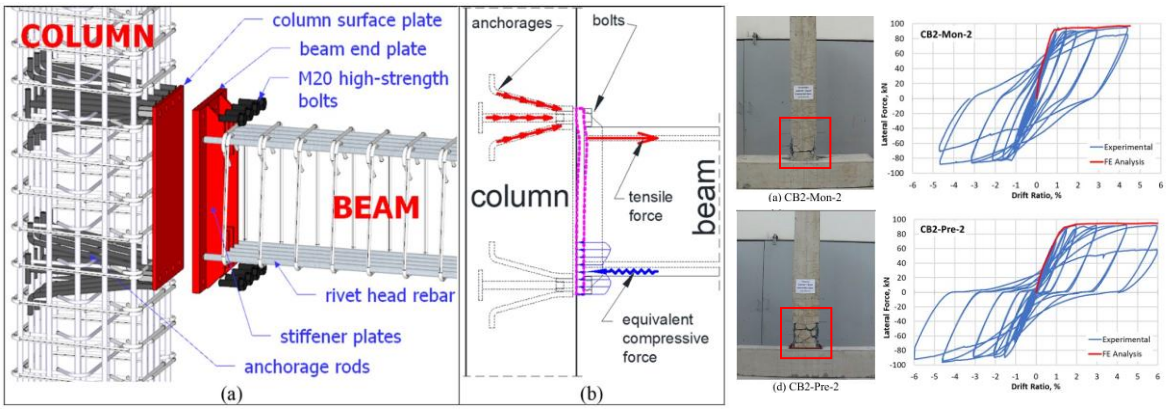

Configuration | Load transfer path | Failure mode and hysteresis behavior

Figure 1-5 Endplate-Inspired Connection

It is worth noting that connections between concrete components and joints significantly impact various performance characteristics [30], like initial stiffness. Therefore, their design must undergo rigorous evaluation and scrutiny to ensure structural reliability.

The connection illustrated in Fig 1-5 resembles the end-plate connection commonly used in steel structures, simulating monolithic behavior. The results indicate that monolithic specimens primarily failed due to shear failure at the panel zone following initial flexural failure, with failure drift ratios ranging from 3% to 4.5%. Precast connections exhibited higher energy dissipation, shear failure at the plastic hinge zone, delayed yielding, and superior drift capacity of up to 6%, demonstrating enhanced ductility. This improvement is attributed to the increased shear strength offered by the anchorage system and column surface plates. [31] However, the extended endplate may pose challenges for slab installations.

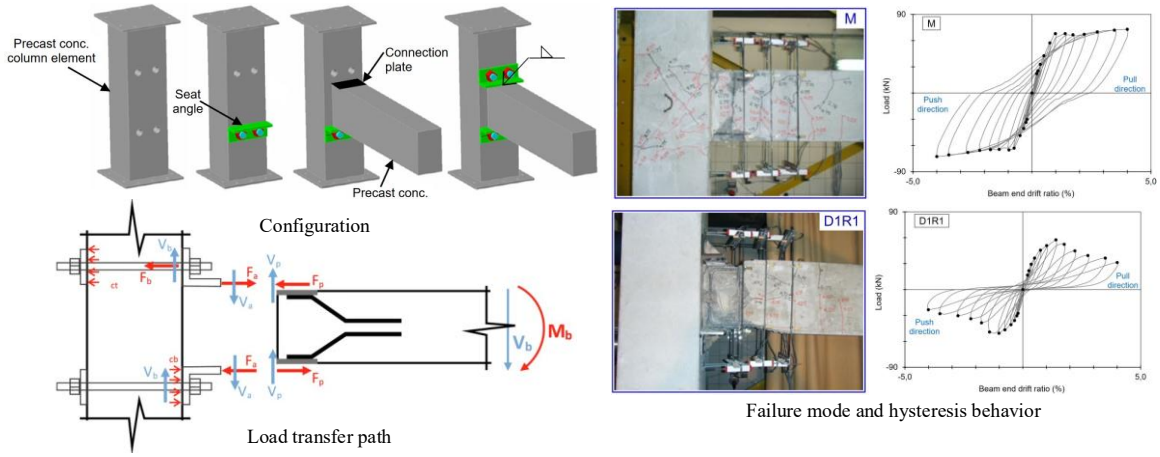

Figure 1-6 Flange cleats-Inspired Connection

The connection shown in Fig. 1-6 resembles flange cleats, where force transfer between beam and column elements is achieved via steel plates anchored in the beam and steel angles attached to the column. Results show that increasing anchor bolts and stiffeners enhances the connection's strength and stiffness. While the connection exhibited high drift capacity with localized damage in the beam and steel components, its energy dissipation was limited due to severe pinching in the hysteresis curve, likely caused by slippage or increased deformation after steel yielding. [30]

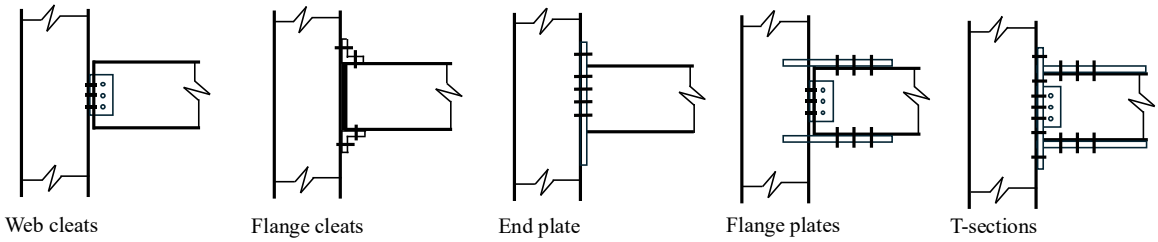

Figure 1-7 Normal bolted connections in steel structure

2. Energy-dissipating connections

Several studies have proposed the integration of dampers at beam ends, serving a dual purpose as both structural connectors and energy dissipation devices. These connections fundamentally rely on energy dissipation through rocking motion mechanisms at the beam-column interface. In this context, rocking motion enables controlled relative rotation and separation between the beam and column, allowing energy to be dissipated through the plastic deformation of metallic components or frictional sliding at the interface[7].

(1) NIST research program

The research program, initiated by the National Institute of Standards and Technology (NIST) in 1987, aimed to evaluate and enhance the seismic performance of precast beam-to-column connections. In Phase I, the program compared the seismic behavior of monolithic and grouted post-tensioned precast specimens. The findings revealed that while both types exhibited similar failure modes, the post-tensioned precast specimens demonstrated superior strength and ductility. However, they dissipated only 30% of the energy per cycle and achieved 80% of the cumulative energy dissipation of the monolithic specimens prior to failure [32]. Phases II and III focused on enhancing energy dissipation by adopting prestressing strands and optimizing the location of post-tensioning steel. These modifications resulted in improved energy dissipation, achieving levels comparable to monolithic connections due to the increased ductility of the precast specimens [33]. In Phase IV, mild steel reinforcement was introduced alongside post-tensioning steel to function as an energy-dissipating element, while the post-tensioning system maintained self-centering behavior. The hybrid system demonstrated enhanced seismic performance, including increased moment capacity, drift capacity, and

energy dissipation [34].

The results of the research program demonstrated the feasibility of hybrid systems that combine external energy dissipation devices with PT steel. However, critical issues such as the additional effects caused by beam elongation [7] and construction constraints imposed by floor slabs remained inadequately addressed.

(2) PRESSS research program

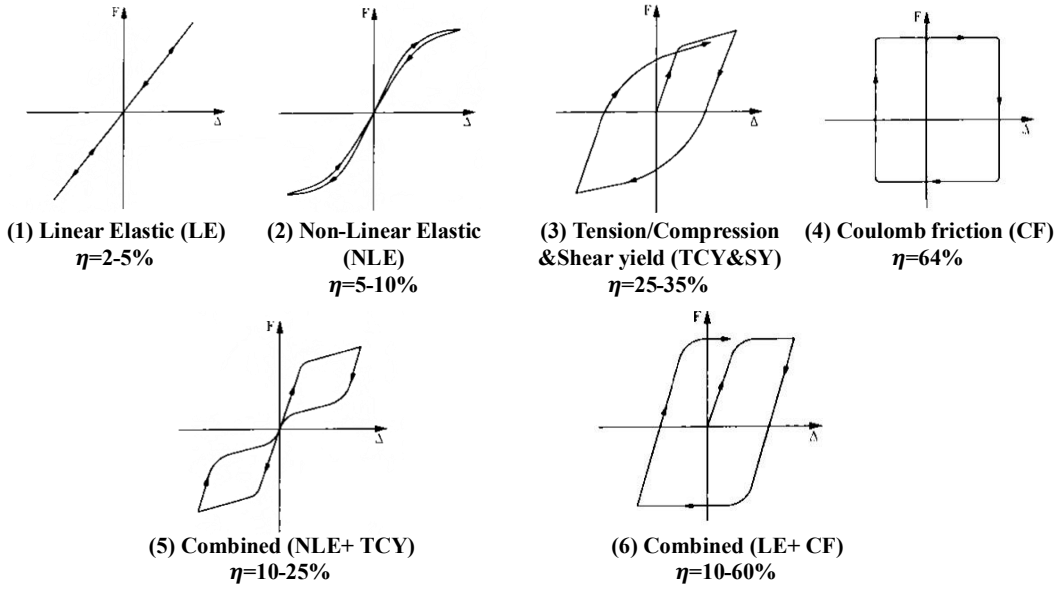

Figure 1-8 Hysteretic characteristics for generic PRESSS connection systems [35]

Similar to the research program conducted by NIST, the PRESSS program, jointly led by the United States and Japan, focused on evaluating various precast concrete connection systems and integrated structural systems for seismic resistance. During the second phase of the program, multiple connection systems were examined, including non-linear elastic (NLE) systems, tension-compression yield (TCY) systems, shear yield (SY) systems, energy-dissipating/Coulomb friction (CF) systems, and hybrid systems. The distinct hysteretic behaviors of these connection types, along with their corresponding equivalent viscous damping ratios, were systematically documented and analyzed [35].

Connections designed based on these systems were systematically tested and analyzed, providing valuable insights into their seismic performance. Among them, Specimens UT-GAP

and UMn-GAP incorporated a reserved gap at the beam-to-column interface, marking the initial development of the ‘slotted beam’ concept [7]. These gaps localized rotational demands and facilitated controlled plastic deformation at the interface, effectively minimizing geometric beam elongation under seismic loading. Both specimens exhibited satisfactory performance, sustaining drift ratios of up to 2.5% and 2%, respectively [36].

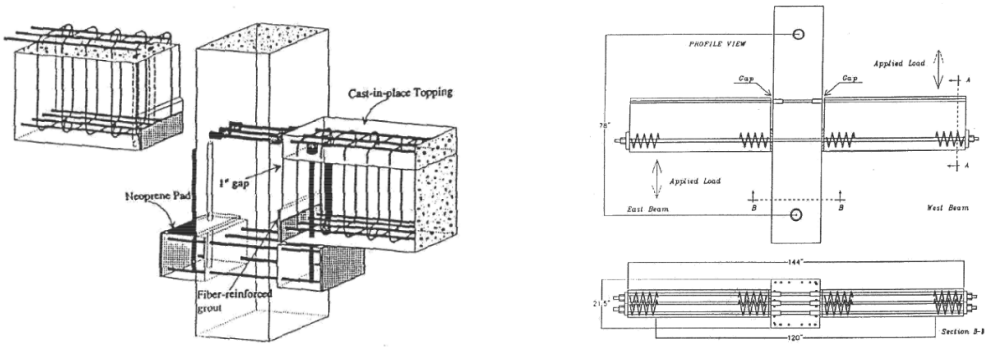

Specimen UT-GAP [36]　　Specimen UMn-GAP [36]

Figure 1-9 Specimens for the ‘Slotted Beam’ Concept in the PRESSS Research Program

Specimen UT-FR employed a friction damper mechanism by enabling sliding along clamped plate surfaces [35]. This approach also effectively mitigated the ‘beam elongation’ phenomenon, demonstrating enhanced strength, high energy dissipation capacity, and repeatable hysteretic behavior up to a drift ratio of 3% under cyclic loading.

Phase III of this program focused on evaluating the seismic behavior of precast frames, emphasizing their structural performance under seismic loading. The five-story PRESSS precast test building demonstrated excellent recentering capability, with the prestressed frame sustaining minimal damage and negligible residual displacement even under seismic intensity twice the design level. In contrast, the tension-compression yielding (TC-Y) frame exhibited higher damping and greater residual displacements, with more extensive damage observed beyond the design-level excitation [37].

The PRESSS program provided a wide range of investigation of connection systems in PC structure, leading the development of dry connections. Especially, the ‘slotted beam’ and ‘sliding effect’ provide two possible solutions to relief ‘beam elongation’ phenomena, reducing

the corresponding deterioration mechanism to protect components. However, this program lacks detailed investigation into the specific mechanisms of individual systems. Additionally, certain connection designs exhibit construction complexity, which may limit their practical application.

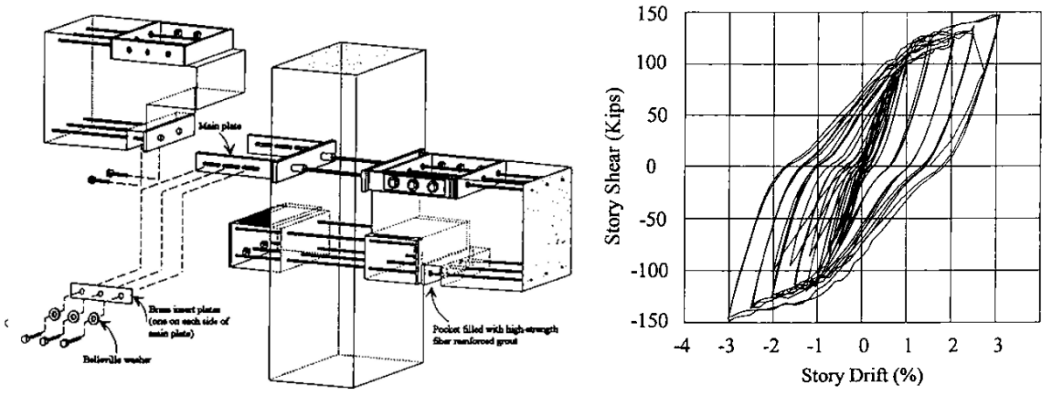

Figure 1-10 Specimen UT-FR and story shear-drift response [35]

(3) Metallic damper

Xie et al. [24,38] proposed a replaceable energy dissipation connector derived from buckling restrained brace (BRB) and testing both connector and beam-to-column connections, exploring the hysteresis behavior of them. The results showed that this kind of connection has a stable and full hysteresis curve, which indicates good energy dissipation behavior. The failure mode is the fracture of the yielding section of energy dissipation steel plate. Beam and column remain elastic after cyclic loading, indicating recovery potential.

Zhang et al. [29] introduced an innovative connector design comprising open slots, high-strength bolts, and screw sleeve. The bottom connector also serves as a concealed corbel, facilitating shear transfer and simplifying the construction process. Experimental results demonstrated that the precast connection achieved 60% of the initial stiffness of the monolithic connection and maintained comparable stiffness beyond a 1% drift ratio. However, due to the high yield strength of Q345 steel used in the connector, the energy dissipation capacity was only 50% of the monolithic counterpart. Subsequently, Zhang et al. [39] proposed an enhanced connection by incorporating longitudinal ribs made of Q235 steel as energy dissipation elements. This improved connection was applied to the entire frame system and evaluated

through shaking table tests. The results showed that the structures remained essentially elastic under frequent earthquakes (0.07g), experienced minor beam damage during fortification-level earthquakes (0.2g), and exhibited concentrated beam damage under rare earthquakes (0.4g), thereby satisfying the specified performance objectives across different seismic intensity levels.

Huang et al. [26,40] developed a replaceable artificial controllable plastic hinge (APFH) featuring a high-strength pin connection as the rotation point and Q235B steel energy dissipation plates as auxiliary energy dissipation devices. Two 1/2-scale precast frames incorporating APFH in beams and grouted sleeve connections in columns were tested and compared with a cast-in-place frame. The results demonstrated that the APFH frame exhibited a beam-hinge failure mode, effectively delaying column plastic hinge formation. Additionally, the APFH frame showed significantly improved ductility and energy dissipation capacity compared to the cast-in-place frame.

(4) Friction damper

Beam-to-column connections incorporating friction dampers have been designed for both precast and precast prestressed concrete frames. In prestressed concrete frames, friction dampers are typically used alongside PT steel to enhance energy dissipation. Song et al. [41,42] developed a self-centering prestressed concrete frame incorporating a welded web friction device, followed by an enhanced bolted web friction damper configuration. The results indicated that the connection exhibited a combined hysteretic response characterized by non-linear elastic (NLE) behavior and Coulomb friction (CF), with the post-tensioned steel contributing to the primary moment capacity while the friction damper provided effective energy dissipation. A minor residual displacement of 2 mm was recorded at the beam end after cyclic loading, with no visible damage to the bolts or steel plates, highlighting the connection's excellent self-centering capability. Additionally, negligible performance differences were observed between aluminum and brass friction plates, indicating both materials are viable as friction pads. Huang et al. [27,43] proposed an innovative self-centering precast concrete (SCPC) beam-to-column connection combining variable friction dampers (VFDs) with grooved steel plates and hidden corbels (HCs) to improve energy dissipation, post-yield

stiffness, and shear transfer. By linking connection behavior to key performance objectives (POs), the study demonstrated staged energy dissipation and stiffness modulation, with theoretical and experimental moment comparisons, offering valuable insights for performance-based seismic design.

In precast concrete frames, friction dampers are widely considered due to their stable energy dissipation capabilities and minimal residual deformations, which contribute to maintaining structural integrity. Qi et al. [44] and Zeng et al. [45] proposed friction energy-dissipating precast beam-to-column connections using pre-embedded steel components, effectively transforming the traditional concrete interface into a steel-to-steel connection, thereby simplifying both design and construction. Their results indicated that connections equipped with friction dampers exhibited significantly enhanced energy dissipation compared to monolithic connections and those without dampers, alongside improved ductility attributed to the controllable sliding mechanism. However, issues related to the deconstruction of embedded steel components and the connection at the central intersection warrant further investigation. Additionally, Zeng et al. [45] reported that the reduced moment capacity of the connection resulted in lower overall stiffness.

(5) Multi-stage connections

In recent years, multi-stage energy dissipation devices have gained attention for their ability to adapt to different seismic intensities, optimizing energy dissipation and failure modes based on displacement demands. This approach aligns closely with the principle of performance-based seismic design, enabling more precise control over structural behavior and providing a more economical, stable and reliable solution.

Samani et al. [46] investigated a semi-active friction damper, adjustable through hydraulic pressure to regulate pre-tightening forces in response to seismic loading. The results demonstrated that the device exhibited reliable performance, with predictable behavior and compliance with the *ASCE/SEI 41-06* specifications.

Chen et al. [47] developed an innovative multi-level energy dissipation damper incorporating

preset gaps to achieve staged yielding behavior under varying seismic intensities. The damper demonstrated stable hysteretic performance with distinct dual-yield points, enabling effective energy dissipation across different earthquake levels.

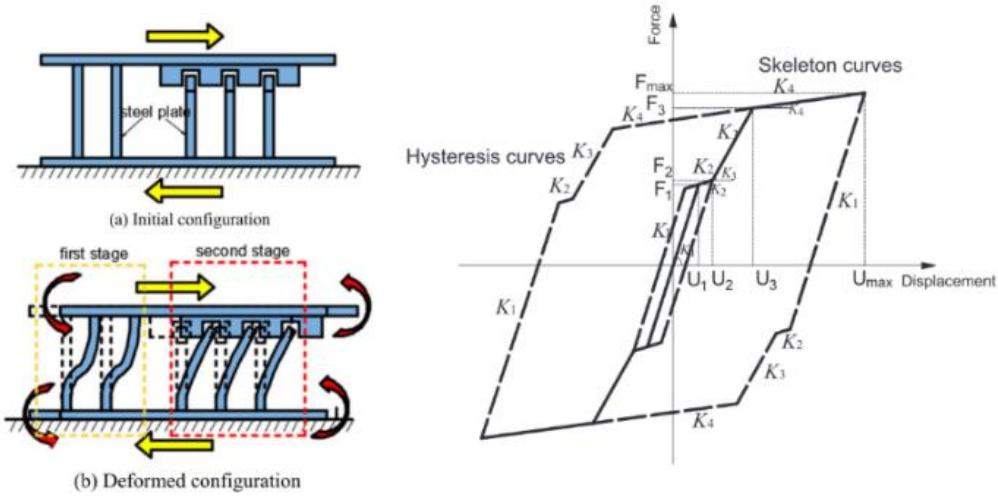

Figure 1-11 A multi-level damper mechanism induced by preset gaps

Li et al.[48] proposed a replaceable graded-yielding energy-dissipating connectors which exhibit stable hysteretic performance and two distinct yield points in the low-cycle loading tests, indicating the potential for graded yielding under varying earthquake intensities.

Xu et al. [49] developed a staged energy dissipation device integrating friction and metallic dampers to provide effective displacement control and stable energy dissipation across three distinct phases: elastic, frictional, and metallic plastic deformation. The results demonstrated a multi-phase hysteretic behavior, characterized by linear elastic (LE) response, Coulomb friction (CF) behavior, and a combined CF-metal yielding mechanism proposed in PRESSS program shown in Fig. 1-12.

Recent studies on multi-stage energy dissipation devices highlight their effectiveness in achieving displacement-controlled hysteretic behavior through graded designs of identical dampers or combinations of different damping mechanisms. However, existing research primarily focuses on the intrinsic performance of these devices, with limited investigation into their integration within structural connections or frame systems.

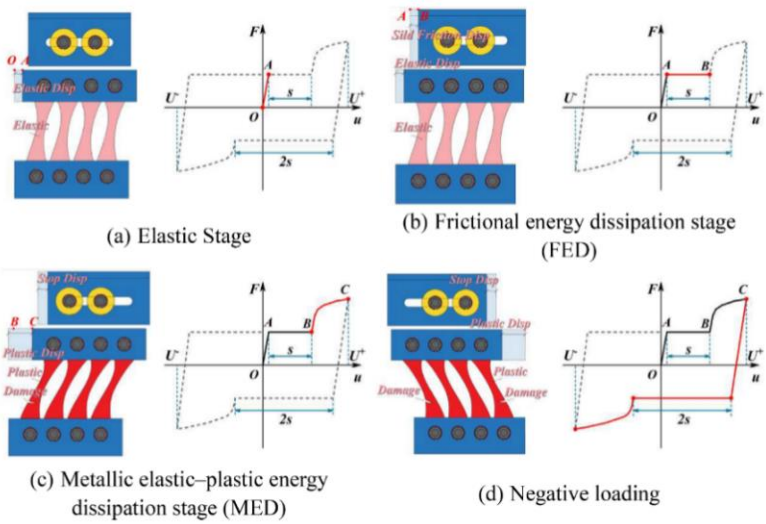

Figure 1-12 A staged energy dissipation device integrating friction and metallic dampers

In summary, metallic dampers, friction dampers, and multi-stage devices are being designed for integration into beam-to-column connections. These systems can generally be classified into four distinct shear transfer mechanisms within the connection. Fig.1-13 illustrates the composition of each system and highlights the key shear and moment transfer components.

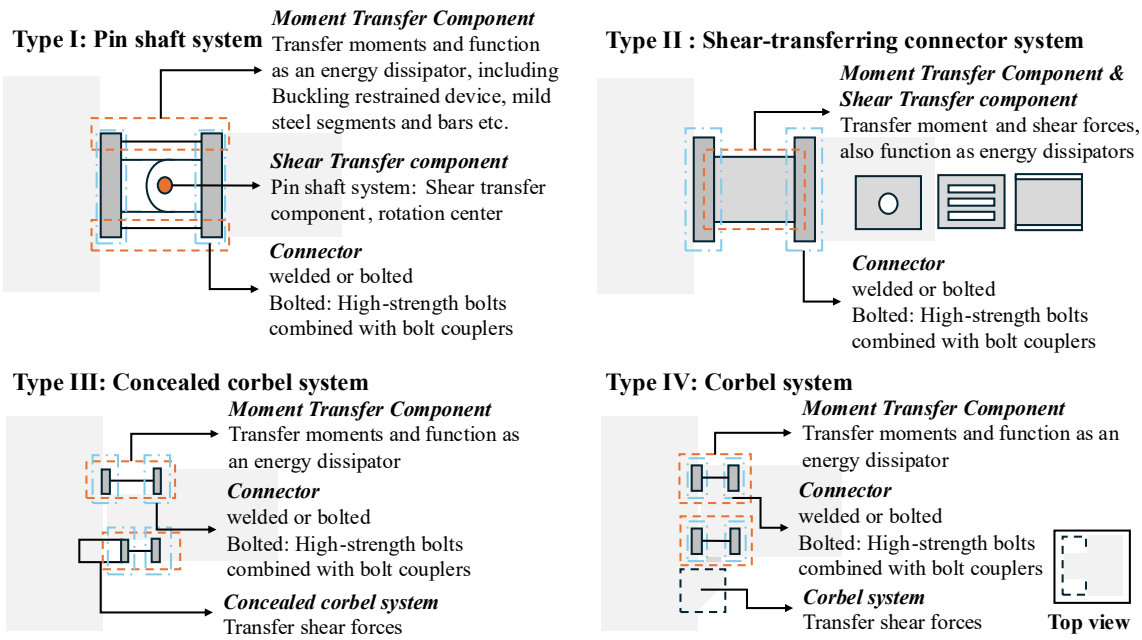

Figure 1-13 Four systems in BCC integrating energy dissipation devices

3. Modular-oriented connections

Modular-oriented connections transform traditional beam-to-column connections into beam-to-beam connections, simplifying load transfer mechanisms and reducing construction complexities.

Ersoy et al. [50] tested two types of beam-to-beam dry connections—one with side plates and one without, as shown in Fig. 1-14, and compared them with a monolithic connection. The results indicated that the connection with side plates demonstrated considerable load-carrying capacity, as well as stiffness degradation and energy dissipation behavior comparable to that of monolithic reference specimens. Additionally, the welding details between steel and reinforcement were noteworthy for further reference and optimization.

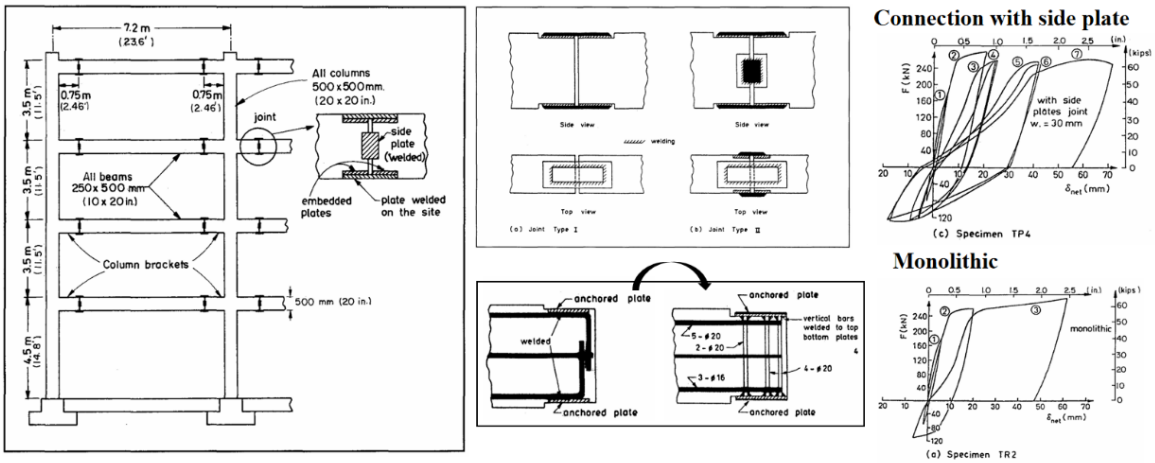

Figure 1-14 Beam-to-beam connections

Besides, beam-to-beam connections must ensure reinforcement continuity through splicing [51,52], welding [53,54], mechanical sleeves [55], or a combination of these methods[9]. However, this continuity requirement poses a challenge to achieving fully demountable connections, as it limits the ease of disassembly and reuse.

In conclusion, each type of BCC has its own advantages and limitations. From the perspective of optimizing BCC performance and achieving demountability, incorporating energy dissipation devices at the beam ends is considered an optimal approach. Currently, extensive research has been conducted on the first three systems in Fig.1-13, whereas corbel systems, despite being a common form in PC frames, have received limited attention. Therefore, this

study will focus on the investigation and design of corbel-based connections.

1.4 Aim and Objective

1.4.1 Aim

To develop and evaluate a demountable frictional energy dissipation beam-column connection for precast concrete systems, especially for column with corbel. This connection aims to enhance seismic performance by dissipating energy, controlling damage, and preserving the integrity of concrete elements and reinforcement to enable their reuse. The research will investigate the connection's theoretical working mechanisms, conduct parametric finite element analysis, and assess its feasibility for repair and reuse in comparison to monolithic connections, contributing to the advancement of sustainable and adaptive construction practices.

1.4.2 Objective

(1) Literature Review: Conduct a comprehensive and systematic review of existing dry connections in precast concrete systems, focusing on their types, working mechanisms, hysteresis behaviors, and application scenarios. Identify gaps in current research to provide a foundation for the proposed demountable connection.

(2) Conceptualization and Design: Design a demountable frictional energy dissipation beam-column connection tailored for precast concrete systems. Define its basic configuration, including bending and shear resistance measures, and detail its components, assembly procedures, and construction methodology.

(3) Theoretical Analysis: Investigate the load transfer path and staged working mechanism of the proposed connection. Develop methods for calculating staged stiffness, energy dissipation characteristics, and rotational stiffness, and propose a constitutive model to characterize its behavior.

(4) Numerical Analysis: Validate the theoretical model through numerical simulations. Analyze the connection's hysteretic behavior, energy dissipation capacity at various stages,

initial stiffness, stiffness degradation patterns, and failure modes. Conduct parametric studies to evaluate the effects of key parameters, including preload force, steel angle thickness, and material properties, on its performance.

(5) Comparison and Feasibility: Compare the seismic performance of the proposed connection with that of monolithic connections. Evaluate its feasibility for repair and reuse, emphasizing its potential advantages in reducing structural damage, waste, and environmental impact while enhancing adaptability and sustainability.

Chapter 2 Design of Demountable Frictional Energy-Dissipative Beam-to-Column connection (DFED-BCC)

2.1. Location of the connection

The strong column–weak beam philosophy aims to prioritize the formation of plastic hinges at the ends of beams rather than at columns, resulting in a beam sway mechanism. This mechanism is considered ideal for frame structures because it provides greater energy dissipation capacity and improved structural resistance under seismic loads [56]. By concentrating inelastic deformations in the beams, this approach reduces the risk of severe structural damage, as beam failure is generally localized and has less impact on the overall structural stability than column or joint failure [56]. Additionally, the beam sway mechanism enhances the feasibility of post-event repair, as the damage is confined to the beam ends [56].

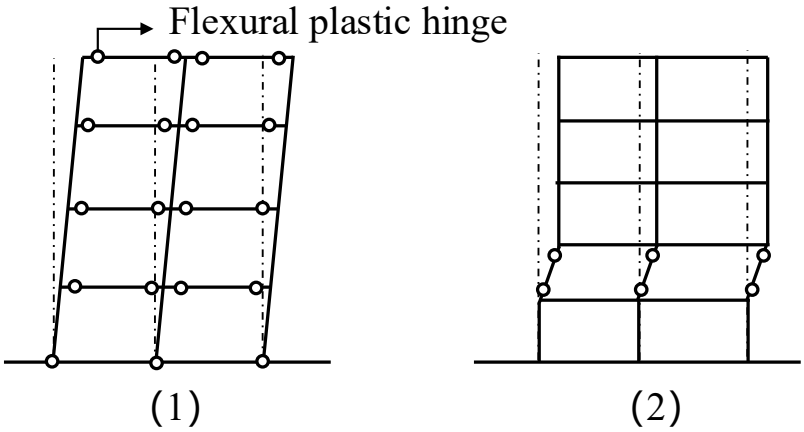

Figure 2-1 (1) Beam side sway mechanism (2) Soft storey mechanism

In current construction practices, the reinforcement in beams and columns are interconnected and cast in place to establish a continuous load transfer path. However, when beam reinforcement yields in high-stress zones, joint failure may still occur due to strain penetration extending into the joint core, even when adhering to the 'strong column-weak beam' design philosophy [57]. Initially, the tensile stress within the concrete joint exceeds its tensile strength, leading to cracking in the high-stress zones near the beam end and joint core. As seismic forces intensify, the longitudinal reinforcement in the beam yields in these high-stress regions, causing

the plastic hinge zone of the beam to extend into the joint core. This strain penetration induces slips along the reinforcement-concrete interface, progressively weakening the bond between concrete and reinforcement, compromising the joint's integrity and impairing the shear transfer mechanism across the joint core [58]. Following reinforcement yielding, the Poisson effect becomes more pronounced, resulting in radial expansion in the yielded sections. This expansion, combined with strain accumulation, further accelerates bond deterioration, increases slip, and weakens the confinement effect of concrete on the reinforcement [59]. With growing rotational demands, compressive forces on the top and bottom of the beam escalate, causing localized brittle crushing in the concrete. As concrete cracking and bond degradation progress, the confinement capacity of stirrups around the longitudinal reinforcement diminishes, impacting the stability of the reinforcement and ultimately reducing the load-bearing capacity of the joint [56].

Plastic hinge relocation strategies, particularly through localized weakening techniques, have been widely employed in steel structures to prevent damage in critical regions such as core joint areas [4]. However, in RC structures, the continuity of reinforcement within beams complicates the selective replacement or repair of damaged sections, posing significant challenges in terms of maintenance and resilience. Given these limitations, alternative connection strategies, such as dry connections incorporating damage-concentrating devices, present a promising approach to enhancing both the repairability and durability of RC joints.

The analysis of the frame's yielding mechanism suggests that an optimal location for damage-concentrating devices is at the beam end, where they can serve as protective elements for the plastic zone. These devices not only function as structural connectors but also act as energy dissipation mechanisms, mitigating damage to reinforcement and concrete components while improving overall structural performance.

As discussed in Chapter 1, damage-concentrating devices commonly include buckling-restrained devices, mild steel sections, and friction dampers. The selection of a suitable device is contingent upon multiple factors, including constructability, load transfer efficiency, seismic performance, and other structural considerations. The subsequent sections will provide a

detailed discussion on these aspects.

2.2. Constructability

As analyzed in Chapter 1, a complete connection consists of three key components, namely the column-to-joint connection, the joint itself, and the joint-to-beam connection. Common connection methods include the use of bolt couplers, embedded steel sections, among others. However, bolt couplers demand high construction accuracy, making their implementation challenging in practice, while embedded steel sections require a substantial amount of steel, leading to increased material costs. Given these considerations, the embedded bolt method emerges as an optimal solution, offering a balance between constructability, cost-effectiveness, and structural performance.

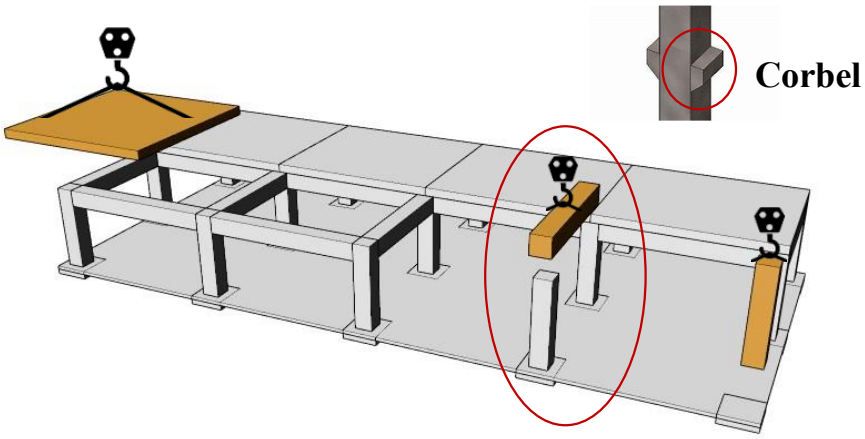

Figure 2-2 Construction of precast concrete frame

However, certain challenges arise due to the constraints imposed by the corbel and embedded bolts. As illustrated in Fig. 2-2, the typical construction sequence of a PC frame progresses from the foundation to the columns, followed by the beams [60]. This sequence necessitates the installation of beams from top to bottom, introducing specific construction challenges.

As shown in Fig. 2-3, three potential connection locations are considered. Although both type (1) and type (3) can be designed to achieve favorable structural performance potentially, the presence of bolts and the corbel significantly hinder their practical implementation. Consequently, Type (2) is selected as the optimal connection configuration, balancing constructability and performance requirements.

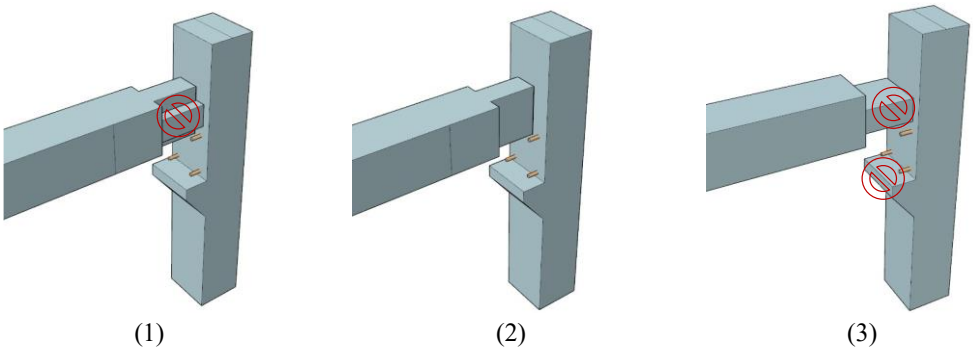

Figure 2-3 Potential connection locations

Additionally, the limited space between the column and beam necessitates the disassembly of the connection into components smaller than the available space to facilitate installation. Given these constraints, a friction damper emerges as the optimal solution, as it effectively meets the forementioned requirements while ensuring structural efficiency and constructability.

2.3. Proposed design of the connection

Building on the previous analysis, the following figure illustrates the configuration of the Demountable Frictional Energy-Dissipative Beam-to-Column Connection (DFED-BCC). Joints are typically classified by both geometric configuration and behavior, including categories such as interior and exterior joints. Here, an exterior beam-column joint is presented as a representative example, chosen for its capacity to encompass a broad range of construction challenges, such as connection sequence and spatial arrangement, offering a generalized perspective on joint design and assembly.

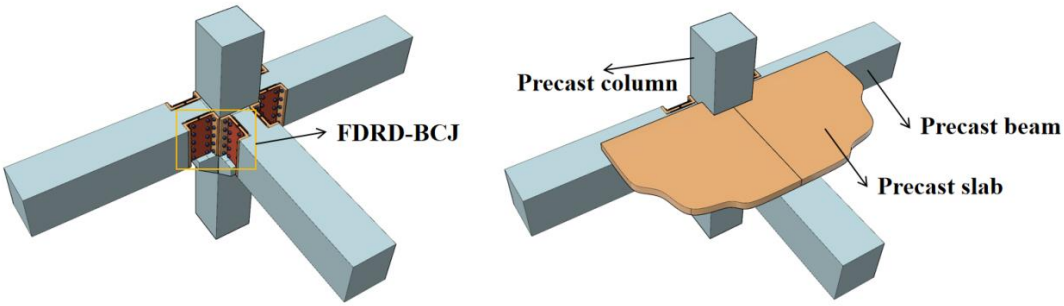

Figure 2-4 Proposed design of the connection

2.3.1. Introduction of DFED-BCC

The DFED-BCC is an innovative dry connection that integrates friction dampers, serving both as an energy dissipation mechanism and a connector. This versatile design accommodates various dimensions and shapes of precast concrete beams and columns, offering potential for broad adoption in the construction sector. The DFED-BCC is compatible with columns both with and without corbels. A corbel provides a stable construction platform, minimizing the need for additional heavy equipment and enhancing its practical accessibility.

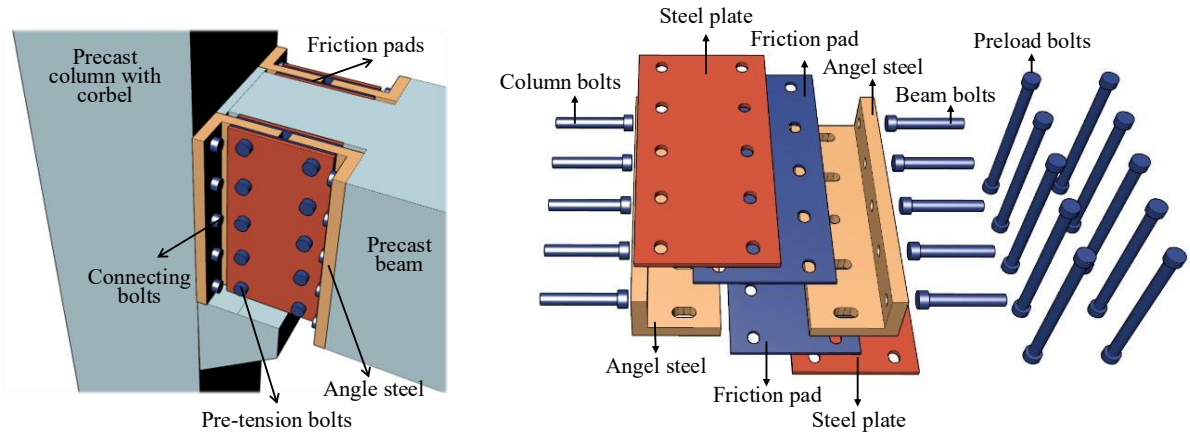

Figure 2-5 Components of DFED-BCC

The DFED-BCC consists of connecting bolts and friction dampers, as illustrated in Fig. 2-5. The embedded bolts facilitate the connections between columns, beams, and friction dampers, ensuring structural integrity and load transfer. The detachable nature of the friction dampers simplifies assembly by allowing the connection to be divided into two parts: one affixed to the column and the other to the beam.

The load capacity of the friction dampers is primarily governed by the number of friction surfaces, bolt preloading forces, and the friction coefficient of the friction pads. Consequently, the load-bearing capacity of the DFED-BCC can be readily adjusted by modifying the number of bolts, altering bolt preloading levels, or selecting different friction pad materials, providing a flexible and adaptable solution for diverse structural demands.

Moreover, the simple geometries of the steel plates and angle steels used in the DFED-BCC eliminate the need for additional water jet cutting or welding during the manufacturing process.

This streamlined production enhances cost efficiency while maintaining ease of fabrication, making the DFED-BCC a practical and economically viable connection solution.

2.3.2. Rotation point

In the DFED-BCC, the angle plates connecting to the column are designed with slotted holes for bolts to accommodate slip, except for the central bolt, which serves as the designated rotation point. This arrangement is strategically developed based on the load transfer mechanism and the behavioral characteristics of the bolts. When a moment is applied at the beam end, the slip behavior of the bolt regions above and below the rotation point exhibits symmetry. Consequently, the frictional forces generated across these regions are balanced and symmetric, ensuring that the rotation point remains free from additional unbalanced lateral effects. This configuration effectively maintains the rotation point as a neutral pivot, thereby optimizing the performance of the connection under loading conditions.

If the rotation point is positioned at the mid-height of the beam, the displacement at the beam end, denoted as Δx relative to the rotation point, is distributed symmetrically along the geometric path. This configuration reduces both the horizontal and vertical displacement demands required to achieve the same drift ratio. Given that the drift ratio, as defined in *ACI 318*, represents the relative displacement between the top and bottom of a story divided by the story height.

$$\text{Drift ratio} = \frac{\Delta x}{h} \tag{2.1}$$

Where Δx is the storey drifts, determined with the δ_x value computed along any of the two edges of the building, and equal to $\delta_x - \delta_{x-1}$. h is the storey height.

Since the beam-to-column connection tests typically involve the application of vertical displacement at the beam end to simulate seismic effects, using the horizontal displacement of the beam's end as an example to analyze the influence of the rotation point on the BCC connection as shown in Fig. 2-6.

$$\Delta\theta = \frac{\Delta h_b}{l_b} \tag{2.2}$$

$$\Delta x_{top} = h_b \times \Delta\theta \tag{2.3}$$

$$\Delta x_{mid} = \frac{h_b}{2} \times \Delta\theta \tag{2.4}$$

$$\Delta x_{top} = 2\Delta x_{mid} \tag{2.5}$$

Where $\Delta\theta$ represents the rotation angle. h_b denotes the height of the beam. Δh_b is the change in beam height due to rotation. l_b is the length of the beam. Δx_{top} represents the corresponding horizontal displacement when the rotation point is positioned at the top of the beam. Δx_{mid} represents the corresponding horizontal displacement when the rotation point is positioned at the middle of the beam.

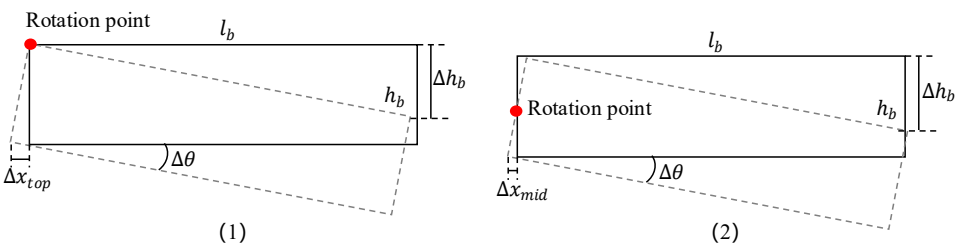

Figure 2-6 Location of rotation point

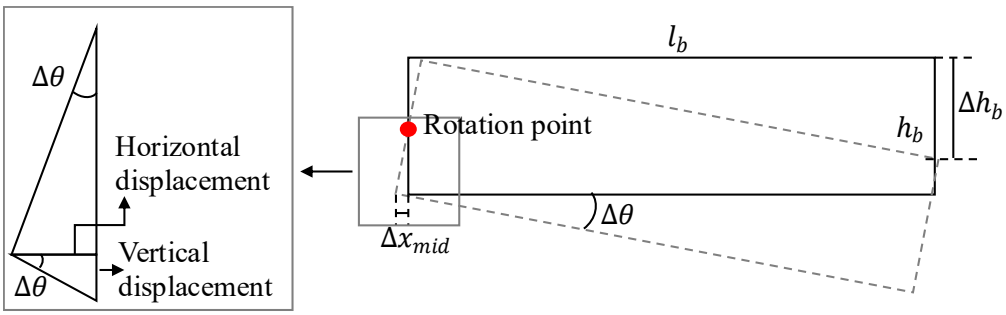

Figure 2-7 Displacement with Rotation Centered at Midpoint

Moreover, positioning the rotation point at the mid-height of the beam can significantly reduce both horizontal and vertical displacement demands, offering several distinct advantages. Firstly, the reduction in horizontal displacement decreases the required slot length in the friction dampers, thereby minimizing dimensional constraints. This enables friction dampers to better

accommodate varying beam and column dimensions, enhancing the flexibility and adaptability of beam-to-column connections.

Secondly, the vertical displacement, resulting from rotational effects, is proportional to the horizontal displacement and is calculated as $\Delta x \times \sin \Delta\theta$ as shown in Fig. 2-7. Given that the slots on the steel plates are primarily designed for horizontal slips, this vertical displacement can induce additional stress at the slot edges. Over time, these stress concentrations may lead to localized plastic deformation at the slot edges, compromising the durability and long-term reliability of the connection. By locating the rotation point at the mid-height of the beam, these stresses are significantly alleviated, ensuring that a slight clearance between the slot width and bolt diameter during production is sufficient to accommodate the anticipated displacement demands. This design strategy effectively maintains the connection's stability while extending its service life. Additionally, this configuration facilitates the potential addition of extra rows of bolts, which can increase the frictional resistance, thereby adapting to higher load-carrying demands and further optimizing the performance of the connection under varying conditions.

2.4. Load transfer mechanism in DFED-BCC

Shear force failures are typically brittle, emphasizing the importance of adhering to the 'Strong shear and weak bending' design principle. As a result, evaluating shear force transfer path is a critical aspect in the design of beam-to-column connections (BCC).

A column with a corbel is a widely adopted design in the construction sector for two main reasons. First, it facilitates the transfer of shear forces. In most scenarios, the beam generates a downward shear force on the column, which is effectively transferred via the corbel located below the beam end. Another advantage of using corbel is its ability to serve as support during construction, eliminating the need for additional temporary support. However, in cases where the beam span is short, seismic forces may induce shear forces greater than those caused by vertical loads, resulting in a reversal of shear force direction to upward [4]. Under such conditions, the corbel transitions from serving as a shear force mechanism to bearing reaction forces, necessitating additional load transfer mechanisms.

A secondary corbel is often added above the beam end to address this reversed shear force, but this can introduce construction challenges, particularly with slab integration. The DFED-BCC offers a more efficient and practical solution by establishing a novel load transfer path, accommodating both sagging and hogging moment conditions, as illustrated in Fig. 2-10.

The following load path analysis assumes that upper and lower portions of the angle steel exhibit symmetrical strain behavior. The symmetry ensures that the compressive and tensile forces remain balanced, thereby preventing the bolts at the rotation point from being subjected to additional axial forces. This hypothesis is consistent with the assumptions made by Kishi and Chen [61] in their study on the initial stiffness of web-angel connections.

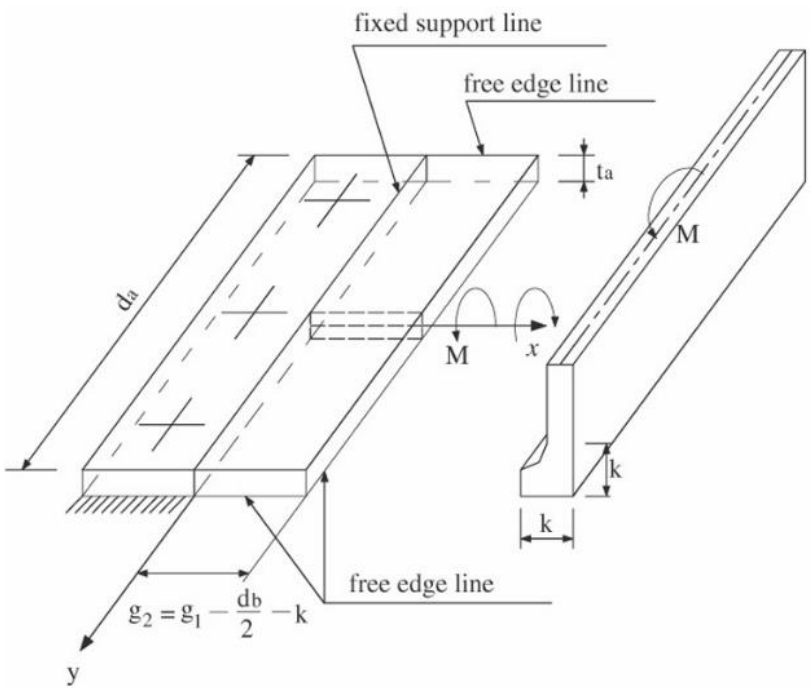

Figure 2-8 Assumption in Kishi–Chen's initial stiffness model

They transformed the problem into a bending problem of a moderately thick plate. The fundamental assumptions include the premise that the center of rotation of the angel is located at the midpoint of the outstanding leg. Additionally, the edge of the bolt heads in the outstanding leg, which are fastened to the column flange, is treated as a fixed boundary condition, while the remaining three edges of the outstanding leg are considered free, as illustrated in Fig. 2-8.

Actually, the rotation point is not located precisely at the midpoint, which may be attributed to the constraints imposed by the upper and lower boundary conditions. As demonstrated in the FEA in Chapter 3, the middle bolt was subjected to axial force. They may also be influenced by the variation in the cross-sectional shape of the steel plate under tensile and compressive loading. A similar analysis was discussed in the study by Yang and Lee [62], where they modified the lower edge of the outstanding leg to a hinge-supported line and assumed that a linearly distributed triangular load was applied along the edge of the plate as illustrated in Fig. 2-9. However, in the proposed connection design, the presence of the middle bolt alters the load distribution, making it inconsistent with the assumptions in their study. To facilitate a more tractable analysis, this study adopts an idealized assumption, simplifying the boundary conditions same to the Kishi–Chen's model.

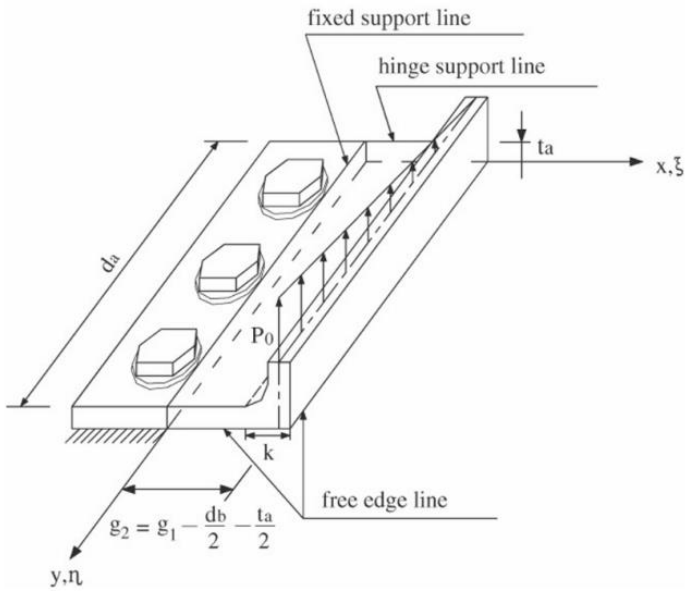

Figure 2-9 Assumption in Yang–Lee's initial stiffness model

When the DFED-BCC system, under sagging moment conditions, the moment is resisted by the friction forces generated by pre-loaded bolts positioned above and below the rotation point. Meanwhile, the embedded bolts in the column primarily handle the transfer of shear forces, ensuring a clear and efficient load transfer path between the beam and the column.

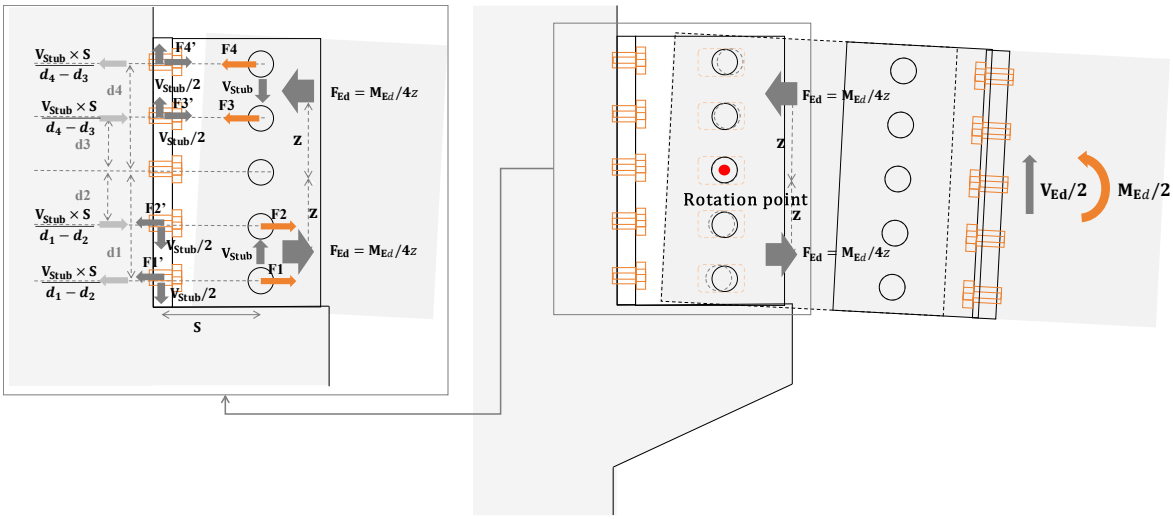

Figure 2-10 Load path: Sagging moment

Under hogging moment conditions, the moment is similarly resisted by the friction forces generated by the pre-loaded bolts. The embedded bolts and the corbel work together to transfer the shear forces, providing a dual mechanism for enhanced reliability. This combined system not only ensures effective shear force transfer but also mitigates the adverse effects of beam section reduction, thereby maintaining the structural integrity and load bearing capacity of the connection.

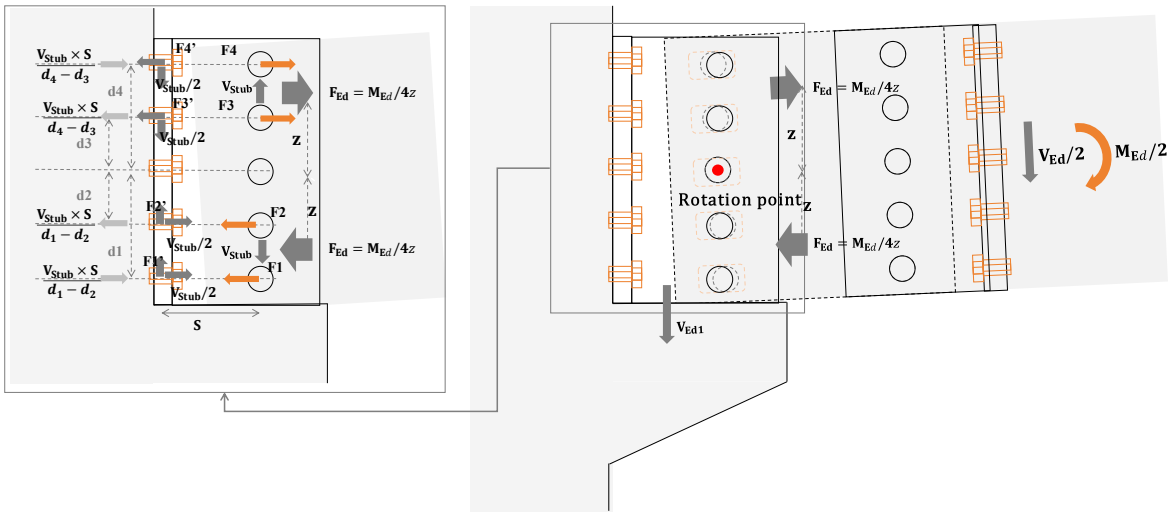

Figure 2-11 Load path: Hogging moment

For systems requiring higher load-bearing capacity, a connection incorporating two rows of bolts, as illustrated in the Fig. 2-11, can be utilized. The load transfer mechanism is analogous to that of a single-row bolt connection. However, due to the central position of the rotational

axis, the resulting rotational deformation follows a curved path.

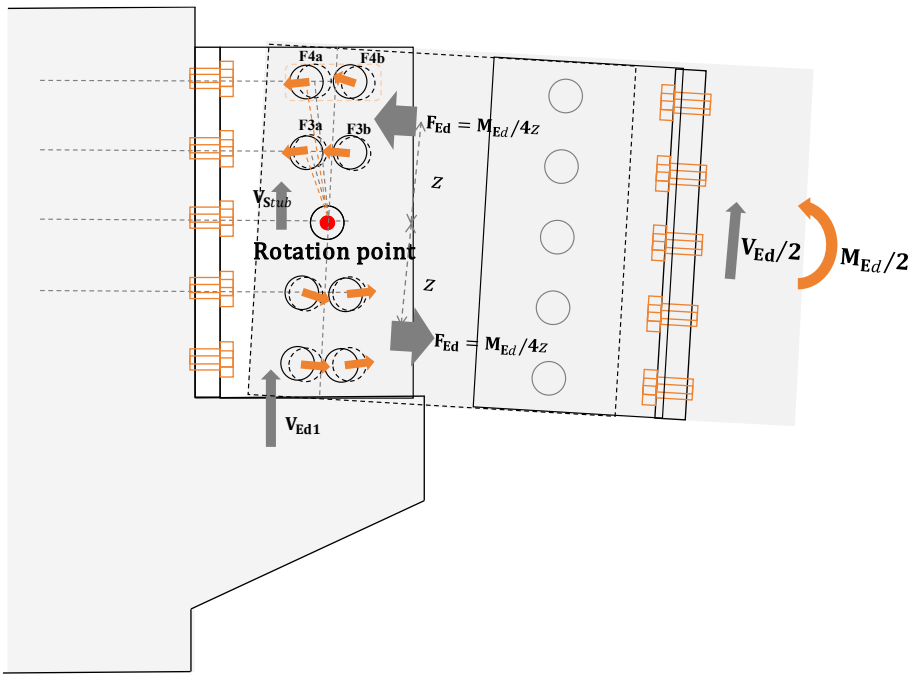

Figure 2-12 Load path in connection with two rows of bolts

To calculate if there is a need to reserve a curved path or straight path for sliding. The height difference of A_1 and A_2 need to be calculated. Assuming the maximum drift ratio loading during the test is 5%. A value of 10mm is used to reserve more space for calculation.

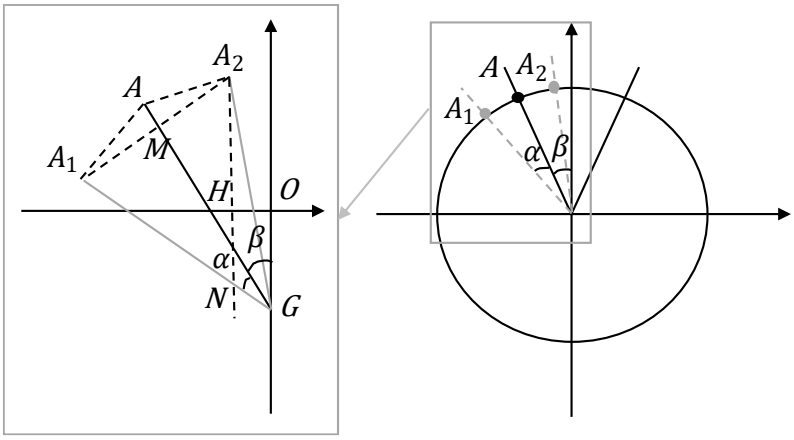

Figure 2-13 Schematic of height difference

To determine whether a curved or straight path needs to be reserved for sliding, the height difference between A_1 and A_2 must be calculated. Assuming the maximum drift ratio during testing is 5%, the corresponding vertical displacement is $\Delta h = 9mm$. For safety and to

accommodate additional tolerances, a value of 10 mm is used in the calculations to reserve sufficient space.

$$sin\alpha = \frac{10}{1800} = \frac{1}{180} \tag{2.6}$$

Assume the spacing between two rows of bolts is 20mm

The radius of circle equal to half of the beam height minus 30mm gap at the edge.

$$l \approx \frac{h}{2} - 30 \tag{2.7}$$

Thus,

$$sin\beta = \frac{20/2 + 10}{h/2 - 30} \tag{2.8}$$

Since $\angle AA_1A_2 = \alpha,\ A_1M = A_2M = \left(\frac{h}{2} - 30\right) \times sin\alpha = \frac{\left(\frac{h}{2}-30\right)}{180},\ A_1A_2 = \frac{\left(\frac{h}{2}-30\right)}{90}$

$$\angle A_2A_1O = \beta,\ A_2H = \frac{\left(\frac{h}{2}-30\right)}{90} \times \frac{30}{h/2-30} = \frac{1}{3}mm \tag{2.9}$$

The maximum potential height difference between $A_1$and $A_2$is calculated to be 2/3=0.67mm.

It's OK to reserve a straight path.

In conclusion, the integrated design of the DFED-BCC establishes a well-defined and controllable load transfer path. Adopting this connection system offers the potential for achieving a more cohesive and multifunctional connection within precast concrete frames, enhancing both structural performance and design flexibility.

2.5. Replacement and upgrade method

Friction dampers dissipate energy through sliding friction, adhering to the principle of 'braking rather than breaking'. This approach focuses energy dissipation on the wear of replaceable components, such as friction pads, rather than causing damage to primary structural elements. As the coefficient of friction of the pads diminishes over time or following seismic events, they are designed for straightforward replacement, ensuring the damper's continued performance and functionality.

The service life and durability of friction dampers are largely determined by factors such as the material properties, thickness, and wear resistance of the friction pads. Designers can select friction materials tailored to specific performance requirements, allowing for customized solutions in various structural applications.

Moreover, the functionality of the DFED-BCC can be easily upgraded due to the adjustability of friction forces. Upgrades can be achieved by replacing friction pads with higher-performing materials or by increasing the pre-loading forces of the bolts. This adaptability not only enhances the structural system's performance but also facilitates the reuse of structural components when functional requirements evolve or are upgraded. By accommodating such modifications with minimal intervention, the DFED-BCC aligns sustainability objectives, extending the service life of the connection and promoting environmentally responsible design practices.

Chapter 3 Numerical analysis

3.1. Selection of modeling methods

ABAQUS is employed in this study for numerical analysis due to its robust capabilities in nonlinear analysis, comprehensive contact modeling features, and extensive library of constitutive material models. It enables precise simulation of material degradation under cyclic loading, accurately captures key mechanisms such as bolt preloading and frictional slip in the proposed connection, and effectively models bolt–hole dynamic interactions using advanced contact algorithms. These capabilities align closely with the critical aspects under investigation in the proposed connection, making ABAQUS a highly suitable tool for this study.

The objective of this section is to investigate the deformation characteristics, mechanical response, and seismic performance of the proposed connection under cyclic loading with increasing displacement. This analysis serves as the foundation for developing a fundamental hysteresis model to facilitate theoretical evaluations. However, a comprehensive parametric study of design variables is more appropriately conducted using a finite element model validated by experimental results. Therefore, this section specifically focuses on the effects of preload and material properties on the connection's behavior. Accordingly, one monolithic connection and four demountable beam-to-column (DfD) connections were designed for simulation analysis.

In ABAQUS, several modeling approaches are commonly employed to simulate the behavior of concrete beam-to-column connections under cyclic loading. The first approach utilizes a two-dimensional (2D) model, where concrete is modeled using beam elements combined with embedded reinforcement. The second approach, a three-dimensional (3D) model, employs eight-node brick elements with reduced integration (C3D8R) for both concrete and steel components, while reinforcement is modeled using three-dimensional two-node truss elements (T3D2). The third approach uses C3D8R elements for all structural components. Considering

the balance between accuracy and computational efficiency, the second approach was selected to simulate the proposed connection.

In monolithic RC connections, the bond-slip relationship between reinforcement and concrete plays a critical role in determining mechanical performance. In ABAQUS, embedded reinforcement is commonly used, which inherently assumes perfect bonding between the reinforcement and the surrounding concrete. As a result, the simulated hysteresis curves are often overly full, failing to capture the pinching effects observed in physical tests and consequently overestimating energy dissipation and stiffness. To address this limitation, several methods have been adopted to simulate bond-slip behavior more realistically.

(1) Defining cohesive contact between reinforcement and concrete [63,64].

(2) Using connector to simulate bond-slip behavior [65,66].

(3) Employing nonlinear spring elements to model bond-slip relationships [67,68].

(4) Imitating the pinching effect by reducing the elastic modulus and yield strength of reinforcement [69,70].

(5) Implementing a hysteretic model for reinforcement with stiffness degradation upon reloading, using a user-defined subroutine [71,72].

However, a study by Chen et al. [73] on the bond-slip numerical simulation of reinforced concrete wall-beam-slab joints demonstrated that methods (3) and (5) are relatively reliable, as they provide reasonable predictions of peak load and stiffness degradation. Nevertheless, they still fail to accurately capture the bond-slip behavior, often leading to an overestimation of energy dissipation.

Since monolithic connection behavior is not the primary focus of this study, and achieving an accurate hysteresis response is of greater importance, beam elements in a two-dimensional (2D) model were selected to model the monolithic connection in this research.

3.2. Test arrangements

3.2.1. Test specimens

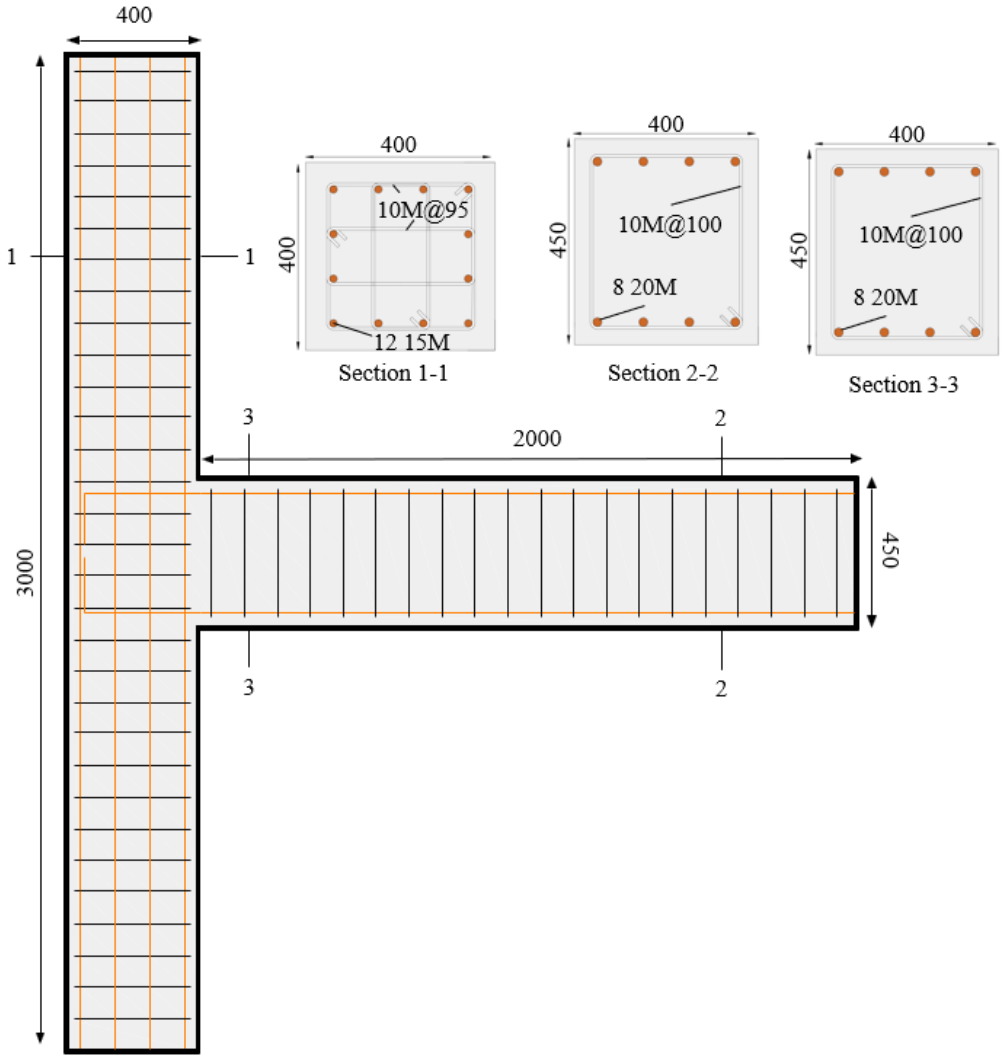

Figure 3-1 Dimensions of monolithic connection

The proposed beam-to-column connections share identical sectional dimensions and reinforcement configurations. The column measures 3000 mm in length with a 400 mm × 400 mm cross-section and is reinforced with twelve 400W rebars of 15 mm diameter. The stirrups, also 400W with a 10 mm diameter, are spaced at 95 mm along the column. The beam has a length of 2000 mm, with a 400 mm × 450 mm cross-section, reinforced with eight 400W

longitudinal rebars of 20 mm diameter. Beam stirrups consist of 10M 400W rebars, spaced at 100mm along the beam. The geometric configurations of the monolithic connection and the proposed DFED-BCC are illustrated in Fig. 3-1 and Fig. 3-2, respectively.

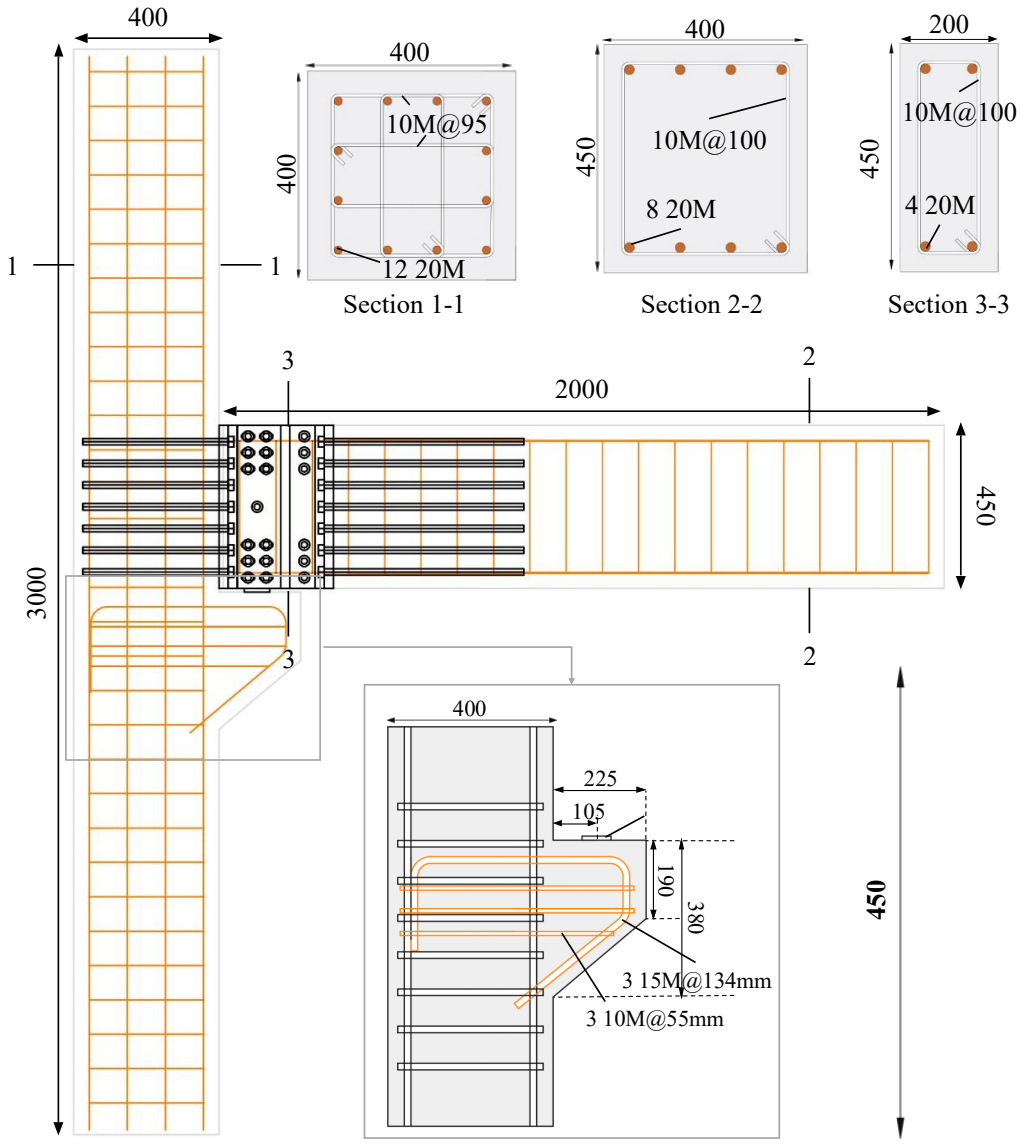

Figure 3-2 Dimensions of DFED-BCC

In the proposed DfD connection, a corbel is integrated to partially resist shear forces and provide temporary support during assembly. Seven M20 high-strength bolts are embedded on each side of the interface between the precast beam and column. Two unequal steel angles are bolted to both the beam and column through these bolts. The inner and outer surfaces of the angles are equipped with friction pads, comprising aluminum-coated steel plates and additional

steel plates. Together, the angles, friction pads, and steel plates form a friction damper, with one unit installed on either side of the connection. Each damper provides two friction interfaces, generating the required resistance. The M20 bolts are preloaded to activate the friction mechanism. Additionally, the angles feature slotted holes aligned with the two bolt rows near the column, enabling controlled sliding. A central bolt is fixed to serve as a rotation point, ensuring the desired mechanical response of the connection. The geometric configuration of the steel components in the DFED-BCC is illustrated in Fig. 3-3, and the detailed parameters of each layer are summarized in Table 3-1.

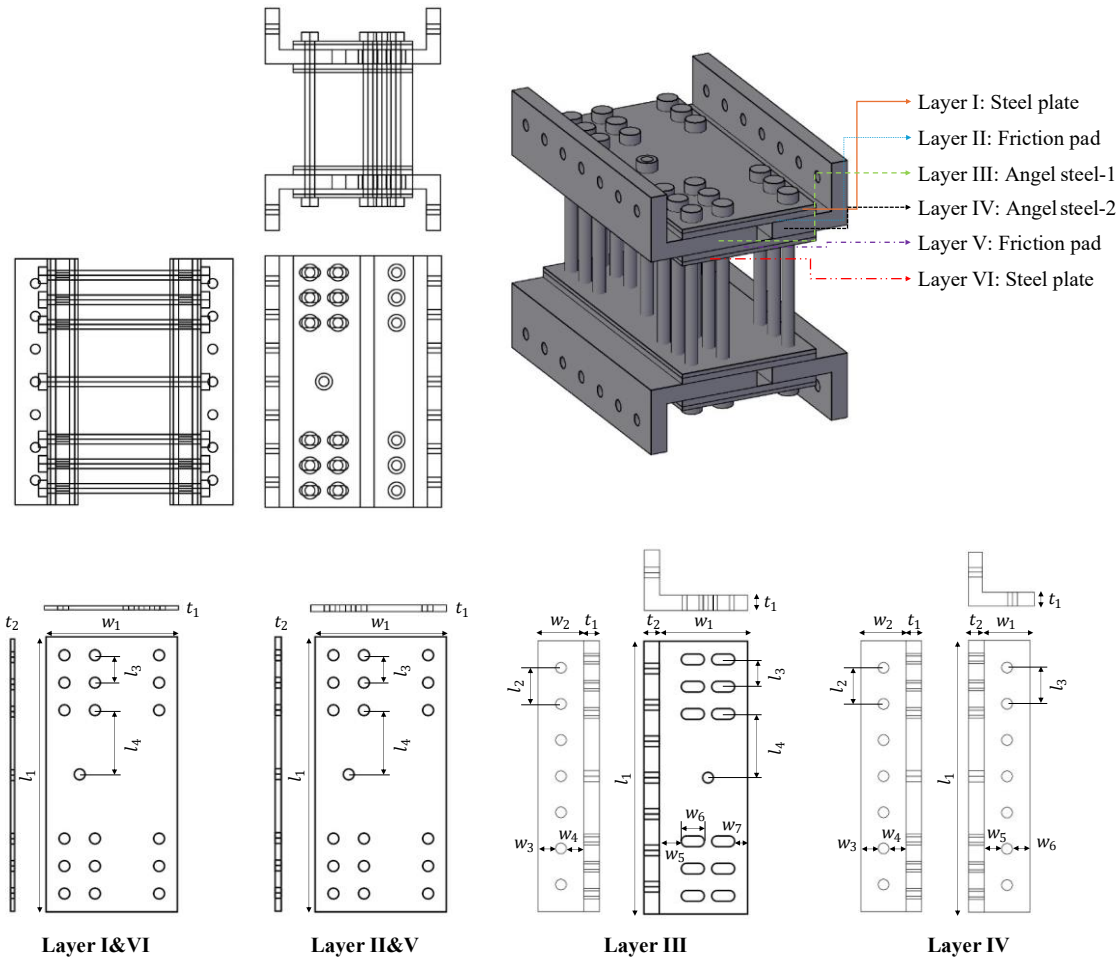

Figure 3-3 Configurations of the steel components in DFED-BCC

Table 3-1 Parameters for the steel components in DFED-BCC

	t1	t2	w1	w2	w3	w4	w5	w6	w7	l1	l2	l3	l4
Layer I&VI	6	6	215	/	/	/	/	/	/	450	/	45	105
Layer II&V	8	8	215	/	/	/	/	/	/	450	/	45	105
Layer III	25.4	25.4	145	74.5	27.25	27.25	36.25	37.5	21.25	450	60	45	105
Layer IV	25.4	25.4	74.5	74.5	27.25	27.25	27.25	27.25	/	450	60	60	/

Unit: mm

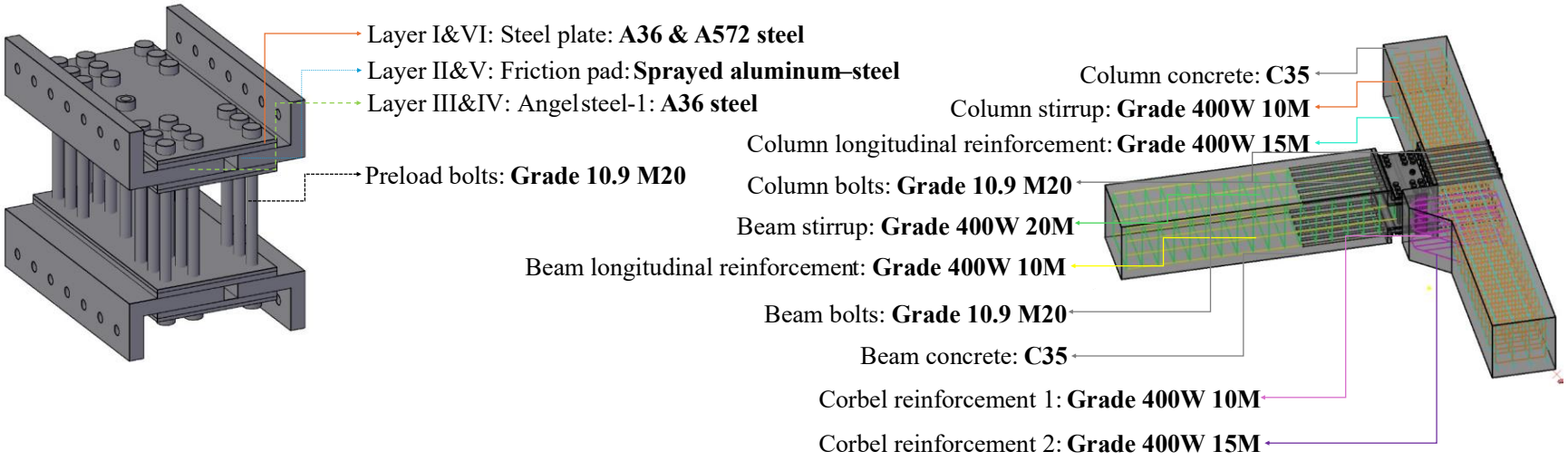

Figure 3-4 Materials of DFED-BCC

3.2.2. Materials

The dimensions and material properties of each component in DFED-BCC are illustrated in Fig. 3-4. In the absence of experimental results, the material parameters are assumed to be conventional values or adopted from existing studies that have been validated through experimental and numerical investigations. Detailed material parameters are provided in ***section 3.4.2***: Constitutive models of materials.

3.2.3. Loading protocol

The loading protocol for the beam-to-column connection followed a variable amplitude (VSA) pattern, with progressively increasing drift levels ranging from 0.3% to 5% over 16 steps, in accordance with *FEMA 461* guidelines. The protocol began with 6 cycles in the first step, followed by 2 cycles per step for the remaining stages. All tests were conducted using a displacement-controlled approach with a constant loading rate of 0.2 mm/s. Testing was concluded when the load capacity dropped below 85% of the peak load, a local failure was observed, or a drift ratio of 5% was reached.

n	16	15	14	13	12	11	10	9	8	7	6	5	4	3	2	1
a_i/a_n	0.006	0.009	0.013	0.018	0.025	0.035	0.048	0.068	0.095	0.133	0.186	0.260	0.364	0.510	0.714	1.000

Figure 3-5 Relative Loading History Deformation Amplitudes

The initial drift level of 0.3% was chosen to capture the initial elongation of the angle steel in the device, as this stage represents the transition from elongation to energy dissipation primarily through friction. Starting at 0.3% ensures that this phenomenon is well captured in the tests. The selection of 5% drift as the upper limit aligns with the maximum drift ratio typically associated with frame structures designed for collapse prevention under severe seismic events. This level captures the ultimate deformation capacity of the beam-to-column connection, providing insight into the ductility and energy dissipation characteristics under extreme loading conditions. The detailed loading protocol is presented in Fig. 3-6.

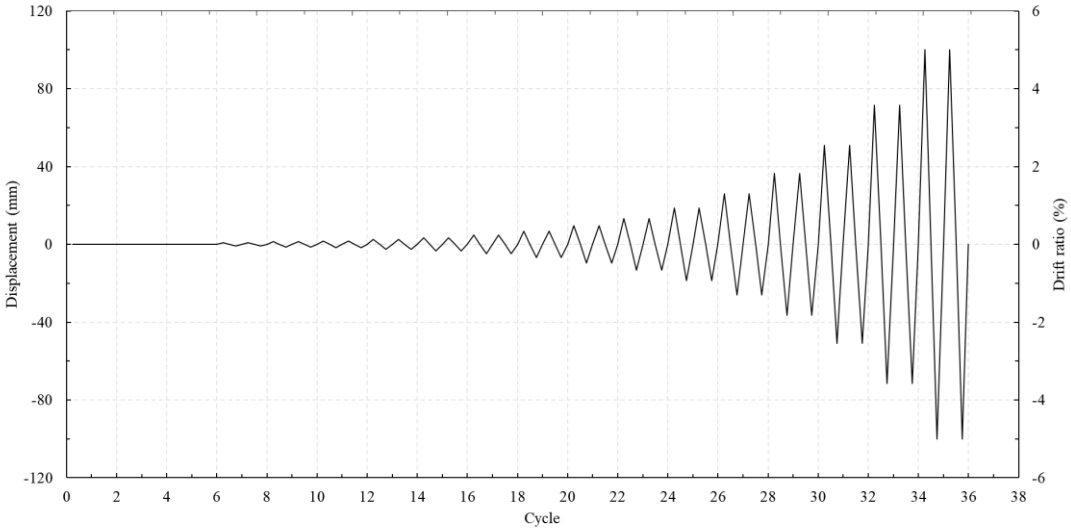

Figure 3-6 Loading protocol

3.2.4. Test matrix

As discussed in ***Section 3.1***, a finite element model validated through experimental results is more suitable for conducting a comprehensive parametric study of design variables. Therefore, this section focuses specifically on the influence of bolt preloading force and material properties on connection performance, providing essential insights for the parameter selection in experimental models. To investigate these effects, four proposed connections are designed with varying bolt preloading forces and different steel angle grades. The specific parameters for each specimen are presented in Table 3-2.

Table 3-2 Test matrix

Specimen	Pre-loading forces (kN)	Steel grade	Thickness of steel angel (mm)
M1	/	/	/
P100-1	100	A36	25.4
P80-1	80	A36	25.4
P60-1	60	A36	25.4
P80-2	80	A572	25.4

3.3. FE model validation

To validate the finite element (FE) model, two beam-to-column connections were selected: one friction-based demountable connection and one monolithic connection. The friction-based connection was adopted from [42] because its load transfer mechanism, dominated by friction

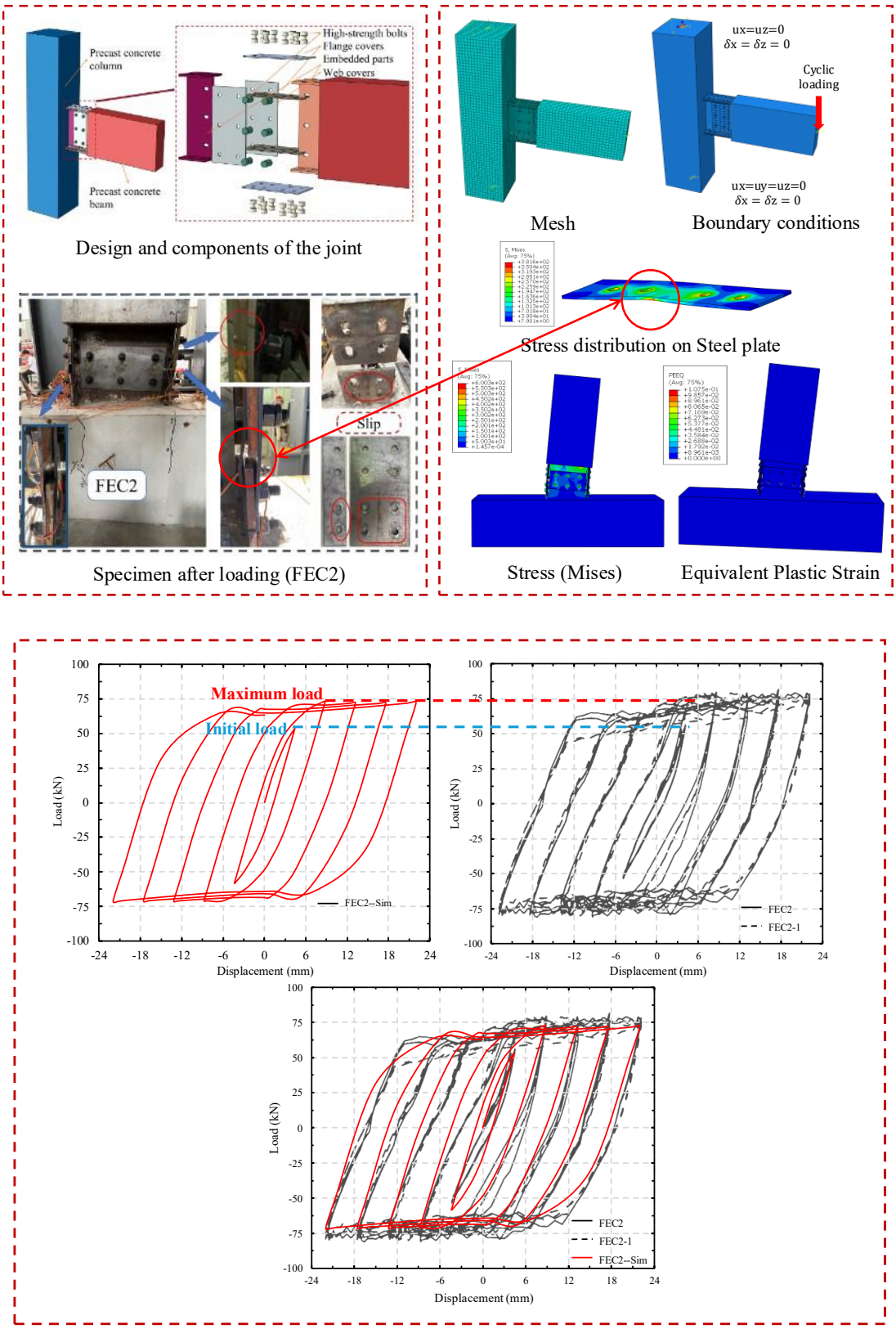

Figure 3-7 Validation of friction-based demountable connection

damping, closely aligned with the proposed frictional design in this dissertation. Since both

designs relied on frictional energy dissipation, this reference provided a suitable benchmark for validating the numerical modeling approach of the friction-based connection.

However, the monolithic connection in [42] was not selected for validation due to two key reasons. First, the beam in [42] fell within the deep beam category, meaning its structural response was predominantly governed by shear action rather than flexural behavior. As a result, its load transfer mechanism was significantly influenced by arching effects, and diagonal shear cracks developed early in the loading process. Furthermore, crack closure-induced friction contributed to substantial energy dissipation even before reinforcement yielding, resulting in a fuller hysteresis loop. Given that beam elements in finite element modeling are formulated based on the plane section assumption and do not explicitly capture shear-dominated failure mechanisms or the contribution of transverse reinforcement (stirrups), directly modeling deep beams using this approach would not yield accurate results.

Second, the beam in the proposed monolithic connection was flexure-dominant, which means that bending moments governed the deformation response, in contrast to the shear-dominant behavior observed in [42]. As a result, the monolithic connection in [22], which also exhibited a flexure-dominated response, was chosen instead. This ensured a more appropriate validation framework, as beam elements with embedded reinforcement could effectively capture both the elastic response and the post-yield nonlinear behavior of flexure-dominant structures. Therefore, the monolithic model in [22] was selected to validate the monolithic beam-to-column connection in this study.

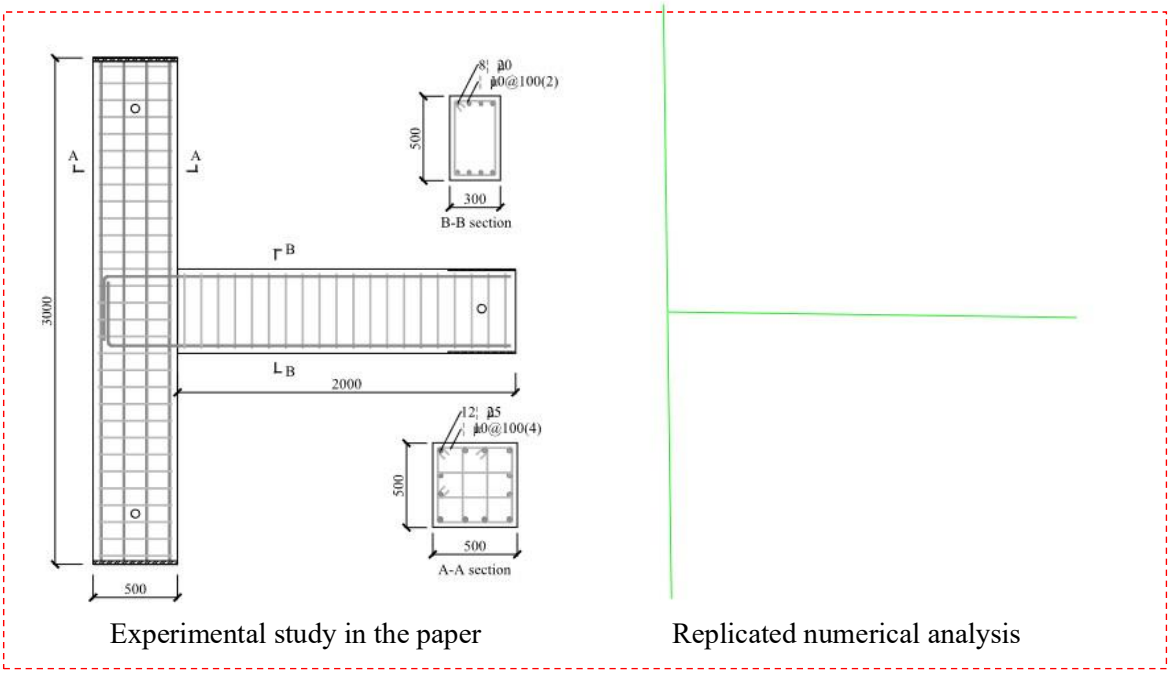

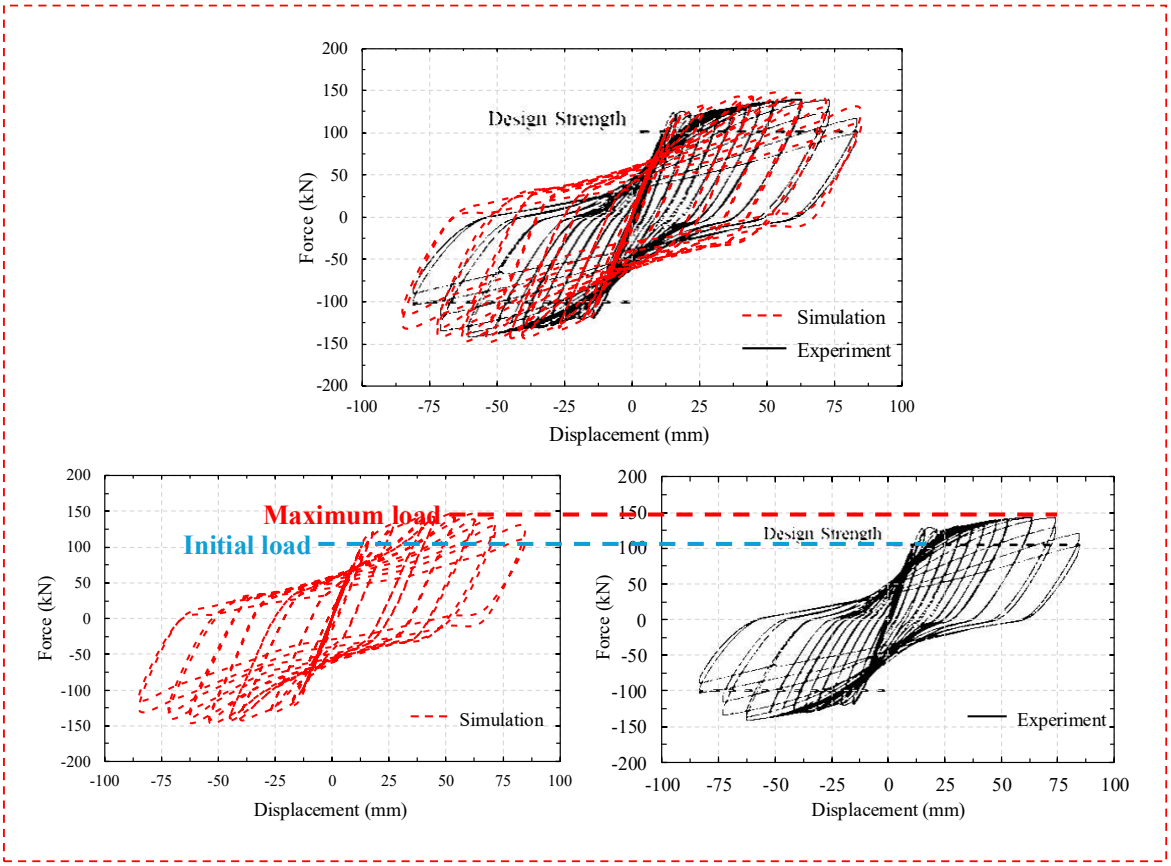

Figure 3-8 Validation of monolithic connection

The validation results for the friction-based demountable connection and the monolithic connection are presented in Fig. 3-7 and Fig. 3-8, respectively. The FE model accurately

captures the key phenomena observed in the experiments. A comparison of the hysteresis curves obtained from the FE simulations and those from experimental results demonstrates strong consistency in terms of initial stiffness, peak load, stiffness degradation, and energy dissipation capacities. This agreement validates the accuracy of the FE model, confirming its reliability for analyzing the proposed DFED-BCC.

The detailed parameters for the FE model are provided in the following section, which introduces the friction-based demountable model in ***Section 3.4*** and the monolithic model in ***Section 3.5***, respectively.

3.4. FE model for DFED-BCC

3.4.1. Basic setup

FEA was performed using ABAQUS 2022. Concrete, steel components, friction dampers, and bolts were discretized using 8-node linear brick (C3D8R) elements with reduced integration, while 2-node linear displacement truss elements (T3D2) were applied to model reinforcement in the beam and column. The size of the mesh was derived from sensitivity analyses, which yielded to the following maximum dimensions: 5mm, 10mm, 10mm, 15mm and 20mm for bolts, plate, concrete, reinforcement, and steel profiles, respectively.

3.4.2. Constitutive models of materials

The materials for each component of DFED-BCC were detailed in ***Section 3.2.2***. This section further discusses the constitutive models for these materials and their specific properties.

(1) Constitutive model for steel

To accurately capture cyclic loading behavior while ensuring numerical convergence, two types of steel constitutive models were selected for different components.

- The combined isotropic and kinematic hardening model based on the work of Chaboche and Lemaitre [74]was chosen for the primary steel components of DFED-BCC, including steel plates, friction pads, and angle steel. This model effectively simulates hardening behavior and cyclic loading response, making it suitable for

components subject to repeated loading.

- A simpler bilinear model was selected for connecting bolts and reinforcement, providing an efficient yet reliable representation of their mechanical behavior.

The detailed material properties for each component are presented in Table 3-2. The parameters of A572 Gr.50 were adopted from a study by Hoveidae [75], which is based on data from [76], while those for A36 were sourced from Elkady [77].

Additionally, an introduction to the Chaboche model is provided here. The Chaboche model is formulated as a combination of isotropic and kinematic hardening, incorporating both yield surface expansion and translation to accurately capture cyclic plasticity behavior. It is based on the von Mises yield criterion and follows an associative flow rule [78].

Table 3-3 Material properties

	$F_y(MPa)$	$F_u(MPa)$	$E\ (Mpa)$	$C\ (Mpa)$	γ	Q_∞	B
A572 Gr.50	345	/	203000	2000	12	160	5
A36	235	/	200000	6895	25	172	2
Grade 10.9	900	1000	/	/	/	/	/
400W	400	540	/	/	/	/	/

(1) Isotropic hardening model

The isotropic hardening model defines the evolution of the yield surface size, σ_0, as the function of the equivalent plastic strain, ε_{pl}. It adopts a simple exponential law [78]:

$$\sigma_0 = \sigma|_0 + Q_\infty(1 - e^{-b_{iso}\varepsilon^{pl}}) \tag{3.1}$$

Where $\sigma|_0$ is the yield stress at zero equivalent plastic strain (defined as the 0.01% proof stress), Q_∞ is the maximum change in the size of the yield surface, b_{iso} is the rate at which the size of the yield surface changes as plastic strain increases.

The size of the yield surface in the ith cycle σ_i^0 can be obtained from:

$$\sigma_i^0 = \frac{\sigma_i^t - \sigma_i^c}{2} \tag{3.2}$$

Where σ_i^t is the maximum tensile stress, σ_i^c is the maximum compressive stress in the elastic range.

The equivalent plastic strain corresponding to σ_i^0:

$$\beta_i^p = \frac{1}{2}(4i - 3)\Delta\varepsilon^{pl} \tag{3.3}$$

Where $\Delta\varepsilon^{pl} \approx \Delta\varepsilon - 2\sigma_t^1/E$

<u>(2) Kinematic hardening model</u>

Kinematic hardening model describes the size of the yield surface in stress space through the backstress, α, as a function of plastic deformation. It is expressed as:

$$\alpha_k = \frac{C_k}{\gamma_k}\left(1 - e^{-\gamma_k \varepsilon^{pl}}\right) + \alpha_{k,1} e^{-\gamma_k \varepsilon^{pl}} \tag{3.4}$$

Where $\alpha_{k,1}$ denotes the kth backstress at the first data point (initial value of the kth backstress), C_k and γ_k are constants from a stabilized cycle.

Each data pair $(\sigma_i, \varepsilon_i^{pl})$ shift to ε_p^0, so it can express as:

$$\varepsilon_i^{pl} = \varepsilon_i - \frac{\sigma_i}{E} - \varepsilon_p^0 \tag{3.5}$$

Where $\varepsilon_1^{pl} = 0$

For each pair $(\sigma_i, \varepsilon_i^{pl})$ values of α_i can be obtained from the test data:

$$\alpha_i = \sigma_i - \sigma^s \tag{3.6}$$

Where α_i is the overall backstress obtained by summing all the backstress at the data point. $\sigma^s = \frac{\sigma_1 + \sigma_n}{2}$ is the stabilized size of the yield surface.

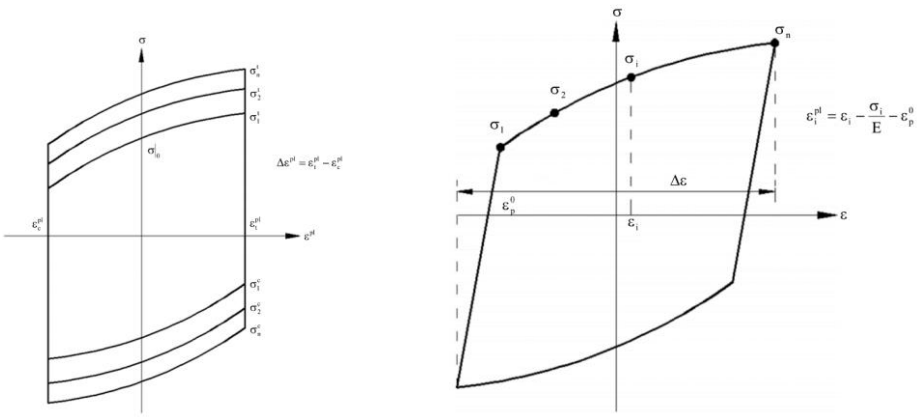

Figure 3-9 Isotropic hardening model and Kinematic hardening model

(2) Constitutive model for concrete

In ABAQUS, three constitutive models are available for simulating the behavior of concrete: the brittle cracking model, the smeared cracking model, and the plastic damage model. The brittle cracking model primarily accounts for the nonlinear behavior of concrete in tension, without considering other mechanical phenomena. Both the smeared cracking model and the plastic damage model simulate cracking behavior in concrete, but through different mechanisms. The smeared cracking model represents concrete as an anisotropic material, distributing cracks across the elements. However, this approach contradicts the assumptions of this study. Additionally, the smeared cracking model does not capture critical mechanical behaviors such as unloading stiffness degradation and reloading stiffness recovery under cyclic loading, which are essential for accurately modeling concrete behavior under dynamic or repeated loading conditions.

The Concrete Damage Plasticity (CDP) model, adopted in this study, assumes that the primary failure mechanisms of concrete are tensile cracking and compressive crushing. This model incorporates two independent damage parameters to characterize stiffness degradation and partial recovery resulting from tensile and compressive damage. These parameters enable a more realistic simulation of the material's nonlinear behavior, particularly under cyclic loading, by capturing the progressive loss of stiffness during loading and partial stiffness recovery during unloading and reloading. The stress-strain relationships were computed using the

following equations based on *ACI 318-18* [79].

- **Compressive strength of cylinder and Compressive strength of cube**

The conversion relationship between the standard compressive strength of cylinder and the standard compressive strength of cube can be calculated by the following equation for concrete compressive strength of cube under 60kN/m^3.

$$f'_c = 0.79 \times f_{ci} \tag{3.7}$$

f_c': Compressive strength of cylinder
f_{cu}: Compressive strength of cube

- **Elastic modulus**

ACI 318-19 [79] 19.2.2.1 suggested when value for density of concrete (w_c) between 90 and 160 lb/ft^3, the elastic modulus of normal concrete (E_c) can be calculated by:

$$E_c = 4730\sqrt{f'_c}\ \text{(MPa)} \tag{3.8}$$

- **Peak strain**

Peak strain for concrete normally between 0.002 to 0.005. The study adopted 0.002 according to Mander [80].

- **Poisson ratio**

The Poisson ratio for normal concrete ranges from 0.1 to 0.2, and it was assumed as 0.2 in this study.

- **Uniaxial compression stress-strain curve**

The uniaxial compression stress-strain curve and concrete uniaxial compression damage parameters were calculated using the following equation, which was proposed by Mander et al. [80] under the American standard.

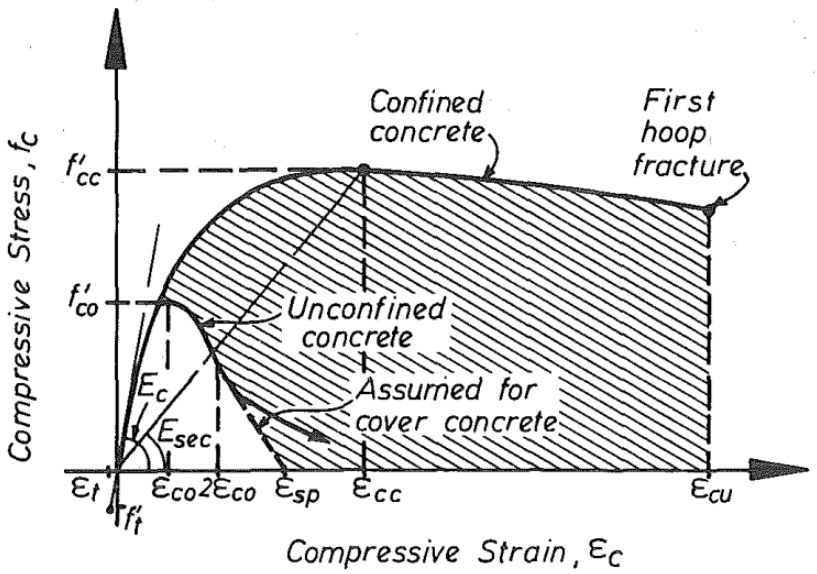

Figure 3-10 Stress-Strain Model proposed for Monotonic Loading of Confined and Unconfined Concrete

$$
\begin{aligned}
f_c &= \frac{f'_{cc} x r}{r - 1 + x^r} \\
x &= \frac{\varepsilon_c}{\varepsilon_{cc}} \\
\varepsilon_{cc} &= \varepsilon_0 \left[1 + 5 \left(\frac{f'_{cc}}{f'_{c0}} - 1 \right) \right] \\
r &= \frac{E_c}{E_c - E_{\sec}} \\
E_{\sec} &= \frac{f'_{cc}}{\varepsilon_{cc}}
\end{aligned}
\tag{3.8}
$$

f'_{cc}: Compressive strength of confined concrete
ε_c: Longitudinal compressive concrete strain

- **Model parameters in CDP model**

The concrete damage plasticity constitutive model in ABAQUS SIMULIA User Assistance 2022 is shown in Fig. 3-11.

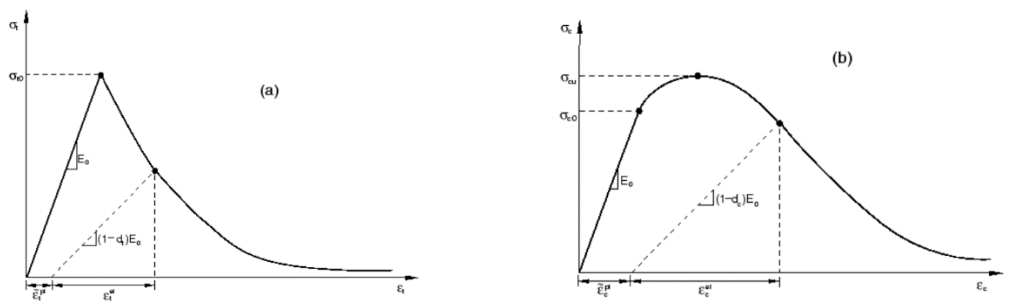

Compression stress-strain relationship of damage plasticity model of concrete

Tensile stress-strain relationship of damage plasticity model of concrete

Figure 3-11 Concrete damage plasticity constitutive model

$$
\begin{aligned}
\tilde{\varepsilon}_c^{in} &= \varepsilon_c - \varepsilon_{0c}^{el} \\
\varepsilon_{0c}^{el} &= \frac{\sigma_c}{E_0} \\
\tilde{\varepsilon}_c^{pl} &= \tilde{\varepsilon}_c^{in} - (\varepsilon_c^{el} - \varepsilon_{0c}^{el}) = \tilde{\varepsilon}_c^{in} - \frac{d}{1-d}\frac{\sigma_c}{E_0} \\
\tilde{\varepsilon}_t^{ck} &= \varepsilon_t - \varepsilon_{0t}^{el} \\
\varepsilon_{0c}^{el} &= \frac{\sigma_t}{E_0} \\
\tilde{\varepsilon}_{0c}^{pl} &= \tilde{\varepsilon}_t^{ck} - (\varepsilon_t^{el} - \varepsilon_{0c}^{el}) = \tilde{\varepsilon}_t^{in} - \frac{d}{1-d}\frac{\sigma_t}{E_0}
\end{aligned}
\tag{3.9}
$$

ε_{0c}^{el}: Elastic compressive strain of concrete without damage
ε_c^{el}: Elastic compressive strain of concrete with damage
$\tilde{\varepsilon}_c^{in}$: Compressive inelastic strain of concrete
$\tilde{\varepsilon}_c^{pl}$:Compressive plastic strain of concrete
$\tilde{\varepsilon}_t^{ck}$: Tensile inelastic strain of concrete
$\tilde{\varepsilon}_t^{pl}$: Tensile plastic strain of concrete

- **Concrete damage factor**

The concrete damage factor can be determined using either the energy equivalence method or the proportional strain method. In this study, the energy equivalence method proposed by Sidoroff [81] was used.

Elastic residual energy of non-destructive materials:

$$W_0^e = \frac{\sigma^2}{2E_0} \tag{3.10}$$

Elastic residual energy of destructive material:

$$W_0^e = \frac{\bar{\sigma}^2}{2E_0} = \frac{\bar{\sigma}^2}{2E_d} \tag{3.11}$$

Equivalent stress:

$$\bar{\sigma} = \frac{\sigma}{1-d} \tag{3.12}$$

Damage elastic modulus:

$$E_d = (1-d)^2 E_0 \tag{3.13}$$

Stress-strain:

$$\sigma = (1-d)E_0\varepsilon \tag{3.14}$$

$$d = 1 - \sqrt{1-D} \tag{3.15}$$

D: concrete compression damage factor
d_c and concrete tension damage factor d_t

3.4.3. Bolt diameter

The bolts were modeled by meshing a solid cylinder with the nominal circular gross area of the bolt to simulate a more accurate stress distribution. This approach provides a realistic representation of the stress state within the bolt.

$$A_s = \frac{\pi}{4}(d - 0.9382 \times p)^2 \tag{3.16}$$

where d is the nominal diameter of the bolt. p is the pitch of the thread.

3.4.4. Bolt preloading forces

The bolt pre-loading forces were modeled using the "Bolt Load" option, with the pre-loading forces applied in the initial step. The preload applied to the bolts in the friction damper corresponded to the design values, as shown in Table 3-2.

3.4.5. Interactions

Fig. 3-12 illustrates the contact interactions within the core region of the connection. The 'surface-to-surface' contact formulation is categorized into three types: concrete-to-steel, steel-

to-steel, and steel-to-friction pad interfaces. All contact pairs employ a hard normal contact behavior to prevent interpenetration and a penalty-based tangential behavior to model frictional resistance. The assigned friction coefficients are 0.3 for concrete-to-steel, 0.2 for steel-to-steel, and 0.4 for steel-to-friction pad, reflecting typical values observed in structural applications.

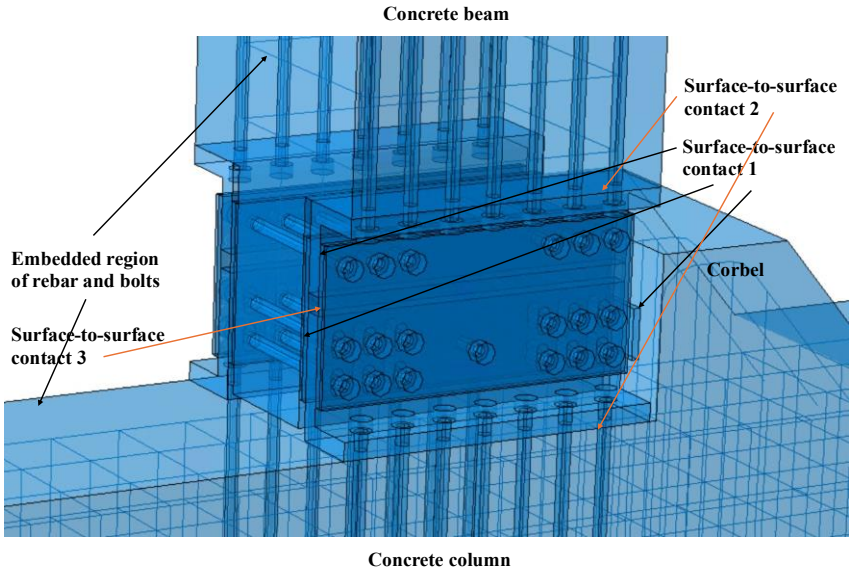

Figure 3-12 Contact relationship of the connection's core area

3.4.6. Boundary conditions

Boundary conditions are the same as validated model in ***section 3.3***.

3.5. FE model for monolithic connection

For the monolithic connection, a user-defined subroutine was employed, incorporating PQ Fiber to simulate the behavior of both reinforcement and concrete. The constitutive model for concrete followed the McKenna model [82], while the reinforcement behavior was represented using the USTEEL02 model. The USTEEL02 model is modified version of the model originally proposed by Clough [83].

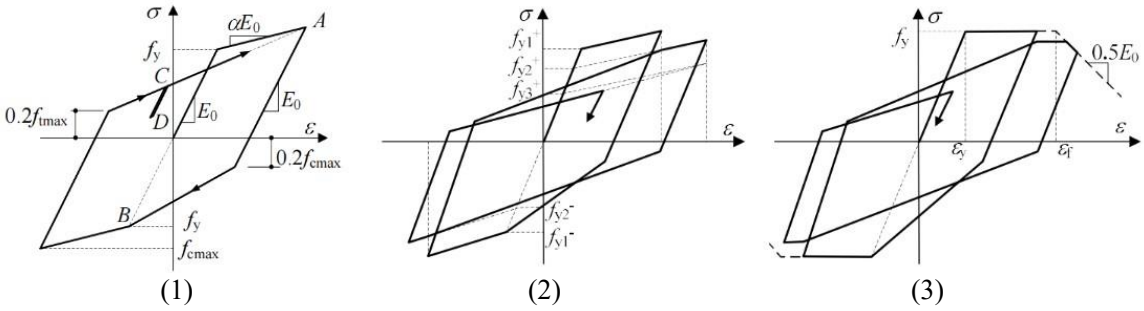

(1) (2) (3)

Figure 3-13 USTEEL02 in user-defined subroutine

This model effectively captures the key behavioral characteristics of RC components under cyclic loading, including the pinching effect, stiffness degradation, and ultimate failure mechanism. These capabilities are primarily attributed to the following three features [84]:

(1) Modification of the Unloading Curve: While based on the Clough model [83], this approach introduces a refinement in the unloading path. Initially, the unloading curve follows an elastic stiffness equal to E_0 until it reaches $0.2f_{cmax}$, as illustrated in Fig. 3-13(1). At this point, the unloading direction is reoriented toward the maximum historical strain point, ensuring a more realistic representation of cyclic loading effects.

(2) Consideration of Flexural Strength Degradation Due to Cumulative Damage: The model accounts for flexural capacity deterioration induced by accumulated damage, as shown in Fig. 3-13(2).

(3) Incorporation of Structural Failure through Backbone Curve Softening: To capture component failure, a descending branch is introduced into the backbone curve in Fig. 3-13(2). Once the failure strain is exceeded, the backbone curve softens with a stiffness of $0.5E_0$ until complete failure. This degradation and failure mechanism primarily reflects the cumulative effects of bond-slip at the reinforcement-concrete interface and the spalling of the concrete cover, rather than the material deterioration of the reinforcement itself [84].

3.6. Results and discussion

3.6.1. Test phenomenon

In this section, the observed behavior of specimen P80-1-25.4 is analyzed across three distinct loading stages, corresponding to different drift ratios: ±0.475% (elastic response stage), ±1.82% (frictional sliding stage), and ± 5.0% (prying-induced plastic deformation stage). These observations serve as validation for the proposed constitutive model of this connection.

The selected drift ratios are specific to the given connection dimensions and loading protocol. Variations in geometric parameters, such as the thickness of the angle steel, bolt diameter, and other dimensional properties, may lead to differences in the structural response and damage evolution. Stage II is omitted from the analysis primarily due to its short duration, which varies depending on the force level in Stage III. At lower force levels, Stage II may not occur at all. Furthermore, the plastic deformation accumulated during Stage II is reflected in the response observed in Stage III, where frictional mechanisms dominate. As a result, the analysis of Stage III inherently accounts for this inelastic behavior, ensuring that the omission of Stage II does not compromise the overall assessment of the connection response.

Several key indicators were selected to evaluate the mechanical behavior of the connection components under loading conditions. These indicators provide critical insights into stress distribution, plastic deformation, and damage evolution, thereby facilitating a comprehensive understanding of the structural performance and failure mechanisms.

For steel components, von Mises stress and equivalent plastic strain (PEEQ) were used to characterize yielding behavior and stress distribution. Von Mises stress, derived from the stress tensor, serves as a fundamental yielding criterion for ductile materials, allowing for the identification of initial yielding and stress redistribution following plastic deformation. PEEQ quantifies the cumulative plastic strain experienced by the material, making it instrumental in identifying potential failure zones, such as plastic hinge formation in the angle steel or localized

yielding in bolts. These indicators are critical for assessing the inelastic response and energy dissipation capacity of the connection.

For concrete components, compressive damage (DAMAGEC) and tensile damage (DAMAGET) were used to evaluate damage evolution based on the Concrete Damage Plasticity (CDP) model. DAMAGEC quantifies the degradation of material stiffness due to compressive inelastic deformation. It represents the loss of stiffness and load-bearing capacity caused by accumulated plastic strain under compressive loading. A DAMAGEC value of 0 corresponds to an undamaged state, while a value of 1 signifies complete loss of strength, typically associated with crushing failure. DAMAGET characterizes the reduction in stiffness due to tensile cracking, reflecting the progressive loss of strength as micro-cracks initiate and propagate under tensile loading. A DAMAGET value of 0 represents an intact material, while a value of 1 indicates complete tensile failure, typically corresponding to extensive crack formation.

(1) Elastic response stage

At the elastic response stage (±0.475% drift ratio), the connection primarily exhibits elastic behavior, with no plastic deformation or damage accumulation (PEEQ = 0). The von Mises stress distribution reveals localized stress concentrations around the bolt holes and at the corners of the angle steel due to geometric discontinuities, load transfer mechanisms, and contact interactions. However, the stress levels remain below the material's yield strength, confirming that the connection remains elastic. Additionally, both DAMAGEC and DAMAGET remain at zero, indicating the absence of crushing failure or tensile cracking in the concrete components.

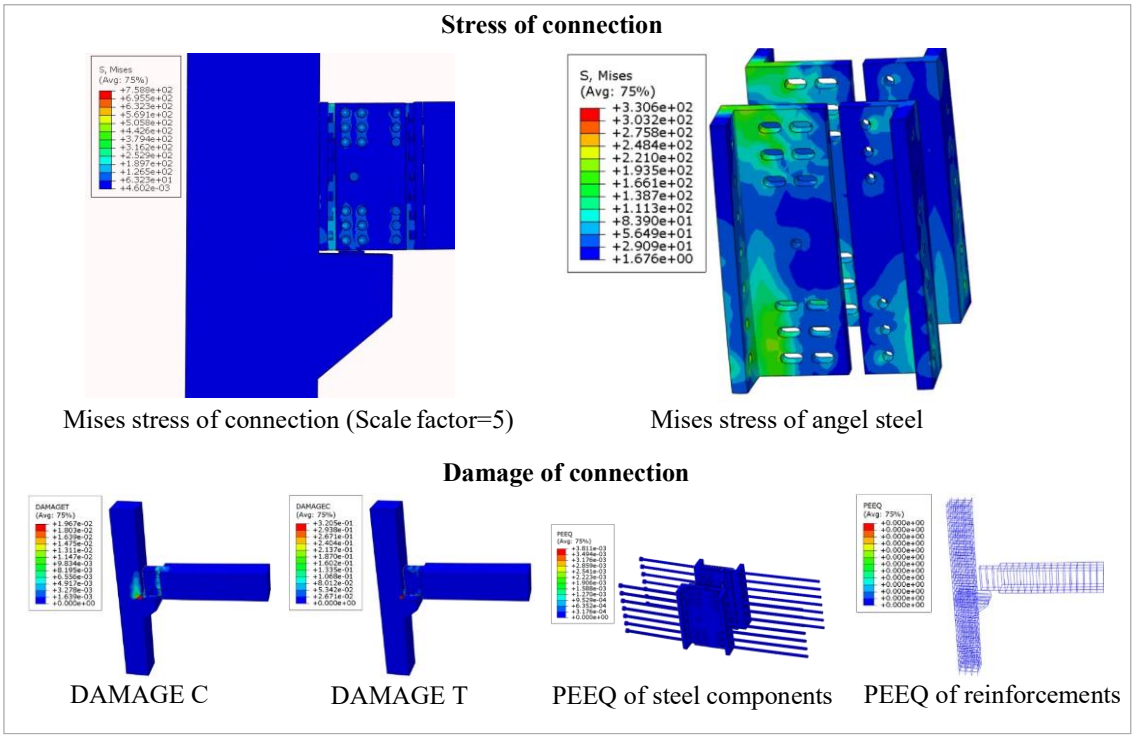

Figure 3-14 0.475% drift ratio hogging moment

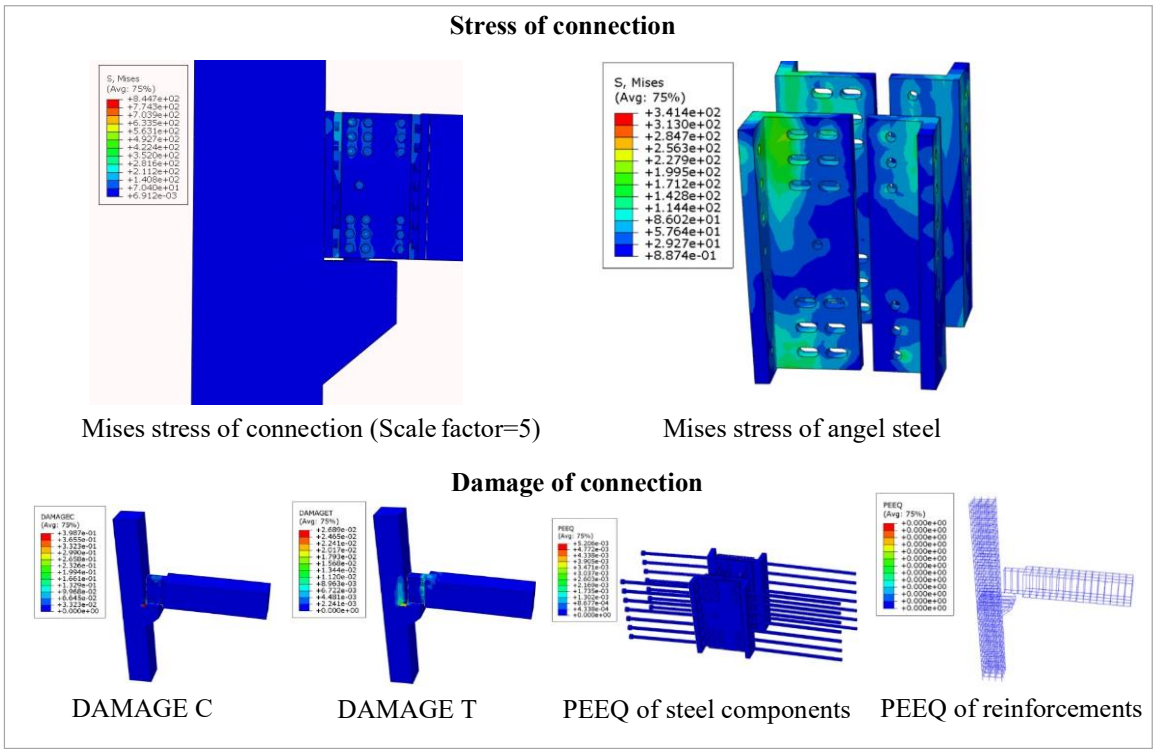

Figure 3-15 -0.475% drift ratio hogging moment

(2) Frictional sliding stage

At the frictional sliding stage (±1.82% drift ratio), the connection transitions from an elastic response to a friction-dominated regime, where energy dissipation occurs through controlled sliding rather than material nonlinearity. The von Mises stress distribution reveals increased stress concentrations around the bolt holes and at the corners of the angle steel, yet most of the structure remains within the elastic range, as indicated by the low equivalent plastic strain (PEEQ) values. The reinforcement remain in the elastic regime, demonstrating that plastic damage is effectively redirected away from the reinforcement, aligning with the damage control design concept to enhance the repairability and resilience of the connection.

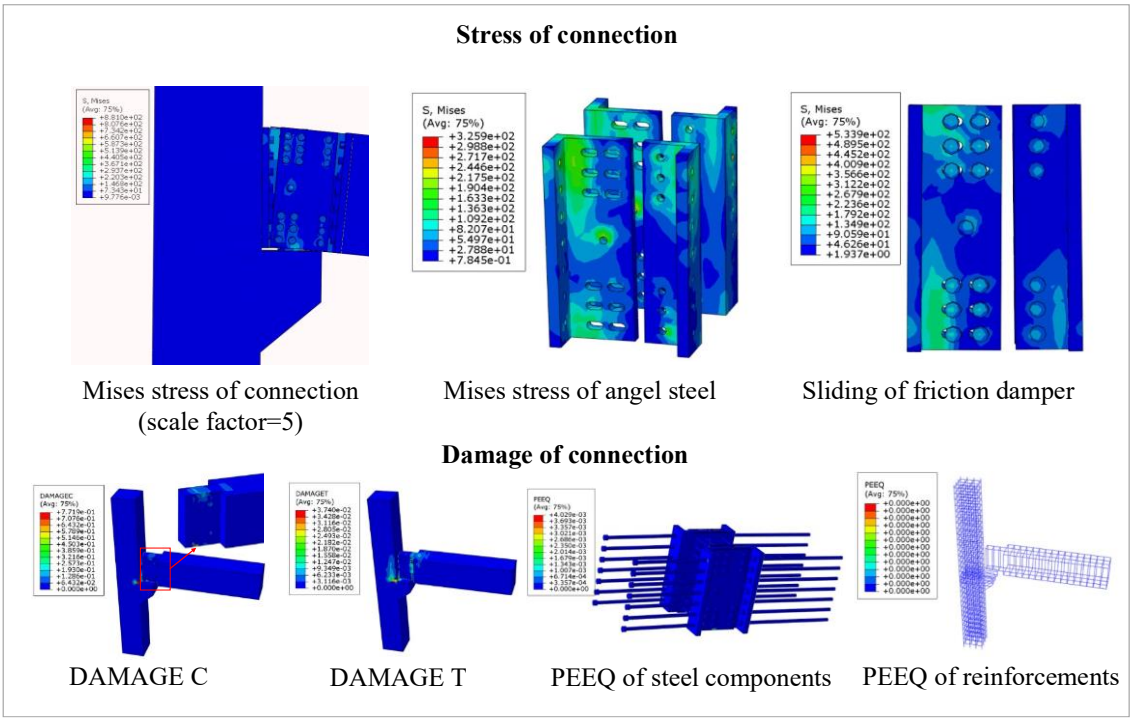

Figure 3-16 1.82% drift ratio hogging moment

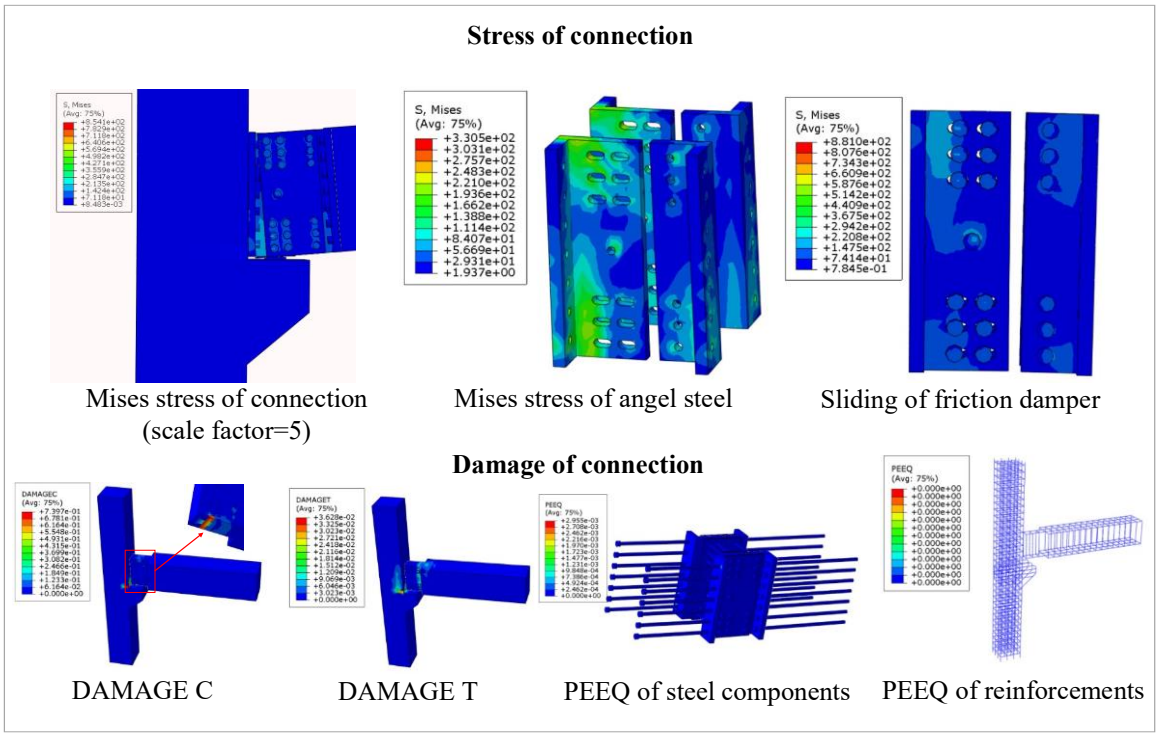

Figure 3-17 -1.82% drift ratio hogging moment

The DAMAGEC and DAMAGET distributions indicate the initiation of concrete damage, primarily concentrated on the top surface of the reduced beam section, the transition between the reduced and unreduced beam sections, and the interface between the corbel and the beam near the column-corbel corner. As displacement increases, the relative movement between the beam and column approaches the predefined gap size, leading to compressive damage (DAMAGEC) at the beam-column interface. Additionally, the corbel and corbel pad induces an asymmetric stress distribution, further contributing to localized compressive damage. This observation suggests potential design improvements, such as embedding a steel plate between the column and beam to reinforce regions prone to damage. Meanwhile, the corbel constrains the beam's movement, and due to its limited length, tensile damage (DAMAGET) develops at the transition between the reduced and unreduced beam sections, as well as on the top surface of the beam. Furthermore, tensile damage at the column-corbel corner is primarily attributed to the tendency of the bolt be pulled out, which induces localized tensile stresses in the surrounding concrete. However, at this drift ratio, the magnitude of DAMAGET remains relatively low, indicating that tensile damage is not yet significant.

(3) Prying-induced plastic deformation stage

At the prying-induced plastic deformation stage (±5.0% drift ratio), the connection exhibits significant inelastic behavior, with a notable increase in stress levels in the angle steel. Stress concentrations develop around the bolt holes, particularly at the top and bottom regions of the angle steel. The segments of the upper and lower rows of bolts near the beam experience plastic deformation under sagging and hogging moments, primarily due to prying action. Despite the high drift ratio, the reinforcement remain within the elastic range, demonstrating effective damage control, which prevents reinforcement yielding and ensures the structural integrity of the connection.

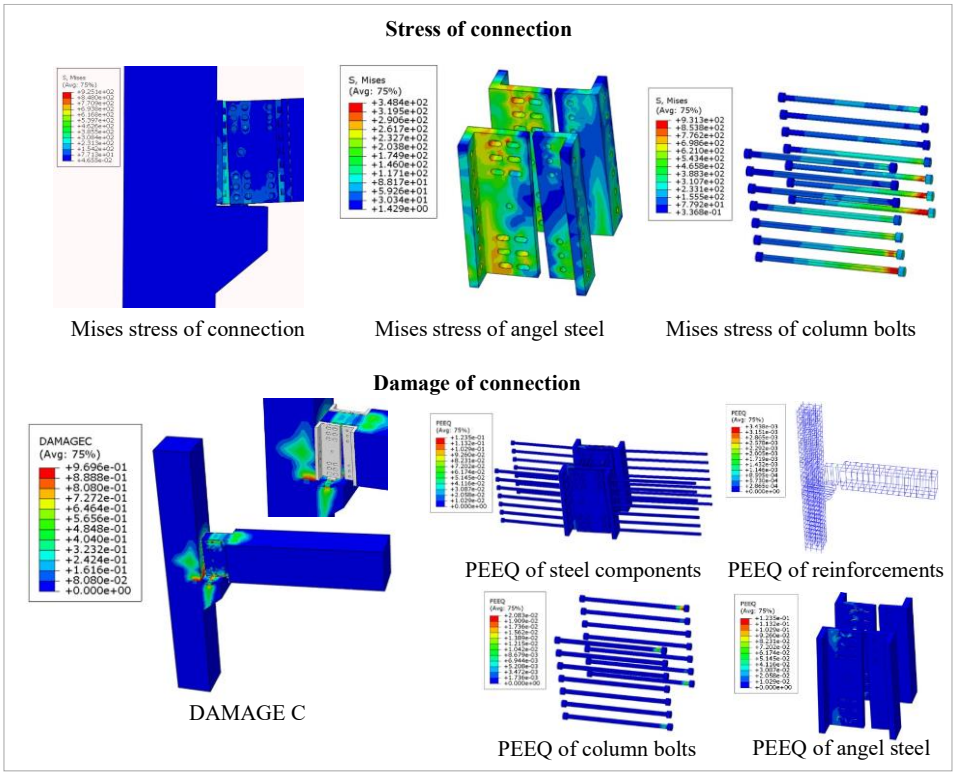

Figure 3-18 5.0% drift ratio hogging moment

The DAMAGEC distribution indicates moderate concrete damage (DAMAGEC < 0.5) in the upper portion of the reduced beam section, the transition between the reduced and unreduced beam sections, and the lower region of the corbel extending along the corbel pad, as well as at the corner of the column-corbel interface. Additionally, severe compressive damage

(DAMAGEC > 0.9) is observed at the interface between the angle steel and the column, where the absence of gaps leads to high localized compressive stresses. As discussed in Stage II, embedding a steel plate in this region could serve as a preventive measure to mitigate excessive compressive damage.

Overall, the observed damage remains within an acceptable range. It should be emphasized that the allowable drift ratio in practical structural applications is typically much lower than the drift ratio reached in this stage. Therefore, this stage (typically occurring at drift ratios exceeding 2%) is primarily conducted to evaluate the ductility capacity of the connection under extreme loading conditions, ensuring that it can undergo significant plastic deformation without experiencing brittle failure. This does not imply that the overall structure remains stable at such drift levels but rather serves to verify the connection's ability to sustain deformation prior to structural instability.

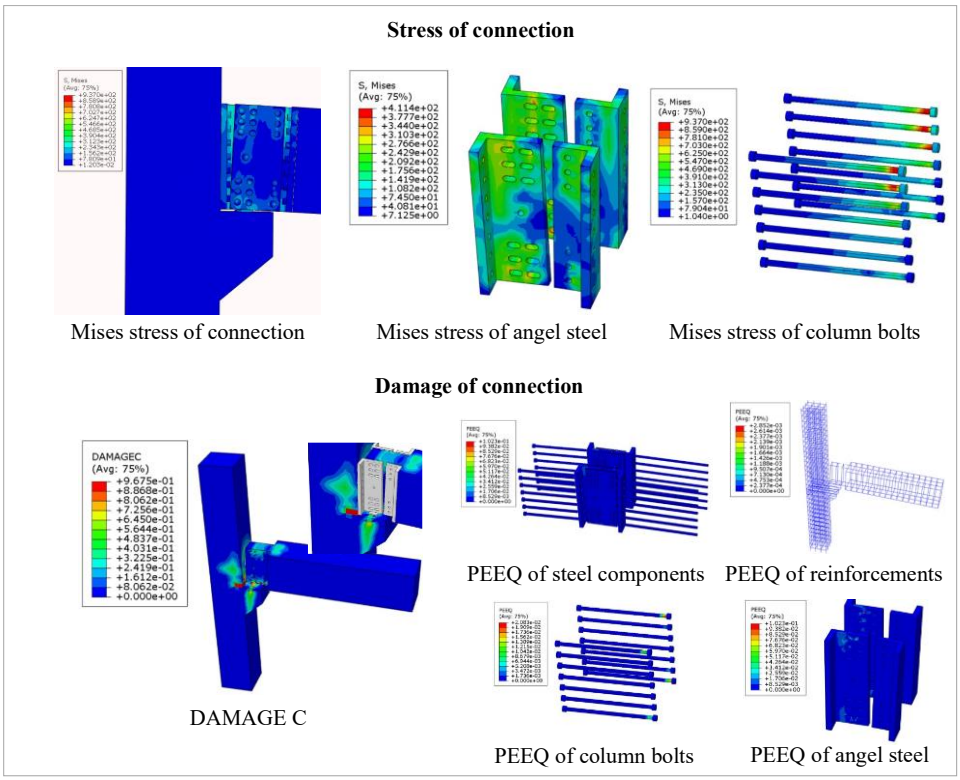

Figure 3-19 -5.0% drift ratio hogging moment

In conclusion, the results provide a comprehensive understanding of the connection's mechanical behavior under increasing drift demands, capturing its transition from an elastic response to inelastic deformation and damage accumulation. The findings validate the proposed constitutive model, confirming that the connection effectively aligns with the intended design strategy by concentrating damage within replaceable components, thereby achieving effective damage control.

3.6.2. Hysteresis behaviors

Fig. 3-21 presents the hysteresis curves of four tested beam-to-column connections, providing insights into their seismic performance [85,86]. The hysteresis loops exhibit stable and full energy dissipation characteristics, typical of friction-based dampers.

Under pretension loads of 60kN, 80kN, and 100kN, the friction damper maintains stable hysteretic behavior up to drift ratios of 2.5%, 3%, and 3%, respectively. Beyond these limits, as the drift ratio increases, a sharp transition in the negative loading direction becomes evident, with the loops losing fullness and indicating the initiation of plastic deformation of connecting bolts. When the drift ratio exceeds 4%, this effect intensifies in both positive and negative directions, indicating progressive localized yielding and damage accumulation.

To further evaluate the performance of the proposed connection, Fig. 3-20 presents a comparison between the hysteresis curves of the P80-1 specimen (A36 steel, pretension load = 80kN) and those of a monolithic connection. Both connections are designed to achieve the same load-bearing capacity. The monolithic connection exhibits a pronounced pinching effect, primarily due to reinforcement yielding, plastic deformation of concrete, and bond-slip between reinforcement and concrete [87]. In contrast, the proposed friction-based connection (P80-1) demonstrates superior deformation capacity, sustaining larger drift ratios while maintaining a highly stable hysteretic response and excellent energy dissipation capability.

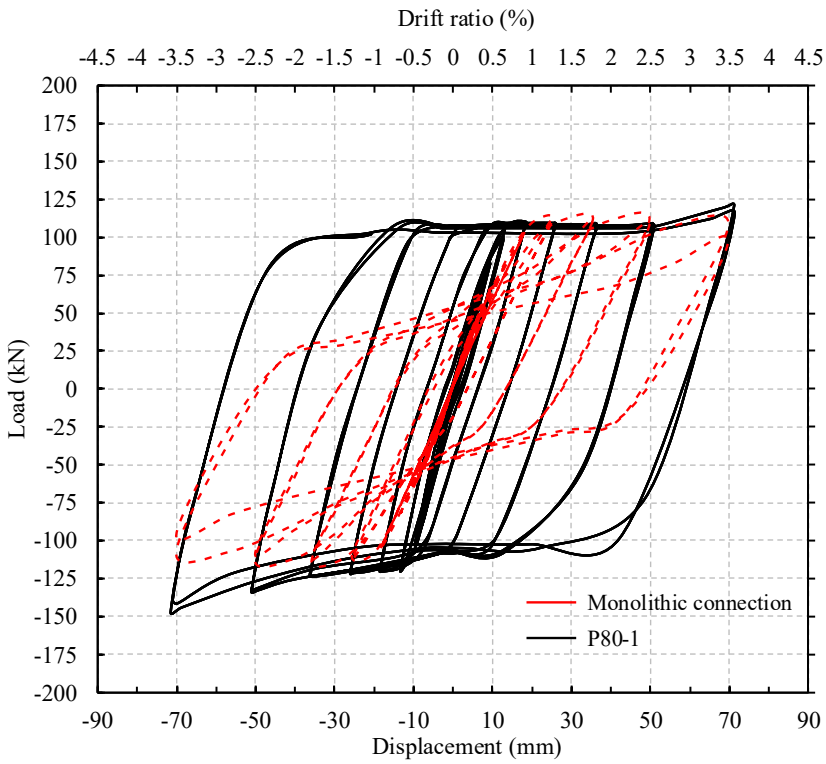

Figure 3-20 Comparison of the hysteresis curves of monolithic connection and P80-1

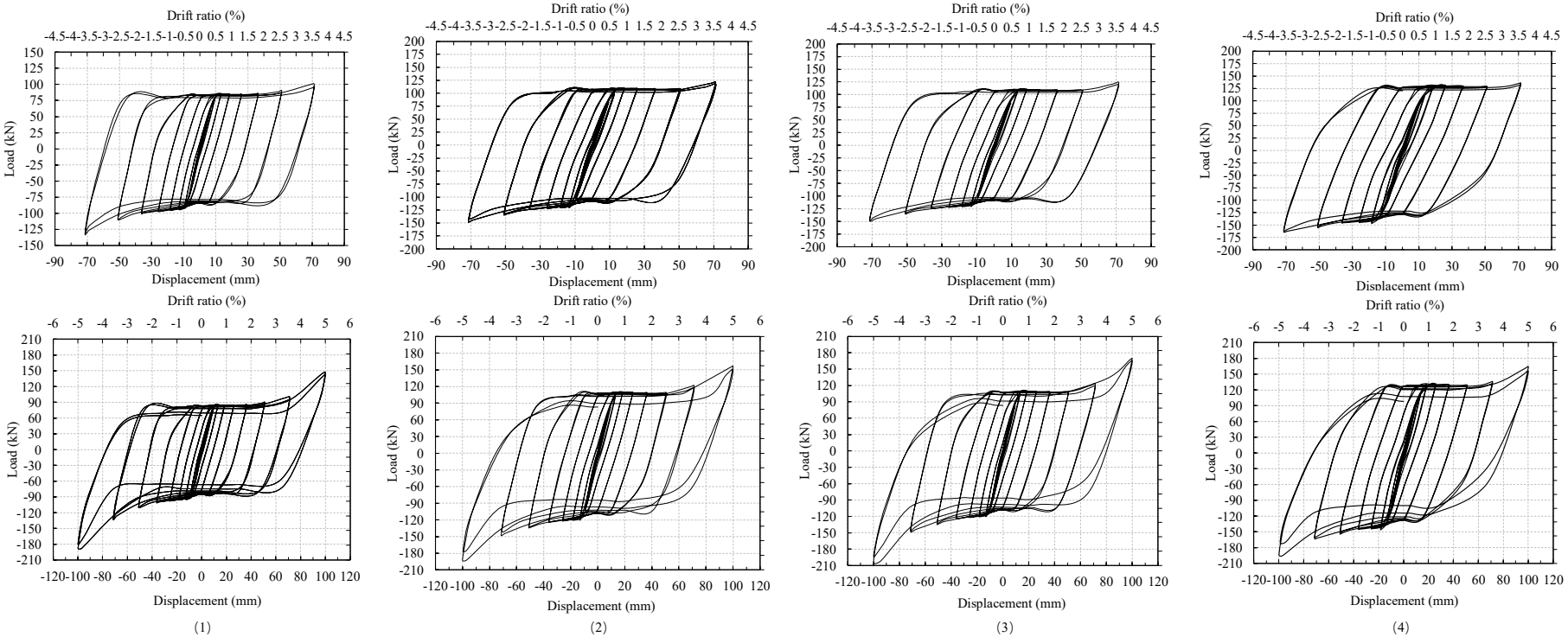

Figure 3-21 Hysteresis curves (1) Pretension load=60kN, A36 (2) Pretension load=80kN, A36 (3) Pretension load=100kN, A36 (4) Pretension load=80kN, A572

3.6.3. Skeleton curves

Fig. 3-22 presents the skeleton curves of P60-1, P80-1, and P100-1, illustrating the progression of the load-displacement response. The behavior progresses from an elastic stage to a frictional sliding stage, after which plastic deformation accumulates in the connecting bolts, resulting in a subsequent increase in load capacity.

It is observed that the stable force during frictional sliding and the drift ratio at the onset of sliding vary among the specimens. Specifically, as the bolt pre-loading forces increase, both the stable force and the drift ratio required for initial sliding increase.

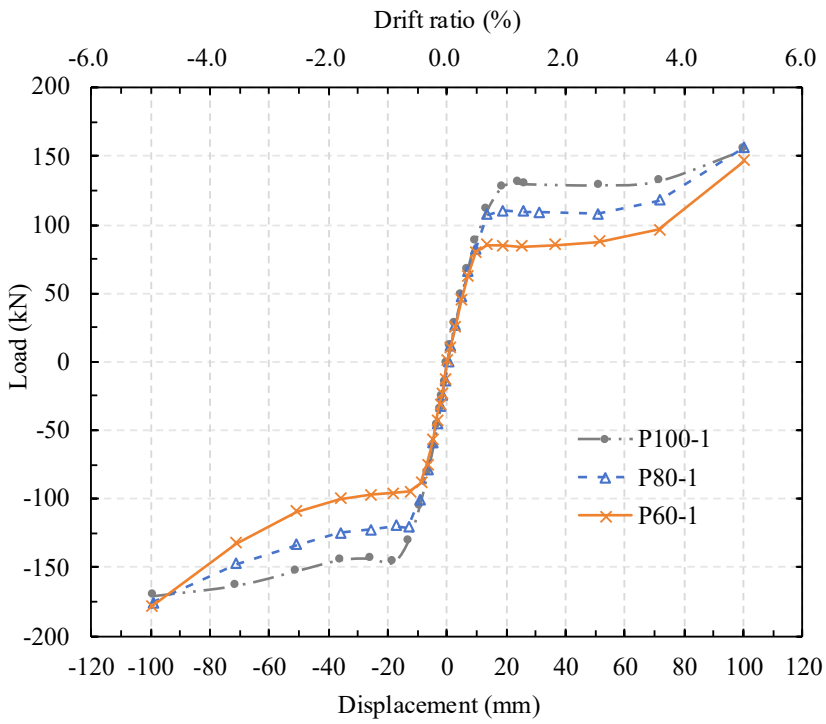

Figure 3-22 Skeleton curves of P100-1, P80-1 and P60-1

As bolt pre-loading force increases from P60-1 to P80-1 by 33.33%, the stable force increases by 29.55%, and the drift ratio at first sliding increases by 40.91%. When normalized with respect to the increase in bolt pre-loading force, the stable force increases by 0.89 per unit increase, while the drift ratio increases by 1.23 per unit increase. When the bolt pre-loading force increases from P80-1 to P100-1 by 25.00%, the stable force increases by 18.45%, and the drift ratio at the onset of sliding increases by 21.51%. The normalized increase in stable force is 0.74, and that of the drift ratio is 0.86 per unit increase in bolt pre-loading force.

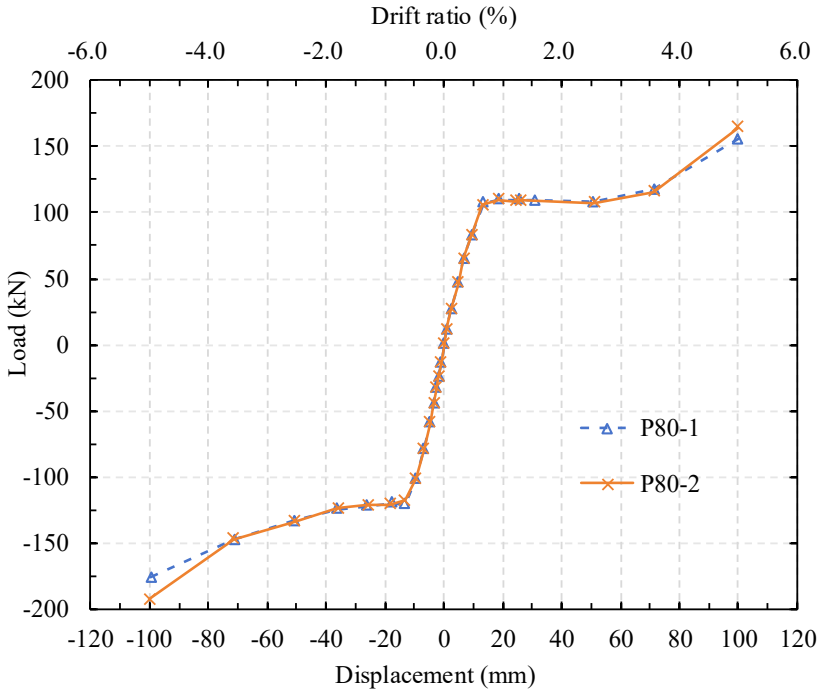

Figure 3-23 Skeleton curves of P80-1 and P80-2

These results indicate that when the bolt pre-loading force is relatively low (P60-1 to P80-1), increasing it leads to a more substantial improvement in both stable force and drift ratio. However, as the bolt pre-loading force increases further (from P80-1 to P100-1), the efficiency of improvement diminishes, suggesting a nonlinear relationship in which higher bolt pre-loading forces require greater plastic deformation of the angle steel before the friction damper is fully activated. Additionally, as the bolt pre-loading force increases, the associated pre-loading losses also become more pronounced, affecting the overall load transfer efficiency and the energy dissipation capacity of the system.

Fig. 3-23 compares the skeleton curves of P80-1 and P80-2. The results indicate that, except for the response at a 5% drift ratio, the overall behavior of both specimens is nearly identical. This suggests that variations in yield strength and ultimate strength have minimal impact on the hysteretic behavior of the proposed connections.

3.6.4. Stiffness degradation curves

The stiffness degradation behavior of the beam-to-column connection can be evaluated through

the positive secant stiffness derived from the hysteresis curve. The secant stiffness for each cycle is determined using the following expression:

$$K_i = \frac{\sum_{i=1}^{n} P_i}{\sum_{i=1}^{n} \delta_i} \tag{3.17}$$

where K_i is the secant stiffness of the ith cycle. P_i denotes the load value of the ith cycle. δ_i is the corresponding displacement value of the ith cycle. n indicates the total number of cycles.

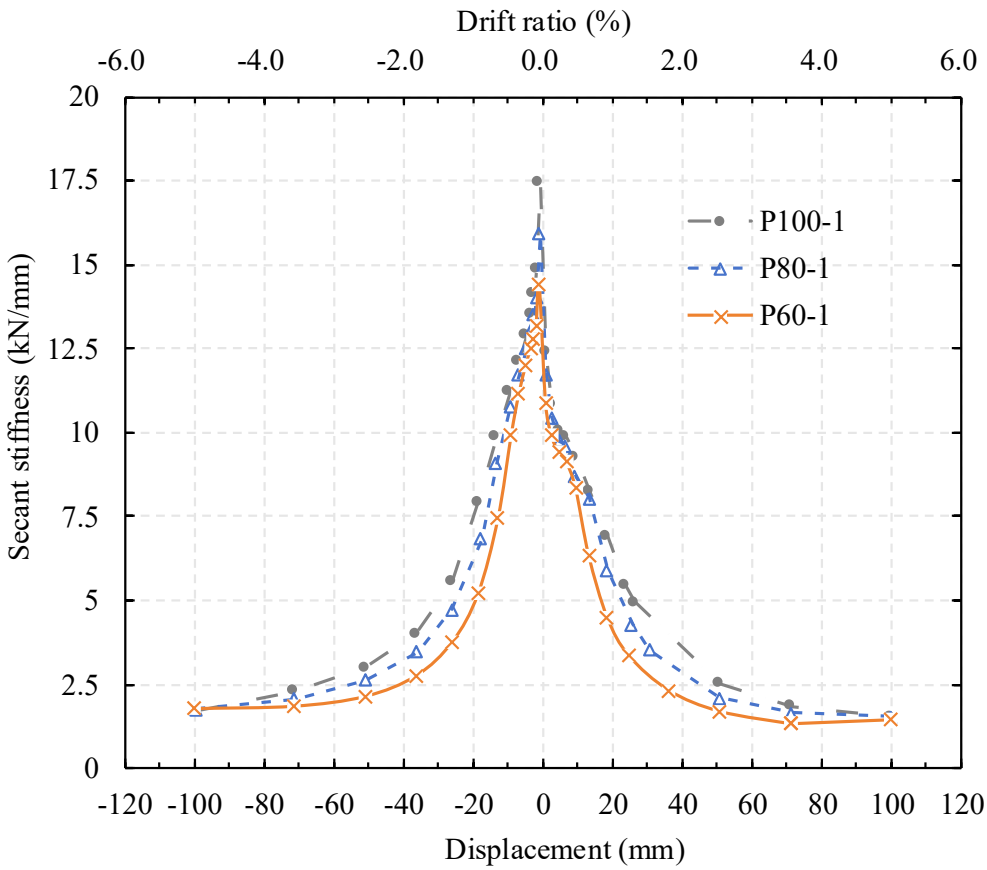

Figure 3-24 Stiffness degradation curves of P60-1, P80-1 and P100-1

Fig. 3-24 presents the stiffness degradation curves of P60-1, P80-1, and P100-1. The results indicate that the proposed connection exhibits distinct semi-rigid behavior, with an initial stiffness significantly lower than that of the monolithic connection.

For specimens with identical geometric configurations, the initial stiffness increases with increasing bolt pre-loading force. Specifically, increasing the bolt pre-loading force from 60

kN to 80 kN results in a 10.29% improvement in initial stiffness. A further increase from 80 kN to 100 kN leads to an additional 9.79% enhancement. Overall, compared to the baseline 60 kN configuration, the cumulative increase in initial stiffness reaches 21.08%.

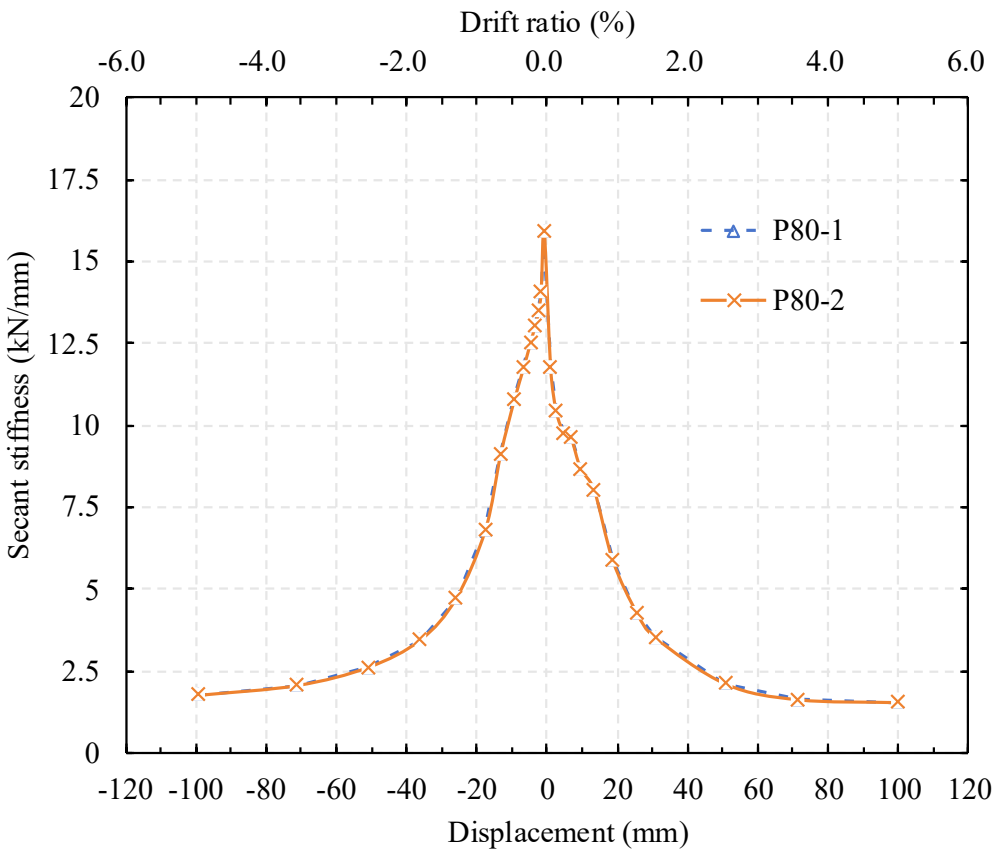

Figure 3-25 Stiffness degradation curves of P80-1 and P80-2

These results demonstrate that the initial stiffness of the proposed connections is significantly influenced by the level of bolt pre-loading force, with higher pre-loading levels leading to greater initial stiffness. This phenomenon can be attributed to the enhanced interface contact stiffness between the angle steel and the beam, provided by the increased pre-loading force. As a result, the deformation zones of the angle steel become more constrained, reducing the effective deformation width and thereby improving the overall initial stiffness of the connection.

Fig. 3-25 presents the stiffness degradation curves of P80-1 and P80-2, which exhibit nearly identical behavior. This indicates that the yield strength and ultimate strength of steel have a negligible influence on the stiffness degradation characteristics of the proposed connection.

3.6.5. Energy dissipation capacity

Energy dissipation is a critical parameter for evaluating the seismic performance of structural connections. Fig. 3-26 presents the cumulative energy dissipation of the proposed connections compared to the monolithic connection. The results indicate that the proposed connections exhibit significantly greater energy dissipation than the monolithic connection at equivalent displacement or drift ratios.

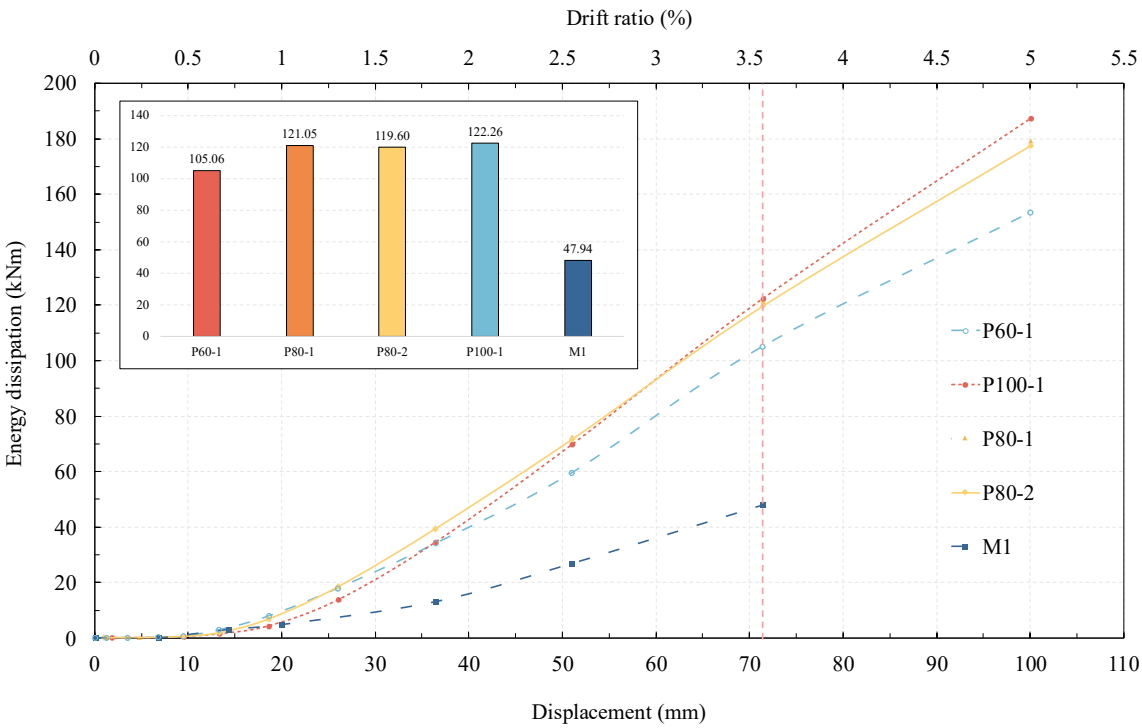

Figure 3-26 Cumulative energy dissipation

Specifically, when the displacement reaches 71.4 mm, P80-1 serves as a reference specimen due to its design load capacity being equivalent to that of the monolithic connection, making it a suitable benchmark for evaluating the seismic performance of precast connections. Both the P100-1 specimen and P80-2 specimens demonstrate an energy dissipation capacities comparable to that of P80-1. In contrast, the energy dissipation capacity of P60-1 is 86.78% of

P80-1, indicating a noticeable reduction. The M1 specimen exhibits the lowest energy dissipation capacity, reaching only 39.72% of P80-1, which is significantly lower than the other specimens. These findings suggest that the proposed connections, owing to their friction-based behavior, achieve substantially higher energy dissipation than the monolithic connection.

Regarding the effect of bolt pre-loading forces, an increase in pre-loading forces generally enhances energy dissipation, as it improves the load-carrying capacity of the connection at a given displacement level. However, a higher bolt pre-loading force does not necessarily result in increased energy dissipation, as observed in the comparison between P80-1 and P100-1. This discrepancy arises because excessive bolt pre-loading force leads to stress concentration, accelerating the formation of plastic damage. As plastic damage accumulates, the hysteresis loops become less stable and less full compared to those observed under small displacement amplitudes, ultimately reducing energy dissipation. This phenomenon is further examined in ***Section 3.6.2***.

Additionally, the material properties of the steel components have minimal influence on energy dissipation, primarily because they maintain similar load-carrying capacities and hysteresis loop stability under identical displacement levels.

Chapter 4 Multi-linear hysteresis model of DFED-BCC

This chapter analyzes the working mechanism of the proposed connection in four distinct stages to provide a comprehensive understanding of its structural behavior and design principles. This staged approach enables a systematic evaluation of the connection's load transfer characteristics, deformation patterns, and overall performance under various loading conditions.

4.1. Progressive Working Mechanism of the Proposed Connection

The working mechanism of the DFED-BCC can be categorized into four distinct stages based on its force-displacement response: the Elastic Phase, Localized Yielding Phase, Frictional Sliding Phase, and Prying-Induced Plastic Deformation Phase. These stages describe the progressive evolution of the connection's mechanical behavior under loading. The following equations and Fig. 4-1 outline the key phases of the DFED-BCC, providing a clear framework for understanding its structural performance.

This chapter presents a preliminary working mechanism based on analytical investigation. The specific coefficients for each phase require further refinement and validation through experimental results and systematic post-experimental parametric analysis. These subsequent studies will ensure the accuracy and practical applicability of the proposed mechanism.

$$P = \begin{cases} P_1 = K_{T1}u & (0 < u < u_1) \\ P_2 = P_1 + K_{T2}(u - u_1) & (u_1 < u < u_2) \\ P_3 = F_f & (u_2 < u < u_3) \\ P_3 = F_f + K_{T4}(u - u_3) & (u_3 < u < u_4) \end{cases} \tag{4.1}$$

where, P_n is the force in n stage. u is the total displacement. K_{Tn} is the tangential stiffness of n stage. F_f is the friction force in the third stage. K_{Tn} in each stage depends on geometry and preload forces of the connection, detail analysis will be presented in the following parts.

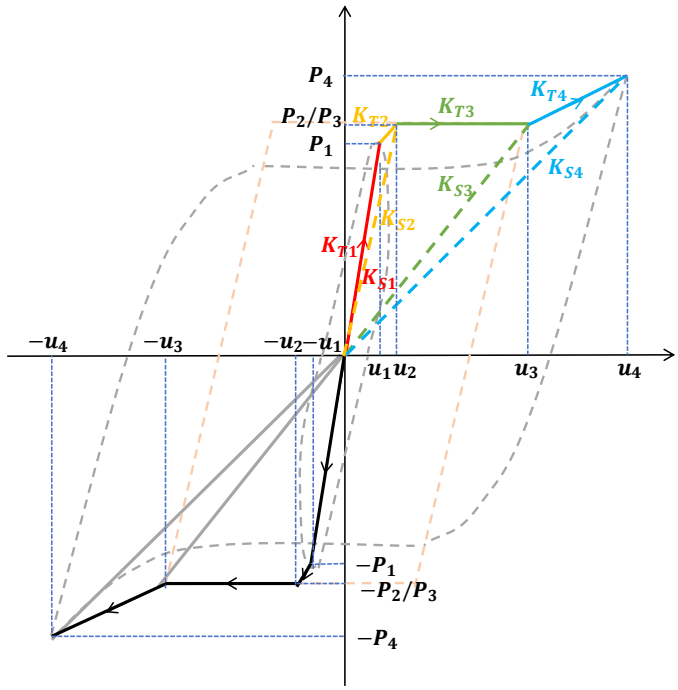

Figure 4-1 Proposed four-stage Multi-Linear Hysteresis Model

Behavior in different stages:

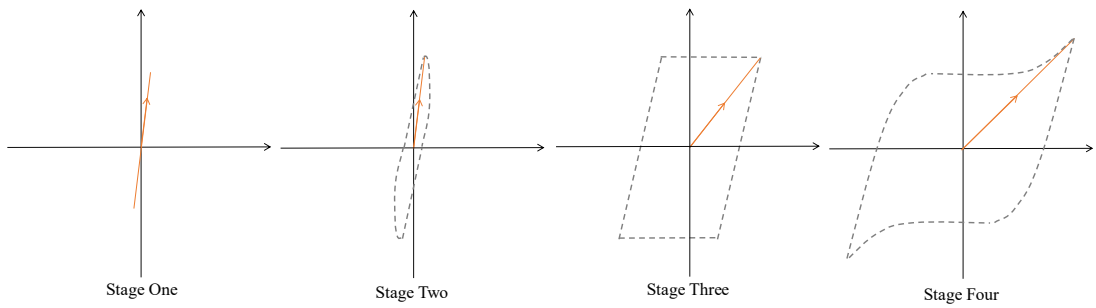

Figure 4-2 Hysteresis behavior of the DFED-BCC in each stage

4.2. Stage one: Elastic stage

In the initial stage, the system remains within the elastic range, during which both the angle steel and bolts experience purely elastic deformation, resulting in a linear force-displacement relationship. During this phase, the deformation remains small, and no theoretical energy dissipation is expected. However, minor frictional resistance or micro-slipping at the interfaces may introduce limited energy dissipation, explaining the deviation from an ideal elastic response. The connection stiffness in this stage is primarily governed by the elastic properties

of its components. As illustrated in Fig. 4-3, the red line represents the elastic stage. The system displacement is predominantly attributed to the elastic deformation of the angle steel, which induces a corresponding rotation of the beam, denoted as Δα.

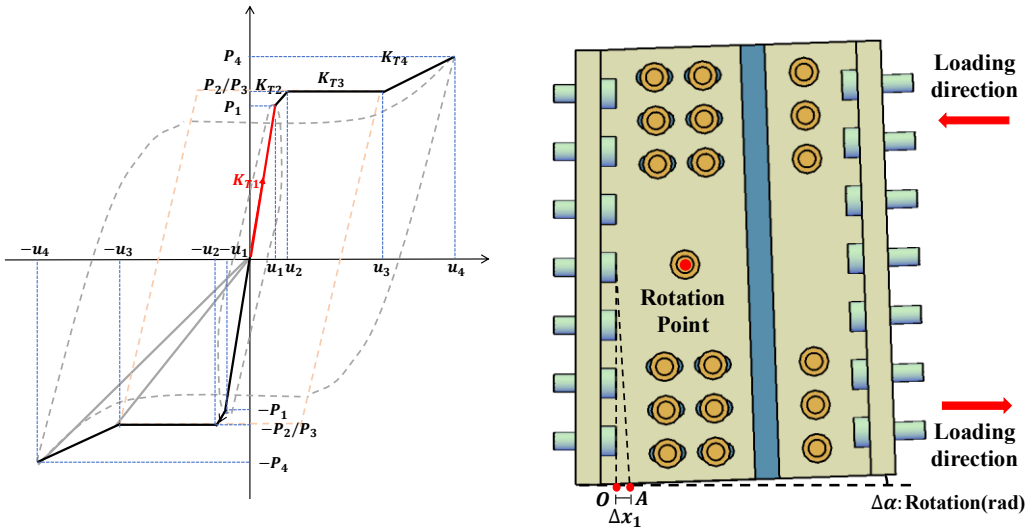

Figure 4-3 Working mechanism in elastic stage

4.2.1. Initial Stiffness

In this stage, the initial stiffness of the connection primarily depends on angle steel, which can be approximated using the model of a double-web angle connection. Kishi and Chen developed an analytical expression for the initial stiffness based on experimental data from Lipson [61]. The assumptions underlying this model can be found in ***Section 2.4***. This model is based on the bending behavior of a moderately thick plate (thickness-to-length ratio >0.05 or 0.1). For a single-web angle connection, the initial rotational stiffness can be expressed as:

$$R_{ki} = G\frac{t_a^2}{3}\frac{\alpha coh(\alpha\beta)}{\alpha\beta\alpha coh(\alpha\beta) - sinh(\alpha\beta)} \tag{4.2}$$

Thus, for double-web connection:

$$R_{ki} = 2G\frac{t_a^2}{3}\frac{\alpha coh(\alpha\beta)}{\alpha\beta\alpha coh(\alpha\beta) - sinh(\alpha\beta)} \tag{4.3}$$

Where R_{ki} represents the initial stiffness; t_a is the web angle thickness; α=4.2967 for a Poisson's ratio of 0.3; Additionally, $\beta = g_c/l_p$ where l_p is the web angle length, and $g_c =$

$g_1 - k - t_a - w/2$ is the gage distance from the fixed support line to the free edge. g_1 denotes the distance from the angle heel to the center of the bolt holes near the beam web on the outstanding leg. k is the fillet radius of the angle w is the nut width of the fastener.

Here, the stiffness of the bolts is neglected, as they are typically embedded, welded, connected using bolt couplers, or subjected to significant preload in this type of connection. These configurations render the contribution of bolt deformation to the overall initial stiffness negligible. Firstly, the bolts experience constrained boundary conditions, such as embedment in concrete or rigid attachment to steel components, which significantly restrict their deformation capacity. Moreover, in bolted connections with substantial preload, load transfer primarily occurs through friction between the connected elements rather than through bolt deformation. Therefore, the assumption of an infinitely rigid bolt is a reasonable simplification in the context of this analysis, ensuring that the primary focus remains on the deformation and stiffness contributions of the angle steel.

As observed in ***Section 3.6.4***, bolt pre-loading forces have a significant influence on the initial rotational stiffness, an effect that is not accounted for in Kishi and Chen's model. To evaluate this impact, the connection with the lowest bolt pre-loading force is taken as the reference. The initial rotational stiffness of P60-1, as obtained from the FEA results and Kishi and Chen's model, is calculated and presented in Table 4-1.

Table 4-1 Comparison of FEA result and Kishi and Chen's model

Kishi and Chen's model	FEA
10149kNm/rad	19574kNm/rad

As expected, the FEA results are significantly higher than those predicted by Kishi and Chen's model. This discrepancy cannot simply be attributed to modeling error, despite the model exhibiting a relatively large deviation [88]. Therefore, it is necessary to introduce a pre-loading coefficient to modify g_c, as pre-loading forces enhance the interface contact stiffness between the angle and the beam web, potentially reducing the effective deformation width. The specific

form and magnitude of this coefficient require further exploration and refinement through additional parametric studies.

4.3. Stage two: Localized yielding stage

As the displacement increases, localized yielding begins to occur in specific regions of the angle steel. This localized plasticity results in a reduction of the system's stiffness, marking the onset of the localized yielding stage. The energy dissipation curve during this phase exhibits the typical characteristics of metallic energy dissipation shown in Fig.4-4. The occurrence of this stage depends on the relationship between the applied bolt preload and the friction forces it generates. If the friction forces do not exceed the maximum forces developed during the elastic stage, localized yielding will not occur; otherwise, this stage will take place. This stage serves as a transition between the elastic stage and the frictional sliding stage.

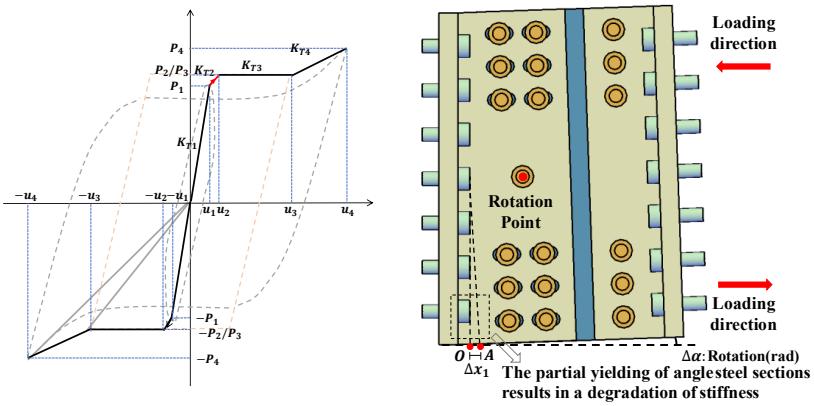

Figure 4-4 Working mechanism in localized yielding stage

4.4. Stage three: Frictional sliding stage

As the displacement continues to increase, stress in the angle steel also rises, resulting in an increase in the forces at the beam end. When the force exceeds the maximum static friction force, relative sliding occurs between the angle steel and the friction pads, causing the connection to function as a friction damper. In this stage, the forces remain constant despite the increasing displacement, leading to zero tangent stiffness. The energy dissipation curve, as shown in Fig. 4-5, exhibits a typical rectangular hysteresis loop, characteristic of a friction damper. Plastic deformation does not accumulate during this stage, and the connection exhibits both significant energy dissipation capacity and stable hysteretic performance. These

characteristics make it the primary design stage for the connection.

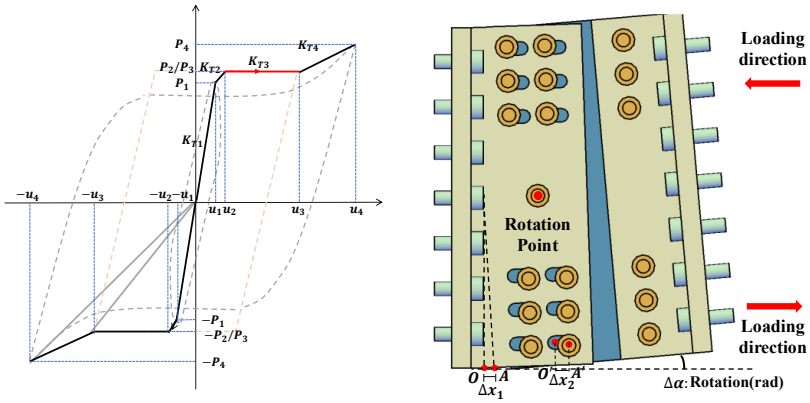

Figure 4-5 Working mechanism in frictional sliding stage

4.4.1. Rotational Stiffness

Assuming the bolt locations are symmetrically arranged, such that $d_1 = d_4, and\ d_2 = d_3$, and considering that the magnitudes of the friction forces are independent of their displacements, it follows that $F_1 = F_2 = F_3 = F_4$. The moment induced by the relative rotation of the friction damper at the BCC, generated by the coupler arising from the relative motion within the friction damper, can be expressed and calculated as follows:

$$M_{eq} = F_1 \times d_1 + F_2 \times d_2 + F_3 \times d_3 + F_4 \times d_4 \tag{4.4}$$

For a given rotation angle, the relative displacements exhibit a linear relationship with the distances between the bolts. This implies that the relative displacement at any bolt location is directly proportional to its perpendicular distance from the axis of rotation.

$$\alpha = sin\alpha = \frac{\Delta l_1}{d_1} = \frac{\Delta l_2}{d_2} = \frac{\Delta l_3}{d_3} = \frac{\Delta l_4}{d_4} \tag{4.5}$$

The rotational stiffness of connection can be expressed as:

$$R = \frac{M_{eq}}{\Delta\alpha} = \frac{F_1 {d_1}^2}{\Delta l_1} + \frac{F_2 {d_2}^2}{\Delta l_2} + \frac{F_3 {d_3}^2}{\Delta l_3} + \frac{F_4 {d_4}^2}{\Delta l_4} \tag{4.6}$$

Given that distance d_1, d_2, d_3 and d_4 are linearly related to d_1, and determined by total bolt spacing d. If there are five bolts, the relationships of spacings are: $d_1 = d_4 = \lambda d_2 = \lambda d_3$, the corresponding

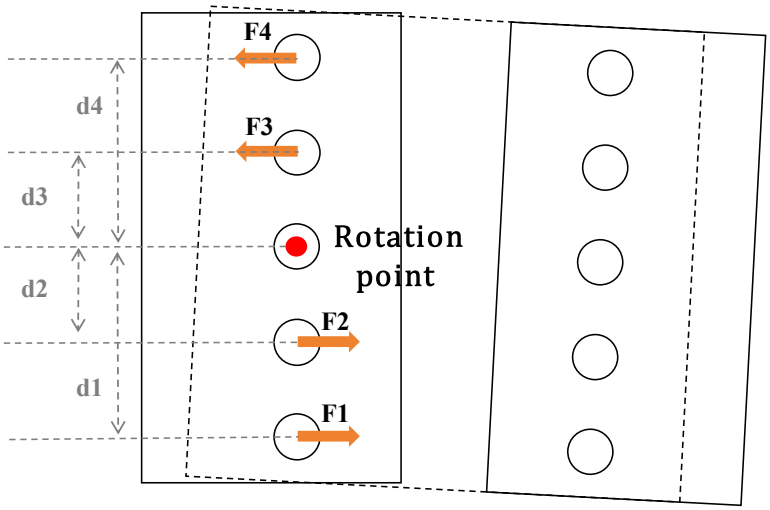

Figure 4-6 Parameters of rotational stiffness

relative displacements can be expressed as: $\Delta l_1 = \Delta l_4 = \lambda \Delta l_2 = \lambda \Delta l_4$. Thus, the rotational stiffness of connection can be written as:

$$R = \frac{F_1 {d_1}^2}{\Delta l_1} + \frac{F_2 {d_2}^2}{\Delta l_2} + \frac{F_3 {d_3}^2}{\Delta l_3} + \frac{F_4 {d_4}^2}{\Delta l_4} = \left(2\frac{1}{\lambda} + 2\right)\frac{F_1 {d_1}^2}{\Delta l_1} \tag{4.7}$$

This is the formula to calculate rotational stiffness of DFED-BCC with five bolts. For configurations with a different number of bolts, a similar formula applies, with the stiffness being linearly related to $\frac{F_1 {d_1}^2}{\Delta l_1}$. The relationship can be expressed generally as $\beta \frac{F_1 {d_1}^2}{\Delta l_1}$.

Dynamic friction forces are determined by dynamic friction coefficient and bolt pre-loading forces: $F = \mu_k N$. The formula for rotational stiffness of connection can be written as:

$$R = \beta \frac{\mu_k N {d_1}^2}{\Delta l_1} \tag{4.8}$$

For a given connection design, where the initial value of the friction coefficient μ_k, and bolt spacing d_1 and β are fixed, the rotational stiffness of the connection is governed solely by Δl_1, assuming the reduction in the friction coefficient is negligible. This relationship implies that the rotational stiffness R decreases linearly with an increase in the relative displacement Δl_1 or, equivalently, with an increasing drift ratio.

$$R \propto \frac{1}{\Delta l_1} \tag{4.9}$$

4.4.2. Axial Stiffness of friction damper

The friction forces can be calculated by:

$$F = k\Delta l = \mu_k N \tag{4.10}$$

Where k is the axial stiffness of the friction damper. Δl is the axial stiffness of the friction damper. μ_k is the dynamic friction coefficient. And N is the bolt pre-loading forces.

The axial stiffness of the friction damper can be expressed as:

$$k = \frac{\mu_k N}{\Delta l} \tag{4.11}$$

So, the rotational stiffness of the connection can be rewritten by:

$$R = \frac{M_{eq}}{\Delta\alpha} = \beta\frac{Fd^2}{\Delta l} = \beta k d^2 \tag{4.12}$$

This relationship indicates that the rotational stiffness of the connection is linearly related to the axial stiffness of the friction damper when $\Delta l \propto \Delta l_1$.

$$R \propto k$$

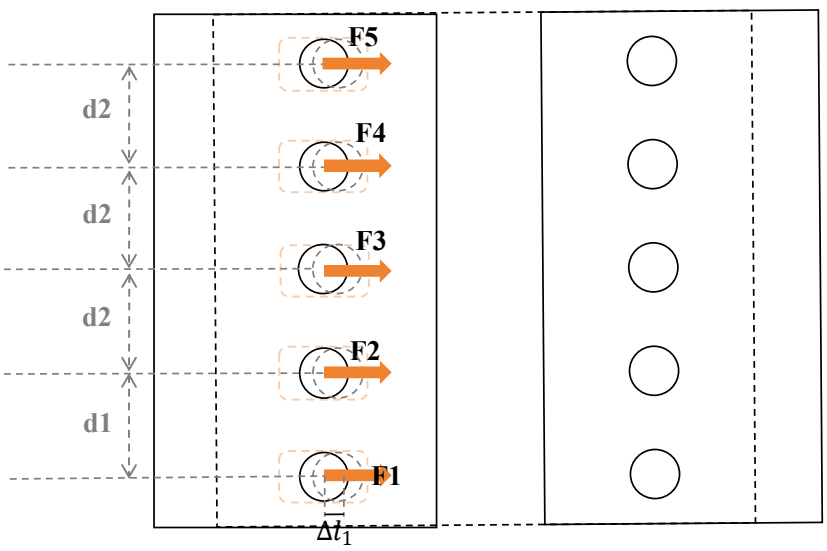

Figure 4-7 Parameters of stiffness

This linear relationship simplifies the design process by allowing designers to estimate the rotational

stiffness of the connection through the axial stiffness of the friction damper. Since determining the axial stiffness involves simpler calculations and testing, this approach provides a practical and efficient method for designing connections with desired rotational properties.

4.5. Stage Four: Prying-induced plastic stage

As the displacement increases, the deformation of the angle steel becomes more significant, resulting in a pronounced prying action. Combined with the rotational effects, this prying action induces plastic deformation in the top and bottom bolts. Consequently, the connection transitions from the frictional sliding stage to a prying-induced plastic stage, marked by a significant increase in internal forces. This transition is evident in the hysteresis curves, where the initially full and stable loops observed in the third stage evolve into pinched loops with tapered ends, indicative of a pinching effect.

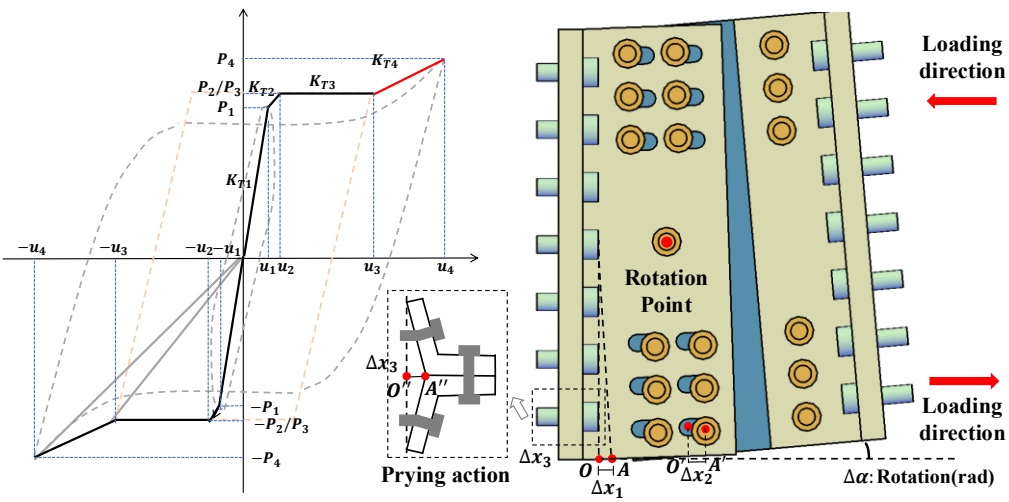

Figure 4-8 Working mechanism in prying-induced plastic stage

Moreover, the elevated internal forces in the connection lead to localized plastic deformation at the contact interfaces between the pretensioned bolts, steel plates, and angle steel. This deformation results in a loss of bolt pretension, reducing the frictional resistance in the flattened regions of the hysteresis curve relative to the third stage. With continued cyclic loading, the accumulation of plastic strain exacerbates the frictional resistance loss, further amplifying the pinching effect and diminishing the overall energy dissipation in subsequent cycles.

In conclusion, the hysteresis behavior of the DFED-BCC is inherently displacement-dependent.

Under normal service conditions or during small seismic events, the connection is expected to exhibit elastic behavior, maintaining high stiffness and structural integrity without any permanent deformation. In this stage, the friction dampers remain inactive, eliminating concerns related to wear or fatigue. During moderate to large seismic events, the connection transitions to operating as a friction damper, effectively acting as "fuses" that limit the forces transmitted to structural members, thereby protecting critical components from excessive loading [89]. Once the displacement exceeds the design limit in the third stage, the hysteresis behavior of the bolts provides a ductile failure mechanism, mitigating the risk of brittle failure.

The allowable displacement limit can be tailored based on the permissible story drift requirements for different structural systems and performance objectives, ensuring the connection satisfies both safety and performance criteria under varying seismic demands.

Chapter 5 Discussion on DFED-BCC

5.1. Performance evaluation

Based on the results presented in Chapter 3, the proposed connection exhibits the characteristics of a semi-rigid connection. From a seismic performance perspective, it demonstrates moderate initial stiffness and favorable energy dissipation capacity, both of which are significantly influenced by bolt preloading forces. Moreover, under the same design load capacity, the proposed connection objectively achieves superior seismic performance compared to monolithic connections. Additionally, as the displacement of the friction damper can be adjusted by modifying the slot length, the connection's seismic response is directly correlated with displacement demand, making it well-suited for performance-based seismic design (PBSD).

From a load transfer mechanism perspective, the primary frictional force stages can be effectively controlled, enabling the precise design of beam-end yielding moments during the design phase. Due to moment equilibrium, this further allows for controlled column moment demand, facilitating the strong-column, weak-beam design principle. Furthermore, the high energy dissipation capacity of the friction damper effectively mitigates stress concentrations in the joint core region, alleviating stress penetration effects and enhancing the integrity of the joint core.

From a constructability standpoint, the proposed connection requires only bolt tightening on-site, eliminating the need for additional welding. The connection’s regular-shaped components further simplify fabrication, removing the necessity for water jet cutting or other specialized machining, leading to process simplification and cost reduction. Moreover, since corbels provide temporary support, the proposed connection is expected to be assembled without additional formwork or temporary supports, enhancing on-site efficiency.

From a sustainability perspective, the proposed connection is designed to protect concrete components and reinforcement, enabling potential reuse of structural elements when a structure is decommissioned due to functional modifications or upgrades rather than damage.

In conclusion, the proposed connection is expected to provide a more structurally efficient, constructible, and sustainable alternative to traditional monolithic connections. By balancing seismic performance, constructability, and sustainability while ensuring a clear load transfer path, it presents a promising solution for resilient and sustainable structures within the framework of modern performance-based and demountable design approaches.

5.2. Research Limitations

The research limitations are examined from two perspectives: the proposed connection and the research methodology.

(1) The proposed connection

First, regarding the proposed connection, one notable limitation was its relatively high residual displacement, which was why friction dampers were typically implemented in prestressed frames. To mitigate this issue, a more detailed investigation was carried out. Potential enhancements included incorporating shape memory alloy (SMA) bars, helical springs, Belleville springs, or ring springs to improve self-centering capability. However, the implementation of these components introduced significant construction complexity. Therefore, their feasibility needed to be carefully evaluated based on the specific structural requirements and performance demands before adoption.

Second, the angle steel used in the proposed connection was recommended to be fabricated based on standard dimensions of unequal-angle steel. However, the feasibility of using off-the-shelf steel components without additional processing required further investigation.

Furthermore, to avoid the use of pre-loaded bolts or bolt couplers, the proposed connection embedded bolts within the beam and column. This method necessitated a thorough evaluation

of the bond behavior between the embedded bolts and concrete, as it could influence the overall connection performance.

Additionally, potential challenges related to transportation and handling need to be carefully assessed to determine whether this approach introduced practical difficulties during construction and assembly.

(2) The research methodology

In the finite element modeling, the contact between the friction pad and steel plate was idealized, whereas, in reality, the friction coefficient evolved with accumulated energy dissipation. This phenomenon was extensively discussed in the study by Latour et al. [90], which provided a more detailed examination of its variation under cyclic loading.

Additionally, the model used to simulate the monolithic connection could only reproduce a hysteresis curve like the experimental response but did not accurately capture the bond-slip relationship. To enhance the realism of the simulation, future studies could consider incorporating nonlinear spring elements to develop a more refined solid model and further investigate these complex behaviors.

Furthermore, the assumptions made in analyzing the load path were idealized. However, FEA results indicated that the rotation point did not lie at midsection, and the top and bottom ends were not fully free, deviating from the initial assumptions. As a result, the equation derived from these assumptions exhibited significant discrepancies, which could be largely attributed to the idealization of boundary conditions and load transfer mechanisms. To establish a more accurate relationship for initial rotational stiffness, the underlying assumptions might need to be revised and refined to better reflect the actual structural behavior observed in numerical simulations.

Reference list

[1] Jaillon L, Poon CS, Chiang YH. Quantifying the waste reduction potential of using prefabrication in building construction in Hong Kong. Waste Management 2009;29:309–20. https://doi.org/10.1016/j.wasman.2008.02.015.

[2] Yee AA. Social and Environmental Benefits of Precast Concrete Technology. Pcij 2001;46:14–9. https://doi.org/10.15554/pcij.05012001.14.19.

[3] Breccolotti M, Gentile S, Tommasini M, Materazzi AL, Bonfigli MF, Pasqualini B, et al. Beam-column joints in continuous RC frames: Comparison between cast-in-situ and precast solutions. Engineering Structures 2016;127:129–44. https://doi.org/10.1016/j.engstruct.2016.08.018.

[4] Hamill P, Bechara CH, Bertolini M, Wilden H, Biebighauser M. Precast Concrete Value Engineering Accommodates Difficult Site. Pcij 2006;51:18–40. https://doi.org/10.15554/pcij.07012006.18.40.

[5] Lee J-Y, Heo JH, Byun H-W, Kim K-H, Shin D. Comparison of emulation evaluation methods of precast concrete moment resistance structures. Engineering Structures 2023;291:116416. https://doi.org/10.1016/j.engstruct.2023.116416.

[6] Hall JF, Holmes WT, Somers P. Northridge earthquake of January 17, 1994: reconnaissance report. vol. 1. Earthquake Engineering Research Institute; 1995.

[7] Au EV. The mechanics and design of a non-tearing floor connection using slotted reinforced concrete beams 2010.

[8] Fenwick R, Megget L. Elongation and load deflection characteristics of reinforced concrete members containing plastic hinges. Bulletin of the New Zealand Society for Earthquake Engineering 1993;26:28–41.

[9] Korkmaz HH, Tankut T. Performance of a precast concrete beam-to-beam connection subject to reversed cyclic loading. Engineering Structures 2005;27:1392–407.

[10] Thomsen A, Van der Flier K. Replacement or renovation of dwellings: the relevance of a more sustainable approach. Building Research & Information 2009;37:649–59.

[11] Abramson DM. Obsolescence: An architectural history. University of Chicago Press; 2016.

[12] Cai W, Wan L, Jiang Y, Wang C, Lin L. Short-Lived Buildings in China: Impacts on Water, Energy, and Carbon Emissions. Environ Sci Technol 2015;49:13921–8. https://doi.org/10.1021/acs.est.5b02333.

[13] Monteiro PJM, Miller SA, Horvath A. Towards sustainable concrete. Nature Mater 2017;16:698–9. https://doi.org/10.1038/nmat4930.

[14] Devènes J, Bastien-Masse M, Fivet C. Reusability assessment of reinforced concrete components prior to deconstruction from obsolete buildings. Journal of Building Engineering 2024;84:108584. https://doi.org/10.1016/j.jobe.2024.108584.

[15] Reinhardt H, Kolpa J, Stroband J. Building with demountable precast concrete components in the Netherlands, part 2. Betonwerk Und Fertigteil-Technik/Concrete Precasting Plant and Technology 1984;50:105–10.

[16] Bird JF, Bommer JJ. Earthquake losses due to ground failure. Engineering Geology 2004;75:147–79. https://doi.org/10.1016/j.enggeo.2004.05.006.

[17] Van De Lindt JW, Goh G-H. Effect of earthquake duration on structural reliability. Engineering Structures 2004;26:1585–97. https://doi.org/10.1016/j.engstruct.2004.05.017.

[18] Savoia M, Buratti N, Vincenzi L. Damage and collapses in industrial precast buildings after the 2012 Emilia earthquake. Engineering Structures 2017;137:162–80. https://doi.org/10.1016/j.engstruct.2017.01.059.

[19] Bournas DA, Negro P, Taucer FF. Performance of industrial buildings during the Emilia earthquakes in Northern Italy and recommendations for their strengthening. Bull Earthquake Eng 2014;12:2383–404. https://doi.org/10.1007/s10518-013-9466-z.

[20] Ding K, Ye Y, Ma W. Seismic performance of precast concrete beam-column joint based on the bolt connection. Engineering Structures 2021;232:111884. https://doi.org/10.1016/j.engstruct.2021.111884.

[21] Tanaka Y, Murakoshi J. Reexamination of dowel behavior of steel bars embedded in concrete. ACI Structural Journal 2011;108:659.

[22] Psycharis IN, Mouzakis HP. Shear resistance of pinned connections of precast members to monotonic and cyclic loading. Engineering Structures 2012;41:413–27.

[23] Bournas DA, Negro P, Molina FJ. Pseudodynamic tests on a full-scale 3-storey precast concrete building: Behavior of the mechanical connections and floor diaphragms. Engineering Structures 2013;57:609–27.

[24] Xie L, Wu J, Zhang J, Liu C. Experimental study on mechanical behaviour of replaceable energy dissipation connectors for precast concrete frames. Structures 2021;33:3147–62. https://doi.org/10.1016/j.istruc.2021.06.053.

[25] Hu G, Huang W, Xie H. Mechanical behavior of a replaceable energy dissipation device for precast concrete beam-column connections. Journal of Constructional Steel Research 2020;164:105816. https://doi.org/10.1016/j.jcsr.2019.105816.

[26] Huang H, Yuan Y, Zhang W, Li M. Seismic behavior of a replaceable artificial controllable plastic hinge for precast concrete beam-column joint. Engineering Structures 2021;245:112848. https://doi.org/10.1016/j.engstruct.2021.112848.

[27] Huang L, Zhou Z, Huang X, Wang Y. Variable friction damped self-centering precast concrete beam–column connections with hidden corbels: Experimental investigation and theoretical analysis. Engineering Structures 2020;206:110150. https://doi.org/10.1016/j.engstruct.2019.110150.

[28] Zhang J, Yuan W, Zhang T. Experimental study of earthquake resilient precast concrete beam-column-slab joints with bearing-double-stage energy dissipation connector. Soil Dynamics and Earthquake Engineering 2025;190:109151.

https://doi.org/10.1016/j.soildyn.2024.109151.

[29] Zhang R, Zhang Y, Li A, Yang TY. Experimental study on a new type of precast beam-column joint. Journal of Building Engineering 2022;51:104252. https://doi.org/10.1016/j.jobe.2022.104252.

[30] Baran E, Mahamid M, Baran M, Kurtoglu M, Torra-Bilal I. Performance of a moment resisting beam-column connection for precast concrete construction. Engineering Structures 2021;246:113005. https://doi.org/10.1016/j.engstruct.2021.113005.

[31] Senturk M, Pul S, Ilki A, Hajirasouliha I. Development of a monolithic-like precast beam-column moment connection: Experimental and analytical investigation. Engineering Structures 2020;205:110057. https://doi.org/10.1016/j.engstruct.2019.110057.

[32] Cheok GS, Lew HS. Performance of Precast Concrete Beam-to-Column Connections Subject to Cyclic Loading. Pcij 1991;36:56–67. https://doi.org/10.15554/pcij.05011991.56.67.

[33] Cheok GS, Lew HS. Model Precast Concrete Beam-to-Column Connections Subject to Cyclic Loading. Pcij 1993;38:80–92. https://doi.org/10.15554/pcij.07011993.80.92.

[34] William C. Stone GSC and John F Stanton. Performance of Hybrid Moment-Resisting Precast Beam-Column Concrete Connections Subjected to Cyclic Loading. ACI Structural Journal 1995;92. https://doi.org/10.14359/1145.

[35] Priestley MJN. The PRESSS Program Current Status and Proposed Plans for Phase Ill. PCI JOURNAL 1996.

[36] Palmieri L, Saqan E, French C, Kreger M. Ductile connections for precast concrete frame systems. Special Publication 1996;162:313–56.

[37] PAMPANIN S, Priestley M, SRITHARAN S. PRESSS PHASE 3: THE FIVE-STORY PRECAST TEST BUILDING VOL. 3-4. SSRP 2000:08.

[38] Xie L, Wu J, Zhang J, Liu C. Experimental study of mechanical properties of beam-

column joint of a replaceable energy-dissipation connector-precast concrete frame. Journal of Building Engineering 2021;43:102588. https://doi.org/10.1016/j.jobe.2021.102588.

[39] Zhang R, Guo T, Li A, Yang TY. Shaking Table Test and Numerical Analysis of a Precast Frame Structure with Replaceable Box Connectors. J Struct Eng 2024;150:04024175. https://doi.org/10.1061/JSENDH.STENG-13398.

[40] Huang H, Li M, Yuan Y, Bai H. Experimental Research on the Seismic Performance of Precast Concrete Frame with Replaceable Artificial Controllable Plastic Hinges. J Struct Eng 2023;149:04022222. https://doi.org/10.1061/JSENDH.STENG-11648.

[41] Song L, Guo T, Chen C. Experimental and numerical study of a self-centering prestressed concrete moment resisting frame connection with bolted web friction devices. Earthq Engng Struct Dyn 2014;43:529–45. https://doi.org/10.1002/eqe.2358.

[42] Tong G, Lianglong S, Guodong Z. Experimental study on beam-column connections of self-centering prestressed concrete frame with web friction devices. China Civil Engineering Journal 2012;45:23–32.

[43] Huang L, Zhou Z, Clayton PM, Zeng B, Qiu J. Experimental Investigation of Friction-Damped Self-Centering Prestressed Concrete Beam-Column Connections with Hidden Corbels. J Struct Eng 2020;146:04019228. https://doi.org/10.1061/(ASCE)ST.1943-541X.0002536.

[44] Qi A, Liu X, Xu R, Yan X. A precast beam-column joint using an innovative friction damper as a connector: Experimental and numerical study. Structures 2022;35:968–89. https://doi.org/10.1016/j.istruc.2021.11.045.

[45] Zeng Z, Miao C, Sun C. Investigation on seismic performance of friction energy-dissipating prefabricated concrete frame joints. Soil Dynamics and Earthquake Engineering 2025;188:109059. https://doi.org/10.1016/j.soildyn.2024.109059.

[46] Samani HR, Mirtaheri M, Zandi AP. Experimental and numerical study of a new adjustable frictional damper. Journal of Constructional Steel Research 2015;112:354–62.

https://doi.org/10.1016/j.jcsr.2015.05.019.

[47] Chen Y, Yu W, Zhang M, Li Y. A novel energy dissipation damper for multi-level earthquakes. Journal of Constructional Steel Research 2022;192:107214. https://doi.org/10.1016/j.jcsr.2022.107214.

[48] Li F, Du Y, Hong N, Li H, Chi P. Seismic performance of prefabricated replaceable graded-yielding energy-dissipating connectors. Engineering Structures 2023;297:116962. https://doi.org/10.1016/j.engstruct.2023.116962.

[49] Xu W, Cai Y, Zhang T, Wang S, Du D, Wan L. Experimental and numerical investigations of a staged energy dissipation device. Thin-Walled Structures 2024;198:111721. https://doi.org/10.1016/j.tws.2024.111721.

[50] Ersoy U, Tankut T. Precast Concrete Members With Welded Plate Connections Under Reversed Cyclic Loading. Pcij 1993;38:94–100. https://doi.org/10.15554/pcij.07011993.94.100.

[51] Baghdadi A, Heristchian M, Ledderose L, Kloft H. Experimental and numerical assessment of new precast concrete connections under bending loads. Engineering Structures 2020;212:110456. https://doi.org/10.1016/j.engstruct.2020.110456.

[52] Khaloo AR, Parastesh H. Cyclic loading of ductile precast concrete beam-column connection. Structural Journal 2003;100:291–6.

[53] Yang S, Lin Y, Guan D, Che Y, Liu W, Guo Z. Experimental investigation of a locally-compressed beam-column connection with bar-typed fuses. Journal of Building Engineering 2023;63:105562. https://doi.org/10.1016/j.jobe.2022.105562.

[54] Xiao J, Ding T, Zhang Q. Structural behavior of a new moment-resisting DfD concrete connection. Engineering Structures 2017;132:1–13.

[55] Liu W, Zhong M, Yang S, He W, Liu W. Seismic performance study on novel precast concrete beam-to-beam connection with threaded sleeve. Structures 2024;64:106572. https://doi.org/10.1016/j.istruc.2024.106572.

[56] Xie L. Research on the mechanism of replaceable energy dissipation connector and its seismic performance in precast concrete frame joint 2020.

[57] Nie X, Zhang S, Jiang T, Yu T. The strong column–weak beam design philosophy in reinforced concrete frame structures: A literature review. Advances in Structural Engineering 2020;23:3566–91.

[58] Lee J-Y, Park J. Effect of strain penetration on RC beam–column joints subjected to seismic loading, Springer; 2019, p. 309–27.

[59] Gao X, Peng H, Li J. Evolution of the yield penetration and bond stress in RC exterior beam-column joints under cyclic loading. vol. 36, Elsevier; 2022, p. 703–18.

[60] Aninthaneni PK, Dhakal RP. Demountable Precast Concrete Frame–Building System for Seismic Regions: Conceptual Development. J Archit Eng 2017;23:04017024. https://doi.org/10.1061/(ASCE)AE.1943-5568.0000275.

[61] Kishi N, Chen W. Moment-Rotation Relations of Semirigid Connections with Angles. J Struct Eng 1990;116:1813–34. https://doi.org/10.1061/(ASCE)0733-9445(1990)116:7(1813).

[62] Yang JG, Lee GY. Analytical models for the initial stiffness and ultimate moment of a double angle connection. Engineering Structures 2007;29:542–51. https://doi.org/10.1016/j.engstruct.2006.06.001.

[63] Keuser M, Kepp B, Mehlhorn G, Rostasy F. Nonlinear static analysis of end-fittings for GFRP-prestressing rods. Computers & Structures 1983;17:719–30.

[64] Burdziński M, Niedostatkiewicz M. Experimental-numerical analysis of the effect of bar diameter on bond in pull-out test. Buildings 2022;12:1392.

[65] Verwaerde R, Guidault P-A, Boucard P-A. A non-linear finite element connector model with friction and plasticity for the simulation of bolted assemblies. Finite Elements in Analysis and Design 2021;195:103586.

[66] Liu H, Chen W, Guo R, Liao W, Du X. Theoretical and numerical study on the bond

behavior between reinforcing steel and concrete. Journal of Building Engineering 2024;90:109398. https://doi.org/10.1016/j.jobe.2024.109398.

[67] Gao X, Li N, Ren X. Analytic solution for the bond stress-slip relationship between rebar and concrete. Construction and Building Materials 2019;197:385–97.

[68] Xu Z, Huang Y, Liang R. Numerical simulation of lap-spliced ultra-high-performance concrete beam based on bond–slip. Buildings 2022;12:1257.

[69] Dehestani M, Mousavi S. Modified steel bar model incorporating bond-slip effects for embedded element method. Construction and Building Materials 2015;81:284–90.

[70] de Terán JRD, Haach VG. Equivalent stress-strain law for embedded reinforcement considering bond-slip effects. Engineering Structures 2018;165:247–53.

[71] Fang Z, Zhou H, Lai S, Xie Q. ABAQUS bond-slip element of reinforced concrete under cyclic loads. Eng J Wuhan Univ 2014;47:527–31.

[72] Feng D-C, Wu G, Lu Y. Finite element modelling approach for precast reinforced concrete beam-to-column connections under cyclic loading. Engineering Structures 2018;174:49–66. https://doi.org/10.1016/j.engstruct.2018.07.055.

[73] Chen F, Yu Z, Yu Y, Liu Q. Study on the bond-slip numerical simulation in the analysis of reinforced concrete wall-beam-slab joint under cyclic loading. Construction and Building Materials 2024;449:138266. https://doi.org/10.1016/j.conbuildmat.2024.138266.

[74] Lemaitre J, Chaboche J-L. Mechanics of solid materials. Cambridge university press; 1994.

[75] Hoveidae N. Ultra-Low Cycle Fatigue Fracture Life of a Type of Buckling Restrained Brace. Rehabilitation in Civil 2018;6. https://doi.org/10.22075/jrce.2017.11262.1185.

[76] Tremblay R, Bolduc P, Neville R, DeVall R. Seismic testing and performance of buckling-restrained bracing systems. Can J Civ Eng 2006;33:183–98. https://doi.org/10.1139/l05-103.

[77] Elkady A. Collapse risk assessment of steel moment resisting frames designed with deep wide-flange columns in seismic regions. McGill University (Canada); 2016.

[78] Nip KH, Gardner L, Davies CM, Elghazouli AY. Extremely low cycle fatigue tests on structural carbon steel and stainless steel. Journal of Constructional Steel Research 2010;66:96–110. https://doi.org/10.1016/j.jcsr.2009.08.004.

[79] ACI Committee. Building code requirements for structural concrete (ACI 318-08) and commentary, American Concrete Institute; 2008.

[80] Mander JB, Priestley MJ, Park R. Theoretical stress-strain model for confined concrete. Journal of Structural Engineering 1988;114:1804–26.

[81] Sidoroff F. Description of anisotropic damage application to elasticity, Springer; 1981, p. 237–44.

[82] McKenna FT. Object-oriented finite element programming: frameworks for analysis, algorithms and parallel computing. University of California, Berkeley; 1997.

[83] Clough R. Effect of stiffness degradation on earthquake ductility requirements 1966.

[84] Qu Z, Ye L. Strength deterioration model based on effective hysteretic energy dissipation for RC-members under cyclic loading, 2010.

[85] Luo X, Cheng J, Xiang P, Long H. Seismic behavior of corroded reinforced concrete column joints under low-cyclic repeated loading. Arch Civ Mech Eng 20: 40 2020.

[86] Xiang P, Deng Z, Su Y, Wang H, Wan Y. Experimental investigation on joints between steel-reinforced concrete T-shaped column and reinforced concrete beam under bidirectional low-cyclic reversed loading. Advances in Structural Engineering 2017;20:446–60.

[87] Xue W, Hu X, Dai L, Zhu B. Cyclic behavior of semi-rigid precast concrete beam-to-column subassemblages with rapid assembly connections. Journal of Building Engineering 2022;46:103671. https://doi.org/10.1016/j.jobe.2021.103671.

[88] Kong Z, Kim S-E. Numerical estimation of the initial stiffness and ultimate moment

capacity of single-web angle connections. Journal of Constructional Steel Research 2016;121:282–90. https://doi.org/10.1016/j.jcsr.2016.02.011.

[89] Nikam SG, Wagholikar SK, Patil GR. Seismic Energy Dissipation of a Building Using Friction Damper 2014;3.

[90] Latour M, Piluso V, Rizzano G. Experimental analysis on friction materials for supplemental damping devices. Construction and Building Materials 2014;65:159–76. https://doi.org/10.1016/j.conbuildmat.2014.04.092.